Simulation and evaluation of flow boiling heat transfer correlations for R-744

Johannes Adrianus Mulder

B.Eng Mechanical

Dissertation submitted in partial fulfilment of the requirements for the degree

Master of Engineering

in the

School of Mechanical and Nuclear Engineering

at the

North-West University

Supervisor: Dr. Martin van Eldik

Co-supervisor: Mr. Werner Kaiser

November 2014

Acknowledgements

I would like to express my thanks to the following people who supported me throughout my studies and assisted me in completing this dissertation:

- My supervisor, Dr. Martin van Eldik for his insight, support and guidance throughout this project.
- My co-supervisor, Mr. Werner Kaiser for his enthusiasm and technical support throughout this study.
- Dr. Martin van Eldik, the North-West University and the NRF for the financial support granted towards my degree.
- My parents, Harko and Isabel Mulder and brothers, Henk and Harko Mulder for their continuous support and motivation.
- My fiancée, Ingrid, for her love and support, your love and prayers carried me through this study.

My Father who art in heaven, hallowed be thy Name. In humbleness I thank thee my Lord for never-ending grace and mercy.

Abstract

Title:	Simulation and evaluation of flow boiling heat transfer correlations for R-744.
Author:	Johannes Adrianus Mulder
Supervisor:	Dr. Martin van Eldik
Co-supervisor:	Mr. Werner Kaiser
School:	School of Mechanical and Nuclear Engineering, North-West University
Qualification:	Master of Engineering (M.Eng)

A need to reduce the use of conventional refrigerants in vapour-compression cycles has shifted attention towards natural refrigerants, one of which is carbon dioxide (CO_2 or R-744). This study focuses on the evaluation of existing correlations to predict the heat transfer characteristics of R-744 flow boiling in an evaporator.

A literature study was conducted on existing correlations developed specifically for R-744 as working fluid. Four correlations were identified, each developed for different ranges of the four main parameters believed to influence heat transfer. These factors are mass flux, evaporation temperature, heat flux and channel diameter.

The objective of the study was to compare experimentally obtained data with these correlations, thereby identifying the most applicable correlation or combination of correlations. A test bench was developed consisting of a counter flow tube-in-tube heat exchanger with water as secondary fluid, whereby experimental data were obtained.

From the study it was concluded that a combination of the Yoon *et al.*(2004) and the Pamitran *et al.*(2011) correlations applied to different regions are the most accurate. This combination predicted on average 55% of the data within ±10% and 88% within ±30% accuracy.

Table of contents

List of figures

List of tables

Nomenclature

A_L	Cross-sectional area occupied by liquid-phase.	m^2
A_p	Total heat transfer area – primary side.	m^2
A_s	Total heat transfer area – secondary side.	m^2
Bd	Bond number.	-
Bo	Boiling number.	-
C	Chisholm parameter.	-
c_p	Specific heat.	J/kgK
d	Tube internal diameter.	m
D_{eq}	Equivalent diameter.	m
E_Y	Enhancement factor with the Yoon *et al.* (2004) correlation.	-
f	Friction factor.	-
F_P	Multiplier factor with the Pamitran *et al.* (2011) correlation.	-
$Fr_{G,Mori}$	Froude number as defined by Mori *et al.* (2000)	-
g	Acceleration of gravity.	m/s^2
h_C	Flow boiling heat transfer coefficient with the Cheng *et al.* (2008a) correlation.	W/m^2K
$h_{cb,C}$	Convective boiling heat transfer coefficient with the Cheng *et al.* (2008a) correlation.	W/m^2K
$h_{cb,TE}$	Convective boiling heat transfer coefficient with the Thome and El Hajal (2004) correlation.	W/m^2K
$h_{cb,Y}$	Convective boiling heat transfer coefficient with the Yoon *et al.* (2004) correlation.	W/m^2K

$h_{dry,C}$	Dry-out region heat transfer coefficient with the Cheng *et al.* (2008b) correlation.	W/m^{2}K
$h_{G,C}$	Vapour heat transfer coefficient with the Cheng *et al.* (2008b) correlation.	W/m^{2}K
$h_{G,TE}$	Vapour heat transfer coefficient with the Thome and El Hajal (2004) correlation.	W/m^{2}K
$h_{G,Y}$	Vapour heat transfer coefficient with the Yoon *et al.* (2004) correlation.	W/m^{2}K
$h_{L,C}$	Wet wall boiling heat transfer coefficient with the Cheng *et al.* (2008a) correlation.	W/m^{2}K
$h_{L,P}$	Wet wall boiling heat transfer coefficient with the Pamitran *et al.* (2011) correlation.	W/m^{2}K
$h_{L,TE}$	Wet wall boiling heat transfer coefficient with the Thome and El Hajal (2004) correlation.	W/m^{2}K
$h_{L,Y}$	Wet wall boiling heat transfer coefficient with the Yoon *et al.* (2004) correlation.	W/m^{2}K
$h_{M,C}$	Mist flow region heat transfer coefficient with the Cheng *et al.* (2008b) correlation.	W/m^{2}K
$h_{nb,C}$	Nucleate boiling heat transfer coefficient with the Cheng *et al.* (2008b) correlation.	W/m^{2}K
$h_{nb,CO2,TE}$	R-744 nucleate boiling heat transfer coefficient with the Thome and El Hajal (2004) correlation.	W/m^{2}K
$h_{nb,P}$	Nucleate boiling heat transfer coefficient with the Pamitran *et al.* (2011) correlation.	W/m^{2}K
$h_{nb,TE}$	Nucleate boiling heat transfer coefficient with the Thome and El Hajal (2004) correlation.	W/m^{2}K

$h_{nb,Y}$	Nucleate boiling heat transfer coefficient with the Yoon *et al.* (2004) correlation.	W/m^2K
h_P	Flow boiling heat transfer coefficient with the Pamitran *et al.* (2011) correlation.	W/m^2K
$h_{R\text{-}744}$	Calculated R-744 heat transfer coefficient.	W/m^2K
h_{TE}	Flow boiling heat transfer coefficient with the Thome and El Hajal (2004) correlation.	W/m^2K
h_{water}	Calculated water heat transfer coefficient.	W/m^2K
h_Y	Flow boiling heat transfer coefficient with the Yoon *et al.* (2004) correlation.	W/m^2K
k	Thermal conductivity.	W/mK
M	Molecular weight.	-
$\dot{m}$	Total mass velocity of liquid and vapour (mass flux).	kg/m^2s
Pr	Prandtl number.	-
p_r	Reduced pressure.	-
q	Heat flux.	W/m^2
$q_{crit,C}$	Critical heat flux with the Cheng *et al.* (2008b) correlation.	W/m^2
Q	Energy	W
Re	Reynolds number.	-
Re_H	Homogeneous Reynolds number as defined by Cheng *et al.* (2008a) correlation.	-
Re_δ	Liquid film Reynolds number as defined by Cheng *et al.* (2008a) correlation.	-
R_{fp}	Fouling factor – primary side.	m^2K/W

R_{fs}	Fouling factor – secondary side.	m^2K/W
R_w	Thermal resistance of heat exchanger wall.	K/W
S_C	Boiling suppression factor with the Cheng *et al.* (2008b) correlation.	-
S_P	Boiling suppression factor with the Pamitran *et al.* (2011) correlation.	-
S_{TE}	Boiling suppression factor with the Thome and El Hajal (2004) correlation.	-
S_Y	Boiling suppression factor with the Yoon *et al.* (2004) correlation.	-
T	Temperature	K
UA	Overall heat transfer coefficient.	W/K
We	Weber number.	-
x	Vapour quality.	-
X	Martinelli parameter.	-
$x_{crit,Y}$	Critical vapour quality with the Yoon *et al.* (2004) correlation.	-
x_{de}	Vapour quality dry-out completion with the Cheng *et al.* (2008a) correlation.	-
x_{di}	Vapour quality of the boundary between annular flow and dry-out inception with the Cheng *et al.* (2008a) correlation.	-
x_{IA}	Vapour quality of the boundary between intermittent and annular flow with the Cheng *et al.* (2008a) correlation.	-
Y_C	Correction factor with the Cheng *et al.* (2008b) correlation.	-

Greek symbols

α	Enthalpy	J/kg
δ	Liquid film thickness.	m
δ_{IA}	Liquid film thickness at the intermittent to annular flow border with the Cheng *et al.* (2008a) correlation.	m
ε	Vapour cross-sectional void fraction.	-
η_{op}	Overall surface efficiency – primary side.	-
η_{os}	Overall surface efficiency – secondary side.	-
θ_{dry}	Dry angle of tube.	rad
μ	Dynamic viscosity.	Ns/m^2
ρ	Density	kg/m^3
σ	Surface tension.	N/m
$\emptyset_f^2$	Two-phase frictional multiplier with the Pamitran *et al.* (2011) correlation.	-

Subscripts

G	Vapour
L	Liquid
LG	Liquid-vapour
Lo	Consider the total vapour-liquid flow as liquid only.
x	Inlet conditions.
y	Outlet conditions.

Chapter 1 - Introduction

1.1 Background

The ability to supply electricity to the ever-increasing demand in South Africa is currently at risk. This has resulted in South Africa experiencing a higher than inflation increase in electricity cost since April 2008. Renewed focus is placed on the development or improvement of energy efficient products such as water heating heat pumps to replace conventional electrical element heating.

However, due to the higher capital cost involved in installing a heat pump, and the simplicity of direct electrical heating, heat pump technology is often overlooked. With the increase in electricity tariffs the feasibility of heat pumps has been drastically increased due to the higher continuous energy savings, which has prompted a large increase in heat pump installations over the last five years.

Water heating heat pumps are based on the well-known vapour compression cycle and makes use of refrigerants as working fluid. Conventional heat pumps, in recent history, make use of hydro-fluorocarbons (HFCs) and hydro-chlorofluorocarbons (HCFCs) as refrigerants. However, if set free into the atmosphere, these refrigerants contribute to global warming and cause damage to the ozone layer. This is reflected in their high global warming potential (GWP) and high ozone depletion potential (ODP) factors respectively (Oh & Son, 2011).

There is increasing pressure from governments world-wide to phase out these refrigerants. An alternative is the use of natural refrigerants, one of which is carbon dioxide (also known as R-744) which has an ODP of 0 and a GWP of 1 (Calm, 2008).

Although natural refrigerants have been used in the early 1900's, the development of CFCs and HCFCs in the 1930's showed an increase in performance and led to the replacement of natural refrigerants. With the recent developments in compressors and system components technology, the performance of R-744 used in a trans-critical vapour compression cycle compares well with the use of conventional refrigerants (HFCs and HCFCs), and is therefore a suitable natural replacement (Neksa, et al., 1998).

1.2 Problem statement

A proper understanding of the heat transfer characteristics of R-744 during evaporation is fundamental to the design and development of trans-critical R-744 heat pumps. Most correlations in literature, used to simulate heat transfer, were not developed specifically for R-744 (Gungor and Winterton, 1987; Jung *et al.*, 1989; Kattan *et al.*, 1998b). These correlations, however, fail to accurately simulate the heat transfer characteristics of R-744 during evaporation.

Correlations have been developed specifically for R-744 by various authors (Thome & El Hajal, 2004; Yoon *et al.*, 2004; Cheng *et al.*, 2008b; Pamitran *et al.*, 2011) but the accuracy of these correlations is not well documented and therefore not widely used. This study aims to address this uncertainty by identifying a correlation or combination of correlations for different flow regions which can be used to accurately predict the heat transfer characteristics of R-744 during evaporation in horizontal tubes. This study will only focus on the two-phase region and will therefore exclude the heat transfer characteristics of superheated R-744.

The test bench facility used at the North-West University (NWU) consists of a closed loop heat pump cycle used to heat up water. This uses a tube-in-tube evaporator, with water as secondary fluid. Due to the limitations of the experimental setup, evaporation through the stratified and stratified-wavy flow regions will not be considered.

1.3 Purpose of this study

The purpose of this study is to determine the applicability of the correlations predicting the heat transfer coefficients of R-744 flow boiling found in literature, to the heat exchanger configuration used in the test bench, at different operating conditions.

1.4 Method of investigation

To identify the correlations available as well as their expected accuracies, an in depth literature survey was conducted. From this survey a short list of four correlations was identified which showed the highest accuracies and applicability. Using Engineering Equation Solver (EES) these correlations were programmed to calculate the heat transfer coefficients for a given set of input variables.

An existing test bench was modified and upgraded to conduct tests for comparison with the correlations. By using the measured data the heat transfer coefficients were calculated for each of the input variables. These experimental heat transfer coefficients were then compared to the heat transfer coefficients of the four correlations. From this comparison the accuracy and applicability of each of the correlations were determined at different operating conditions.

Chapter 2 - Literature survey

In this chapter the comprehensive literature survey that was conducted will be described. In the first two sections an introductory overview is given on the history of refrigerants and on the trans-critical R-744 heat pump cycle. The third section discusses the main parameters which have an influence on the heat transfer characteristics. Finally, the last two sections describe the four R-744 heat transfer correlations identified and the water heat transfer correlations to be used in this study.

2.1 History of refrigerants

Before the ongoing world-wide interest to further develop R-744 as a refrigerant is discussed, a brief overview of the history of R-744 will be given.

Carbon dioxide (R-744) as a refrigerant has been in use since the 19th century with R-744 being one of the very first refrigerants used after the invention of the vapour compression refrigeration cycle. The first system was patented in 1834 by Jacob Perkins and although he used ethyl ether as the refrigerant for his first system, R-744 (and other natural refrigerants) were used as a refrigerant during that time (Pearson, 2005).

The first refrigeration system which used carbon dioxide as a refrigerant was designed and built by Thaddeus S.C. Louw in 1862. The technology was further developed by various individuals including Franz Windhausen. These systems were developed and manufactured mainly for the marine refrigeration industry (Pearson, 2005).

R-744 was considered much safer than other natural refrigerants like ammonia and sulphur dioxide mainly due to the latter being toxic and flammable. The development of R-744 therefore continued and it was widely used as a refrigerant. There are, however, disadvantages to using R-744 as refrigerant, including a lower coefficient of performance compared to other refrigerants. Also, due to a lack of technology at the time, the high pressure at which R-744 needed to operate caused difficulties in the development of these cycles (Oh & Son, 2011).

During the 1930's the technology of refrigeration was drastically changed by the development of dichlorodifluoromethane (R-12) by Thomas Midgeley. This started the era of halocarbon refrigerants which later led to the development of a number of chlorofluorocarbons (CFCs)

and hydrochlorofluorocarbons (HCFCs) which included R-22, R-115 and R-502 (Pearson, 2005). These refrigerants replaced the natural refrigerants used previously mainly because of improved safety, and thus resulted in R-744 being phased out.

In the 1970's the effects of CFC's on the ozone layer were discovered, which eventually meant the end of CFCs due to mounting pressure during the 1980's by environmental groups. A new refrigerant, R-134a, was developed to serve as replacement. This refrigerant has no negative effect on the ozone layer although its performance is lower than that of R-22 (Calm, 2008).

Due to mounting concerns regarding the effects of certain gasses on global warming it can be assumed that R-134a will not be used as a refrigerant in future. This is reflected in its high global warming potential (GWP) of about 1300 and therefore extensive research is being done on the use of alternative refrigerants with a lower GWP. R-744 falls in this category due to a GWP of 1 and is being explored as an alternative (Calm, 2008).

2.2 Trans-critical R-744 heat pump cycle

As indicated in the previous section R-744 is being investigated as a potential refrigerant to be used in heat pump cycles without having a negative impact on the environment. A brief overview is given next on the basic layout of a trans-critical heat pump cycle as well as the properties of R-744 when operating in this cycle.

2.2.1 Layout of a trans-critical heat pump cycle

Similar to that of a conventional heat pump, the trans-critical cycle consists mainly of a compressor, two heat exchangers and an expansion valve. The cycle as depicted on a T-S (temperature vs. entropy) diagram is shown in Figure 2.1. The working fluid (R-744) is being compressed by the compressor which causes the fluid temperature to rise between points 1 and 2. In order to heat water to 60°C in the gas cooler the fluid needs to be heated into the super-critical region, which will be discussed in further detail in the following section.

The heat is transferred to water in a heat exchanger due to the compressed gas having a higher temperature than the water (between points 2 and 3 in Figure 2.1), therefore the fluid experiences a temperature drop in the heat exchanger. In a trans-critical cycle the fluid does not condensate through the two-phase region since the gas flashes instantly from the gas

phase to the liquid phase. Because of this, the heat exchanger known as a condenser in a conventional vapour compression cycle is here known as a gas cooler.

From the gas cooler the fluid is expanded through the expansion valve allowing the pressure and temperature to drop (between points 3 and 4 in Figure 2.1). The fluid enters the two-phase area and is a mixture of liquid and gas when entering the second heat exchanger, called the evaporator. Heat is transferred to the fluid in the evaporator ensuring it is completely super-heated before entering the compressor (between points 4 and 1 in Figure 2.1). Also shown in Figure 2.1 are the typical temperatures and pressures at each of these points.

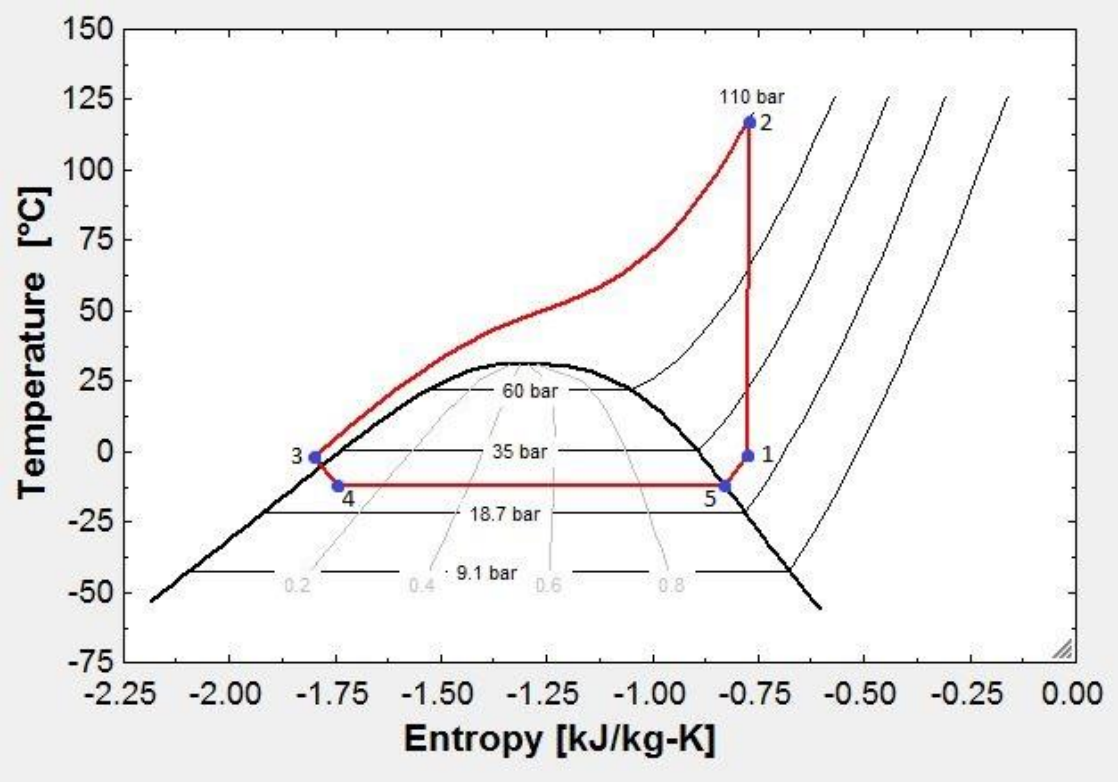

Figure 2.1 – T-S diagram of a trans-critical vapour compression cycle.

2.2.2 Properties of R-744

As described in the preceding section the primary difference between a trans-critical R-744 heat pump system and the more conventional Freon system, is the use of a gas cooler instead of the conventional condenser. This is due to the fluid properties of R-744 which will be discussed briefly.

R-744 has a low critical point (31.1°C and 73.7 Bar) and therefore does not condense in the high pressure heat exchanger (Kim *et al.*, 2004). The high pressure R-744 cools while

flowing through the gas cooler and flash from the gas phase to the liquid phase without the presence of a two-phase region. There is thus no region when the fluid condenses at a constant temperature while heat is exchanged with the secondary fluid. The system is operating in a so-called trans-critical state since the gas cooler is operating above the critical point and the evaporator below the critical point. In Figure 2.2 a P-h diagram is shown illustrating the critical point of R-744.

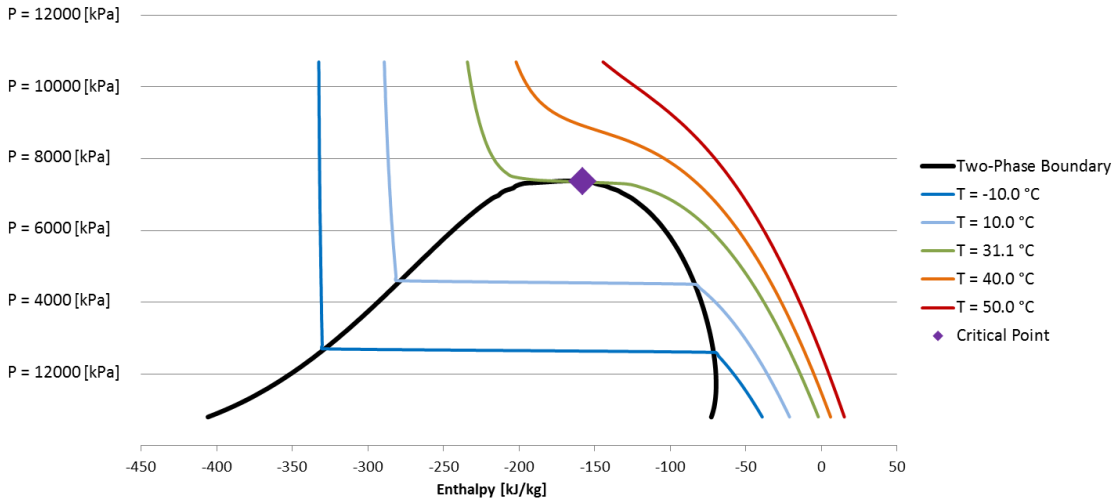

Figure 2.2 – P-h diagram of R-744.

Any conventional type evaporator can be used to heat up the R-744 through the two-phase area below the critical point. R-744 however evaporates at a higher pressure than conventional refrigerants to ensure the necessary temperature difference with the secondary fluid. The evaporation temperatures at various pressures for various refrigerants can be seen in Figure 2.3

The triple point of R-744 (-56.6°C and 5.2 Bar) is higher compared to other refrigerants and can cause it to reach a solid state when the system is not running, causing a sudden increase in pressure (Kim *et al.*, 2004). Also, the density of R-744 in the gas phase can exceed that of water in the liquid phase - it is due to this high vapour density that R-744 has such a high volumetric refrigeration capacity.

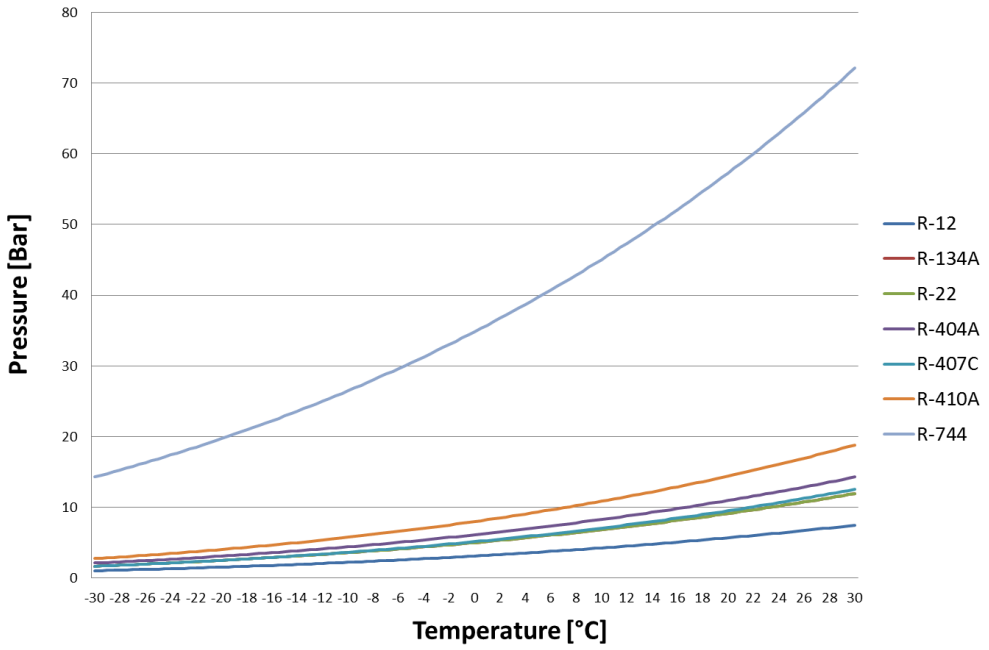

Figure 2.3 – Evaporation temperature comparison of different refrigerants.

2.3 Parameters influencing heat transfer characteristics

It is clear from the latest literature available on this topic that most authors agree that certain parameters have a predictable influence on the heat transfer characteristics of flow boiling with R-744. The following four parameters were identified that directly influence the heat transfer coefficient (Cheng *et al.*, 2006; Pamitran *et al.*, 2011; Yoon *et al.*, 2004):

- Channel diameter.
- Saturation temperature.
- Mass flux.
- Heat flux.

The effect of each one of these parameters will be discussed briefly along with graphs indicating the trends. The correlations evaluated in this study will be compared to these trends to ensure the trends are reflected in the predicted heat transfer coefficients.

2.3.1 Channel diameter

The trend shown by most authors is an increase in the heat transfer coefficient with a decrease in channel diameter, as can be seen from the experimental data of Pamitran *et al.* (2011) as shown in Figure 2.4 (x refers to vapour quality). This is due to nucleate boiling

being more active in a smaller channel, since the relative contact surface area for heat transfer increases when the tube diameter decreases. It is also expected that the annular flow region and the dry-out point will occur earlier in a smaller channel.

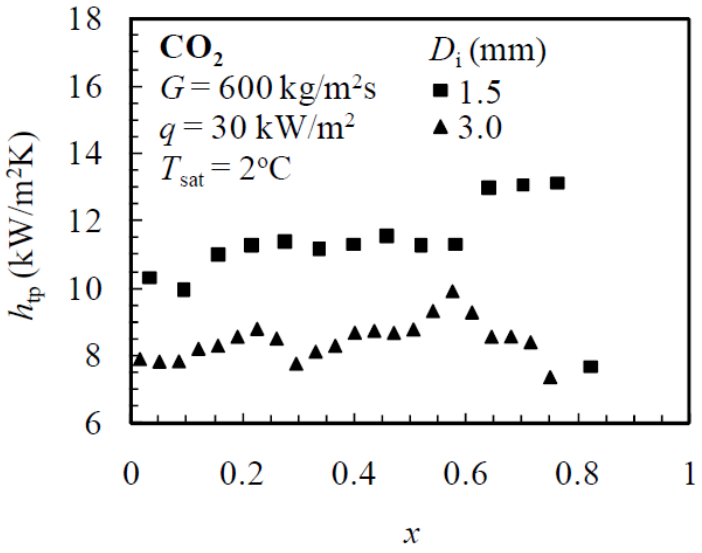

Figure 2.4 – Influence of channel diameter on the heat transfer coefficient (Pamitran *et al*., 2011).

In this study the test facility is limited to a channel diameter of 15.7 mm, and therefore the influence of channel diameter will not be tested. However, correlations in literature are grouped according to the channel diameter to which it is applicable and is therefore important for this study. The different groups are named i) conventional, ii) mini/macro and iii) micro channels, where mini and macro normally refers to the same size channels. According to Kandlikar (2002) the channel diameters can be classified as follows:

i. Conventional channel: $3.0\ \text{mm} < D_{channel}$

ii. Mini/macro channel: $0.2\ \text{mm} < D_{channel} < 3.0\ \text{mm}$

iii. Micro channel: $D_{channel} < 0.2\ \text{mm}$

It needs to be noted that not all authors agree on the same classification and correlations were often developed from databases which include data from more than one group.

Whichever classification is used, it is clear that for this study the channel diameter falls into the conventional grouping. Due to the uncertainty among authors about the exact classification as well as the limited number of correlations available, the assumption has been made that correlations specifically developed for micro-channels will be excluded from this study whilst all other correlations will be considered.

2.3.2 Saturation temperature

In the low quality region the heat transfer coefficient tends to increase with a rise in the saturation temperature. This is due to nucleate boiling which becomes more effective at higher pressures associated with higher saturation temperatures. The vapour bubbles detaching from a heated surface during nucleate boiling plays an important role: as the temperature increases the liquid to vapour density ratio increases. Therefore the vapour bubble buoyancy increases and the bubble detachment increases accordingly (Cho *et al.*, 2000). This trend can be seen in Figure 2.5.

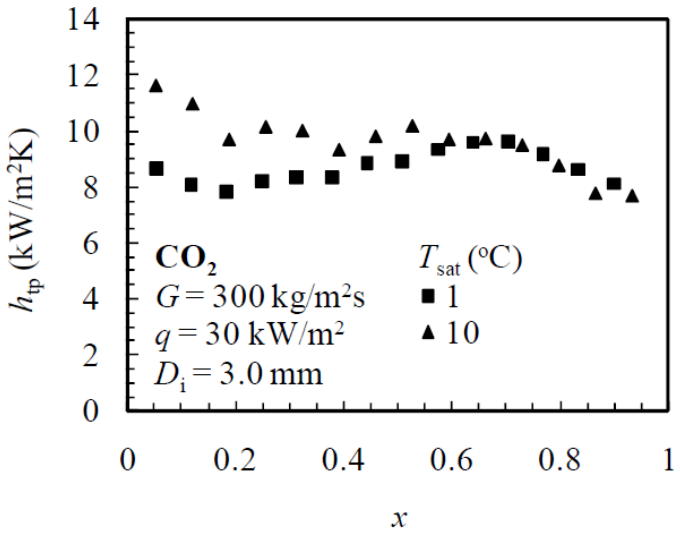

Figure 2.5 – Influence of saturation temperature on the heat transfer coefficient (Pamitran *et al.*, 2011).

The dry-out quality is reached earlier with higher saturation temperatures as shown in Figure 2.6. It starts at the top of the channel due to gravitational forces and occurs due to the higher density ratio associated with a higher saturation temperature. This leads to greater entrainment which in turn causes dry-out to occur at a lower vapour quality (Yun *et al.*, 2005; Choi *et al.*, 2007; Pettersen, 2003).

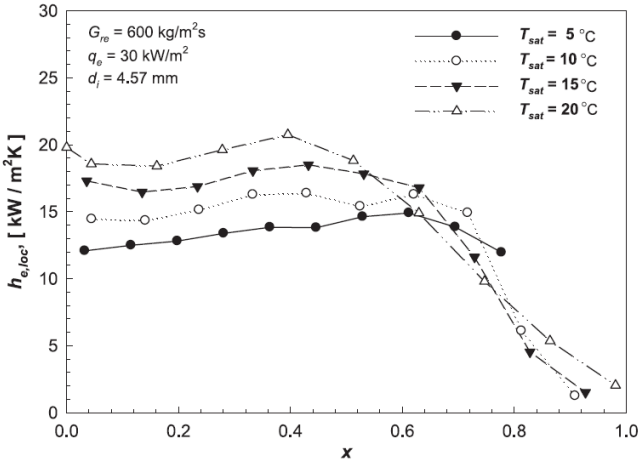

Figure 2.6 – Dry out point at various saturation temperatures (Oh & Son, 2011).

2.3.3 Mass flux

A change in mass flux has a limited effect on the heat transfer coefficient in the low vapour quality region (Pettersen, 2003). However, the mass flux has an influence on when dry-out occurs, which in effect influences the heat transfer coefficient since a sudden drop in the heat transfer coefficient is found post dry-out. Figure 2.7 confirms the negligible influence on the heat transfer coefficient before dry-out and shows the vapour quality at which dry-out occurs. This is again caused by higher entrainment due to the higher mass flux similarly to the effect of a higher saturation temperature.

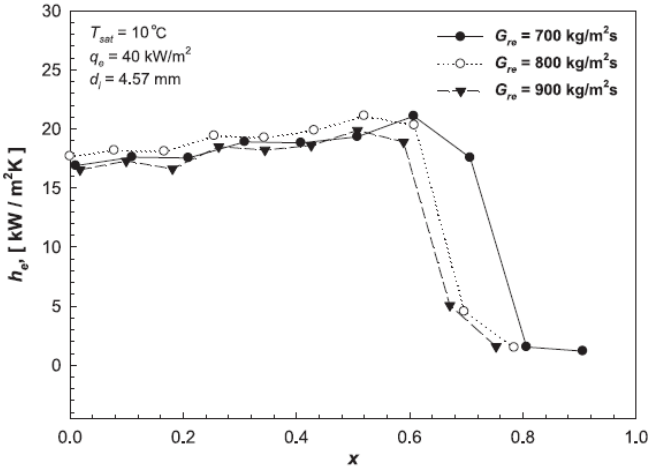

Figure 2.7 – Influence of mass flux on the heat transfer coefficient (Oh & Son, 2011).

2.3.4 Heat flux

The heat transfer coefficient increases with an increase in heat flux in the low and moderate vapour quality regions due to nucleate boiling being the dominant heat transfer mechanism

(Yun *et al*., 2005; Huai *et al*., 2004). In the high vapour quality region nucleate boiling is suppressed and therefore the heat flux has a smaller effect on the heat transfer coefficient as can be seen in Figure 2.8.

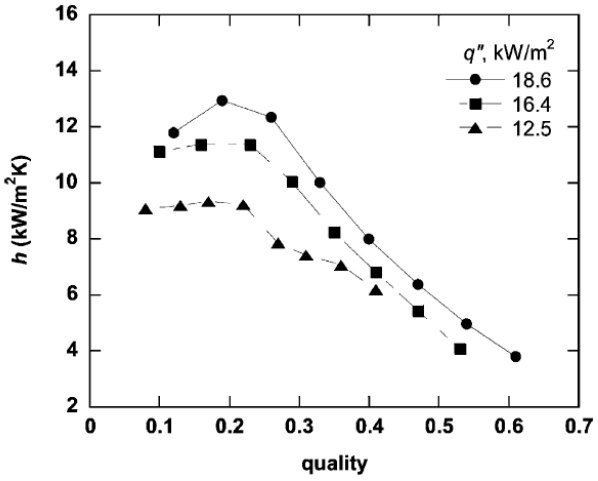

Figure 2.8 – Influence of heat flux on the heat transfer coefficient (Yoon *et al*., 2004).

2.4 R-744 correlations

The following are some of the correlations which were not specifically developed for R-744 but which were considered and evaluated for use in this study:

- Gungor & Winterton (1987).
- Kandlikar (1990).
- Liu & Winterton (1991).
- Kattan *et al.* (1998b).

These non-R-744 correlations tend to under-predict the heat transfer coefficient due to a failure to predict a higher nucleate boiling heat transfer contribution (Oh & Son, 2011). Therefore none of these will be tested in this study. The following four correlations fall in the conventional channel diameter group as described in section 2.3.1 and were specifically developed for R-744:

- Thome and El Hajal (2004).
- Yoon *et al.* (2004).
- Cheng *et al.* (2008b).
- Pamitran *et al.* (2011).

These correlations will each be briefly discussed in the sections to follow and will be used to calculate the predicted heat transfer coefficients.

2.4.1 Thome and El Hajal (2004)

This is the oldest of the four correlations and was published in August 2004. This correlation followed on research conducted at the Swiss Federal Institute of Technology Lausanne in Lausanne, Switzerland.

Five different data sets from previous independent studies were used to set up a database from which the correlation was developed and later tested. This correlation covers channel diameters from 0.79 to 10.06 mm, mass velocities from 85 to 1440 kg/m^{2}s, heat fluxes from 5 to 36 kW/m^2 and saturation temperatures from -25 to 25°C.

The correlation is based on the heat transfer model developed by Kattan-Thome-Favrat which makes use of a flow pattern map (Kattan *et al.*, 1998c). This flow pattern map was not specifically developed for R-744 but was simplified by Thome and El Hajal in an earlier study for use with this correlation (Thome & El Hajal, 2002) (Thome, 2005). Figure 2.9 shows an example of the flow pattern map and also the effect of channel diameters on the flow pattern map. The flow regimes as indicated on the map are as follows:

- S – Stratified flow.
- SW – Stratified wavy flow.
- I – Intermittent flow.
- A – Annular flow.
- MF – Mist flow.

Although different authors use different names for flow regimes, the ones mentioned above are widely used in literature and will thus be used in this study also. Figure 2.10 shows the effect of different saturation temperatures on the flow pattern map of a 6 mm tube.

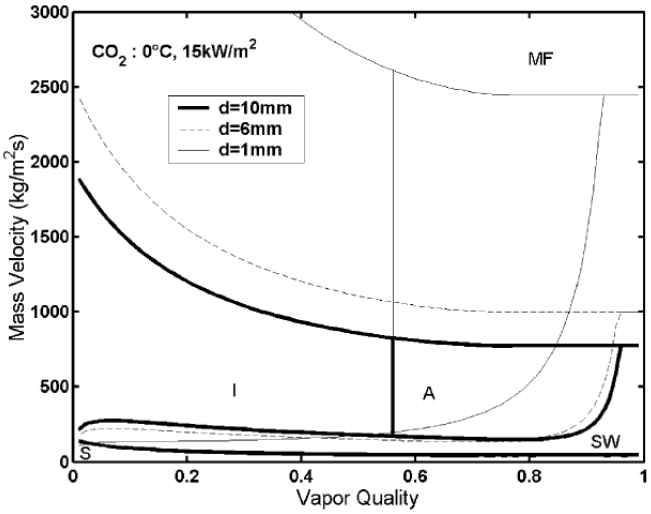

Figure 2.9 – Example of flow pattern map for different channel diameters (Thome & El Hajal, 2004).

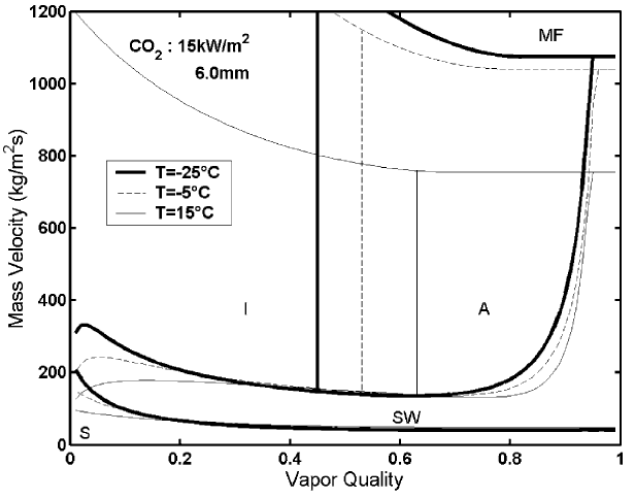

Figure 2.10 – Example of flow pattern map for different saturation temperatures (Thome & El Hajal, 2004).

Thome and El Hajal (2004) compared this flow map with data in existing literature, and taking into account that the lines do not indicate a sudden change but rather a gradual change of flow regime, the map predicted 24 of the 29 data points correctly.

The major changes made to the Kattan-Thome-Favrat model were i) the nucleate pool boiling correlation which was changed and ii) the use of a boiling suppression factor on the nucleate boiling heat transfer coefficient. This was done due to the low critical temperature and high evaporating pressures of R-744 (Thome & El Hajal, 2004).

Applying this correlation and comparing the results to the available 404 data points in the database, the correlation predicted 73% of these points within ±20% and 86% within ±30%. This showed a large improvement on the previously available correlations in predicting the flow boiling characteristics of R-744.

2.4.2 Yoon et al. (2004)

This correlation was published in the same year as the correlation by Thome and El Hajal and followed on research done by LG Electronics Inc. in conjunction with the Seoul National University in Seoul, South Korea. Unlike the previous correlation discussed, this correlation was developed from new data acquired using an experimental setup developed by Yoon *et al*. (2004) as shown in Figure 2.11.

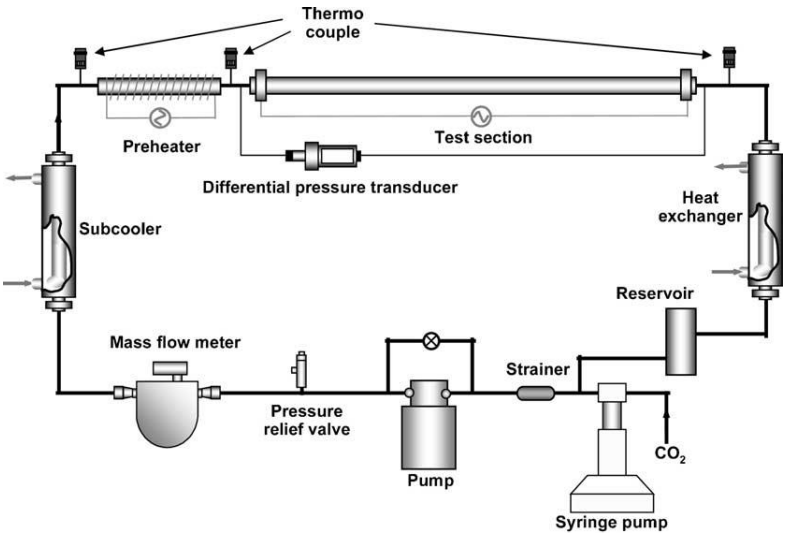

Figure 2.11 – Experimental apparatus used by Yoon *et al.* (Yoon *et al.*, 2004).

The test section consisted of a stainless steel tube with an inner diameter of 7.73 mm and a total length of 5.0 m. At each thermocouple location, temperatures were measured at the top, bottom and on both sides of the tube. Experiments were done for mass velocities from 212 to 530 kg/m^{2}s, heat fluxes from 12.3 to 18.9 kW/m^2 and saturation temperatures from -4 to 20°C. Experiments were restricted to vapour quality ranges below 0.7.

Yoon *et al.* (2004) proposed that due to gravitational forces the flow pattern within the tube differs at the top and bottom of the tube. Therefore the heat transfer coefficient also differs at the top and bottom of the tube. Figure 2.12 indicates the predicted flow pattern of R-744 inside the tube.

It was found that the temperature at the top of the tube suddenly increased at a certain quality due to the ever shrinking liquid film eventually disappearing at the top of the channel. At this point the heat transfer coefficient decreased significantly.

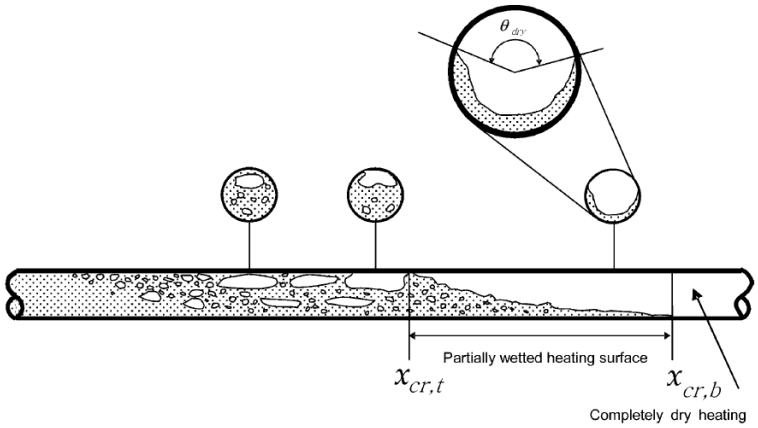

Figure 2.12 – Flow pattern prediction by Yoon *et al*. (Yoon *et al*., 2004).

This phenomenon is well known with halocarbon refrigerants, however with halocarbons this normally happens at a quality of 0.9 whereas with R-744 this happens at a lower quality. For the data set discussed this occurred at a quality of 0.2. Therefore in some sections of the flow the vapour heat transfer mechanism is dominant whilst in other regions the two-phase evaporative heat transfer mechanism is dominant.

Yoon *et al.* developed an equation in order to determine the point at which these mechanisms change, known as the critical point. This equation is based on dimensionless numbers which reflects the influence of mass flux, heat flux and saturation temperature. In Figure 2.13 this phenomenon is shown with temperature readings on the top, side and bottom of the pipe plotted against vapour quality

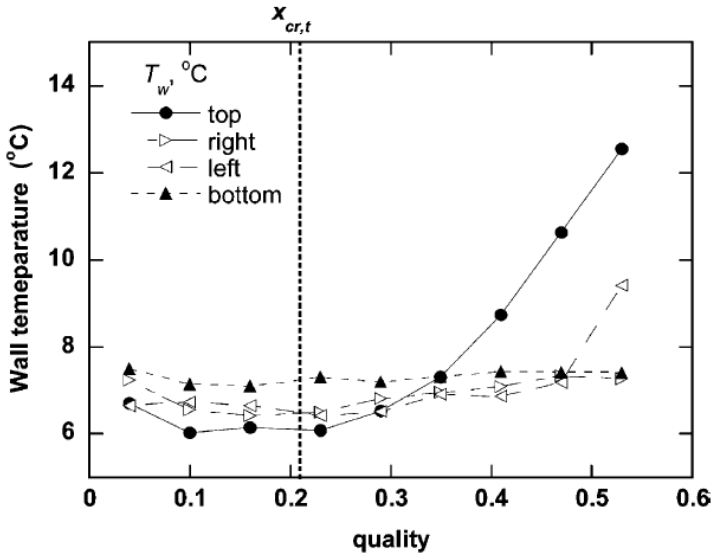

Figure 2.13 – Temperature distribution around the circumference of the evaporation channel (Yoon et *al*., 2004).

Based on this equation a correlation for the heat transfer coefficient before and after the critical point was developed. By improving the coefficients of the correlation by Liu and Winterton, a correlation was developed to represent the R-744 data before the critical point (Jung et al., 1989). For after the critical point a correlation was developed by the superposition of the liquid and vapour heat transfer coefficients for the wet and dry regions. Gungor & Winterton's correlation was used for the development of the wetted area coefficient and the Dittus-Boelter correlation for the dry area albeit with some modification (Gungor & Winterton, 1987).

The new correlation was compared to the experimental data, and the results were as follows:

- Average deviation: 1.5%
- Absolute average deviation: 15.2%
- Root-mean-square (RMS) deviation: 21.1%

2.4.3 Cheng et al. (2008b)

This correlation followed on an extensive study done at the Laboratory of Heat and Mass Transfer at École Polytechnique Fédérale de Lausanne in Lausanne Switzerland. The correlation was published in June 2007 and followed on previous articles by the same authors in 2003 and 2006.

In the earlier studies a model was proposed based on a new flow pattern map developed from the model by Wojtan *et al.* (2005a). The fluid flow pattern under different conditions was predicted by the flow pattern map, with a specific heat transfer correlation applicable to each flow pattern. These heat transfer correlations take into account the heat transfer mechanisms which are dominant in the respective flow patterns. Although reasonably accurate for specific limited ranges of mass flux and heat flux, this model did not extrapolate well outside of these ranges.

The authors improved on this by refining the flow pattern map and increasing the ranges of mass flux and heat flux it was applicable to. Thirteen independent experimental studies were used to form a new database from which the new model was developed. This model covers channel diameters from 0.6 mm to 10 mm. The database included mass velocities from 50 to 1500 kg/m^{2}s, heat fluxes from 1.8 to 46 kW/m^2 and saturation temperatures between -28 and 25°C.

Refinement of the flow pattern map included:

- Modification of the annular flow to dry-out transition boundary to accommodate the heat transfer characteristics of higher mass velocities.
- A new transition boundary criterion between the dry-out and mist flow regions.
- A bubbly flow pattern boundary.

This flow pattern map was applied to a data set by Gasche (2006) showing good results in predicting the flow pattern. The flow pattern map is shown in Figure 2.14 with the corresponding observed flow patterns shown in Figure 2.15.

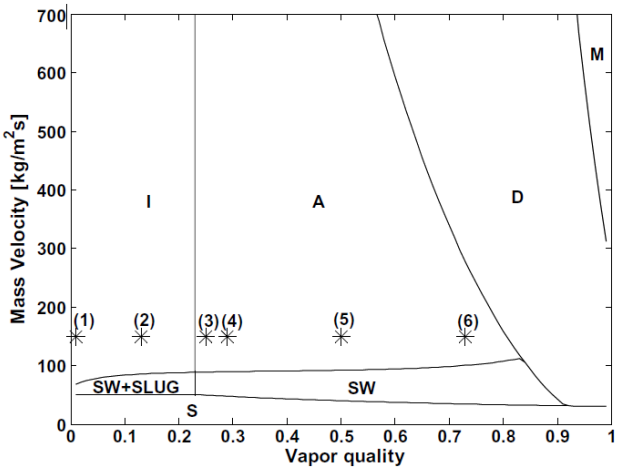

Figure 2.14 – Flow pattern map by Cheng *et al.* presenting data from Gasche (Cheng *et al.*, 2008a).

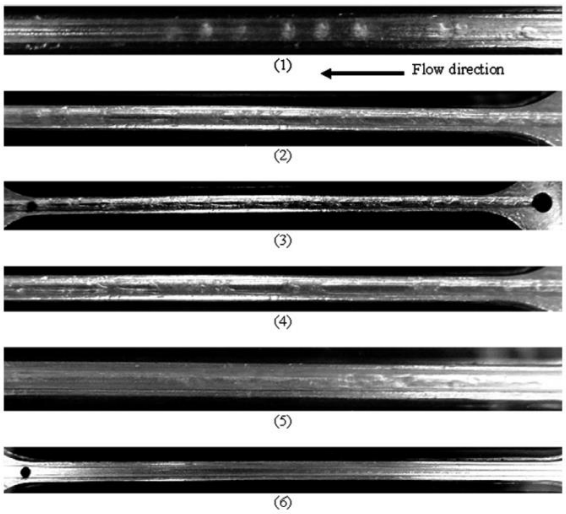

Figure 2.15 – Flow patterns as observed by Gasche (Gasche, 2006).

The new flow pattern map correctly identified the flow patterns of 82% of Gasche's data points. Cheng *et al.* (2008a) recommended that further studies be done to fully explain the width of each transition, since flow pattern maps give the impression that the changes are abrupt, which is not the case.

Based on this new flow pattern map a heat transfer correlation for each of the flow regimes was developed. The results, excluding the data for the dry-out and mist flow regimes, are shown in Figure 2.16.

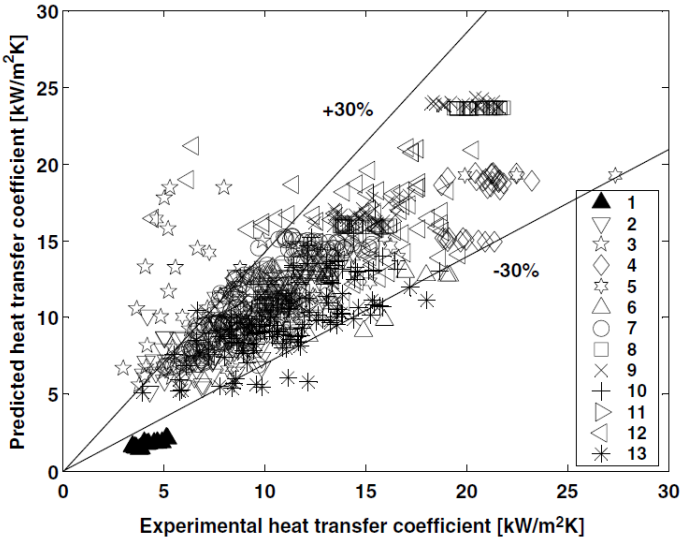

Figure 2.16 – Accuracy of Cheng *et al.* correlation (Cheng *et al.*, 2008b).

The model showed less satisfactory results in the dry-out and mist flow regimes, due to the difficulty in accurately measuring the heat transfer data in these regimes. Despite this the model performed well compared to other correlations with 71.4% of the data points in the database predicted within ±30%. Of the wet data points 83.2% were predicted within ±30%, 47.6% of the partially wet data points and 48.2% of the dry data points (all within ±30%).

2.4.4 Pamitran et al. (2011)

This is the most recent of the four correlations evaluated. Two universities were involved in this study, namely the University of Indonesia in Depok, and Chonnam National University in the Republic of Korea. The study focused on developing a new evaporation heat transfer correlation for use with propane (C_3H_8), ammonia (NH_3) and R-744.

Similar to the study by Yoon *et al. (2004)* an experimental test facility was used to acquire a new database from which the correlation was developed as shown in Figure 2.17. This

database encompasses the entire vapour quality range and includes mass fluxes from 50 to 600 kg/m^{2}s, heat fluxes from 5 to 70 kWm^2 and saturation temperatures from 0 to 10°C. Two different tube inner diameters were used, namely 3.0 and 1.5 mm.

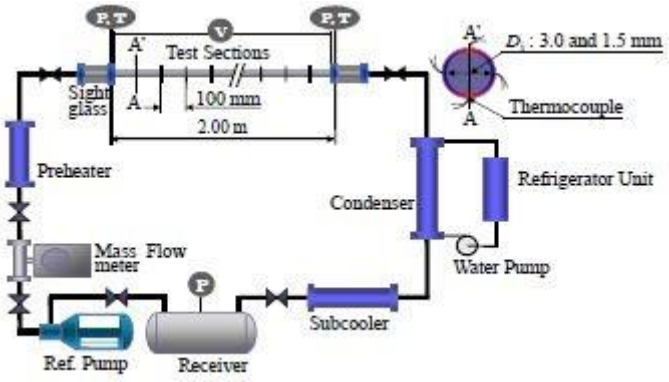

Figure 2.17 – Experimental apparatus used by Pamitran *et al.* (Pamitran *et al.*, 2011).

Pamitran *et al.* (2011) confirmed that R-744 has a high nucleate boiling heat transfer contribution due to its low surface tension and high operating pressure. Through the superposition of the two heat transfer coefficients for the two mechanisms governing heat transfer during flow boiling, a new combined correlation was developed (with these two mechanisms being nucleate boiling and forced convective evaporation).

The liquid heat transfer coefficient was derived from the Dittus-Boelter correlation and a convective two-phase multiplier was added to account for the enhanced convection due to the presence of both liquid and vapour (Dittus & Boelter, 1930). The nucleate boiling heat transfer was predicted by using the Cooper correlation which is a pool boiling correlation (Cooper, 1984). To account for the suppression of nucleate boiling due to high mass flux a suppression factor is included for nucleate boiling, derived from the convective boiling heat transfer multiplier by Jung *et al.* (1989).

The new correlation was compared to the experimental data and the results for R-744 can be seen in Figure 2.18. R-744 showed the best results compared to C_3H_8 and NH_3, with a mean deviation of 17.12% and an average deviation of 0.32%.

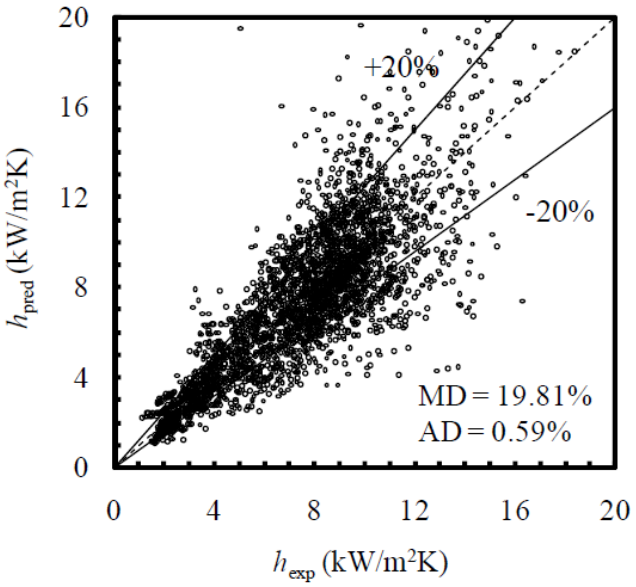

Figure 2.18 – Accuracy of Pamitran *et al.* correlation (Pamitran *et al.*, 2011).

2.4.5 Summary

For the current study four correlations developed specifically for R-744 were identified to be evaluated based on their high accuracy in predicting the flow boiling heat transfer of R-744 in the two-phase region. Although other R-744 flow boiling heat transfer correlations are available in literature they mainly focus on micro channels ($D_{channel}$ < 0.2 mm) and therefore were excluded. Table 2.1 gives a summary of the four correlations and their respective ranges.

Table 2.1 – Summary of ranges for each of the four selected correlations.

	Channel diameter [mm]	**Mass velocities [kg/m^{2}s]**	**Heat fluxes [kW/m^2]**	**Saturation temperatures [ºC]**
Thome & El Hajal (2004)	0.79 – 10.06	85 – 1440	5 – 36	-25 – 25
Yoon *et al.* (2004)	7.53	200 – 530	12 – 20	-4 – 20
Cheng *et al.* (2008b)	0.6 – 10.0	50 – 1500	1.8 – 46	-28 – 25
Pamitran *et al.* (2011)	3.0 & 1.5	50 – 600	5 – 70	0 – 10

2.5 Water correlations

Although the focus of this study is on the evaluation of R-744's characteristics during flow boiling, the secondary fluid in the heat exchanger (being water) also needs to be included. The correlations for the heat transfer coefficient of water flowing in a tube are well known and readily available in various textbooks and journals and are therefore only mentioned briefly. These will be divided into coefficients for laminar flow and turbulent flow.

2.5.1 Laminar flow

For this study it is assumed that the fluid (water) is incompressible, has constant properties and the flow is fully developed. With these assumptions a theoretical model can be used to predict the heat transfer coefficient which will be discussed in Chapter 3 (Borgnakke & Sonntag, 2009).

2.5.2 Turbulent flow

For the turbulent flow region the flow conditions are more complicated and therefore an empirical correlation is more suitable. The most well-known correlation is that of Dittus-Boelter and this correlation is well proven in literature (Dittus & Boelter, 1930). The Dittus-Boelter equation has been confirmed experimentally for the following conditions:

- Fully developed flow.
- $0.6 \leq$ Prandtl number ≤ 160.
- Reynolds number ≥ 10000.
- Channel length / channel diameter ≥ 10.
- Small to moderate temperature differences.

The correlation developed by Gnielinski is more complex, however it has shown higher accuracy (Gnielinski, 1975). This correlation also includes the transitional region unlike the Dittus-Boelter equation and is accurate for the following conditions:

- Fully developed flow.
- $0.5 \leq$ Prandtl number ≤ 2000.
- $3000 \leq$ Reynolds number $\leq 5 \times 10^6$.
- Channel length / channel diameter ≥ 10.

It uses the Moody diagram to determine the value of the friction factor for tubes which are not smooth.

2.6 Chapter summary

In Chapter 2 a brief history was given of refrigerants and the trans-critical R-744 heat pump cycle after which a description was given of the influence of the four main parameters on the heat transfer coefficients of R-744. Following this the four different flow boiling heat transfer correlations for R-744 were identified. These four correlations were discussed separately to indicate the basic workings and accuracies thereof. The correlations to be used in calculating the heat transfer coefficients on the water side were also briefly discussed. In Chapter 3 the theoretical details for each of these correlations will be discussed.

Chapter 3 - Theoretical background

In Chapter 3 the theory describing the correlations identified in Chapter 2 will be discussed in more detail. This will form the basis for the EES program setup that follows in the next chapter. In the first part of this chapter the four R-744 correlations will be discussed followed by the two water correlations in the second part.

3.1 R-744 correlations

Each of the four correlations chosen in the literature survey will be discussed separately.

3.1.1 Thome and El Hajal (2004)

This correlation makes use of the flow pattern map as developed by Kattan-Thome-Favrat and for this study the evaporation process is divided into three regions, namely: intermittent flow, annular flow and mist flow.

This correlation, however, does not have a specific heat transfer correlation for the mist flow region and therefore the same basic equation is used in all the regions, given by:

$$h_{TE} = \frac{d\,\theta_{dry} h_{G,TE} + d\left(2\pi - \theta_{dry}\right) h_{L,TE}}{2\pi d} \tag{3.1}$$

The parameter θ_{dry} indicates the angle of dryness as shown in Figure 3.1 which is zero for the intermittent, annular and mist flow regions. The dry-angle will influence the heat transfer coefficient in the stratified and stratified wavy flow regions. However these two regions are not included in this study since they only occur at very low mass fluxes which is outside the limits of the test bench used in this study. These limits will be discussed further in Chapter 4.

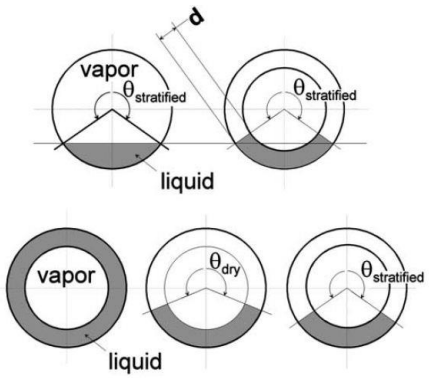

Figure 3.1 – Dry-angle and film thickness of fluid in evaporation channel (Thome & El Hajal, 2004).

For this study equation (3.1) therefore reduces to the following:

$$h_{TE} = h_{L,TE} \tag{3.2}$$

Thome and El Hajal defined the correlation for $h_{L,TE}$ in equation (3.2) as follows:

$$h_{L,TE} = \left[\left(S_{TE} h_{nb,CO_2,TE}\right)^3 + h_{cb,TE}^3\right]^{1/3} \tag{3.3}$$

The nucleate boiling heat transfer coefficient in equation (3.3) is based on the Cooper correlation excluding the surface roughness correction:

$$h_{nb,TE} = 55 p_r^{0.12} \left(-log_{10} p_r\right)^{-0.55} M^{-0.5} q^{0.67} \tag{3.4}$$

with the following modification used to improve its accuracy when applied to R-744:

$$h_{nb,CO_2,TE} = 0.71 h_{nb,TE} + 3970 \tag{3.5}$$

The convective boiling heat transfer coefficient in equation (3.3) is calculated as follows, with the term in the first bracket being the liquid film Reynolds number and the term in the second bracket the liquid Prandtl number:

$$h_{cb,TE} = 0.0133 \left(\frac{4\dot{m}(1-x)\delta}{(1-\varepsilon)\mu_L}\right)^{0.69} \left(\frac{c_{pL}\mu_L}{k_L}\right)^{0.4} \frac{k_L}{\delta} \tag{3.6}$$

The vapour void fraction in equation (3.6) is determined with the Rouhani and Axelsson drift flux model:

$$\varepsilon = \frac{x}{\rho_G}\left(\left(1 + 0.12(1-x)\right)\left(\frac{x}{\rho_G} + \frac{1-x}{\rho_L}\right) + \frac{1.18}{\dot{m}}\left(\frac{g\sigma(\rho_L - \rho_G)}{\rho_L^2}\right)^{\frac{1}{4}}(1-x)\right)^{-1} \tag{3.7}$$

The boiling suppression factor in equation (3.3) is defined as follows:

$$S_{TE} = \frac{(1-x)^{\frac{1}{2}}}{0.121 Re_L^{0.225}} \tag{3.8}$$

3.1.2 Yoon et al. (2004)

As discussed in Chapter 2, Yoon *et al.* (2004) developed an equation to determine the critical point during evaporation. This is the point where dry-out starts to occur at the top of the channel and is given by:

$$x_{crit,Y} = 0.0012Re_L^{2.79}(1000Bo)^{1.640.06}Bd^{-4.76} \tag{3.9}$$

For the region $x < x_{crit,Y}$ Yoon *et al.* proposed that the heat transfer mechanism be similar to the existing correlations for annular flow. Yoon *et al.* used Liu and Winterton's (1991) correlation but modified the coefficients to improve the accuracy according to their experimental data. The following equation is used to calculate the two-phase heat transfer coefficient:

$$h_Y = ((S_Y h_{nb,Y})^2 + (E_Y h_{cb,Y})^2)^{\frac{1}{2}} \tag{3.10}$$

The nucleate pool boiling heat transfer coefficient in equation (3.10) is calculated using Cooper's pool boiling correlation:

$$h_{nb,Y} = 55p_r^{0.12}(-log_{10}p_r)^{-0.55}M^{-0.5}q^{0.67} \tag{3.11}$$

The suppression factor (S_Y) is used to account for the smaller effect that the nucleate pool boiling heat transfer mechanism has in this area. The following equation is proposed to calculate the suppression factor in equation (3.10):

$$S_Y = \frac{1}{1 + 1.62 \times 10^{-6}E_Y^{0.69}Re_L^{1.11}} \tag{3.12}$$

As can be seen from equation (3.12) the suppression factor (S_Y) is a function of the enhancement factor (E_Y), which is used to account for the larger effect of the forced convective heat transfer mechanism in this area. The following equation is proposed to calculate the enhancement factor in equation (3.12):

$$E_Y = \left(1 + 9.36 \times 10^3 xPr_L\left(\frac{\rho_L}{\rho_G} - 1\right)\right)^{0.11} \tag{3.13}$$

The forced convective heat transfer coefficient in equation (3.10) is calculated using the Dittus-Boelter equation:

$$h_{cb,Y} = 0.023 \frac{k_L}{d} Re_L^{0.8} Pr_L^{0.4} \tag{3.14}$$

For the area where $x > x_{crit,Y}$ the two-phase heat transfer coefficient is calculated as a superposition of the heat transfer coefficient for the liquid and vapour flows respectively. The dry angle (θ_{dry}) is the weighting factor as shown in the following equation:

$$h_Y = \frac{\theta_{dry} h_{G,Y} + (2\pi - \theta_{dry}) h_{L,Y}}{2\pi} \tag{3.15}$$

The heat transfer coefficient for the vapour ($h_{G,Y}$) is again calculated using the Dittus-Boelter equation similar to equation (3.14) however with the vapour conditions. The heat transfer coefficient for the wetted area of the tube ($h_{L,Y}$) is calculated using the Gungor and Winterton (1987) correlation as follows:

$$h_{L,Y} = E_Y \times h_L \tag{3.16}$$

Where h_L is also calculated with the Dittus-Boelter equation and E_Y is again an enhancement factor, for this section it is calculated with the following equation:

$$E_Y = 1 + 3000 Bo^{0.86} + 1.12 \left(\frac{x}{1-x}\right)^{0.75} \left(\frac{\rho_L}{\rho_G}\right)^{0.41} \tag{3.17}$$

The dry angle (θ_{dry}) is used to give an indication of the portion of the tube which is wetted and the portion which is dry as indicated in Figure 3.1. Since the dry angle is dependent on the flow pattern of R-744, the equation is a function of dimensionless numbers (Reynolds number, boiling number and Bond number). The Martinelli parameter is also used since the "dry" area increases as the quality increases. The equation used to calculate the dry angle in equation (3.15) is:

$$\frac{\theta_{dry}}{2\pi} = 36.23 Re^{3.47} Bo^{4.84} Bd^{-0.27} \left(\frac{1}{X}\right)^{2.6} \tag{3.18}$$

3.1.3 Cheng et al. (2008b)

This correlation uses a flow pattern map which predicts the flow pattern at specific flow conditions with an associated heat transfer coefficient for that area. For this study the evaporation will be divided into four flow patterns according to the quality, namely: intermittent flow, annular flow, dry-out region, and mist flow.

Three equations are used to determine the three quality boundaries, with the boundary between intermittent and annular flow given by:

$$x_{IA} = \left(1.8^{1/0.875} \left(\frac{\rho_G}{\rho_L}\right)^{\frac{-1}{1.75}} \left(\frac{\mu_L}{\mu_G}\right)^{\frac{-1}{7}} + 1 \right)^{-1} \tag{3.19}$$

The boundary between annular flow and the dry-out region (dry-out inception) is given by:

$$x_{di} = 0.58e^{\left(0.52-0.236We_G^{0.17}Fr_{G,Mori}^{0.17}\left(\frac{\rho_G}{\rho_L}\right)^{0.25}\left(\frac{q}{q_{crit,C}}\right)^{0.27}\right)} \tag{3.20}$$

The equation for dry-out completion is given by:

$$x_{de} = 0.61e^{(0.57-0.502We_g^{0.16}Fr_{G,Mori}^{0.15}(\frac{\rho_G}{\rho_L})^{-0.09}(\frac{q}{q_{crit,C}})^{0.72})} \tag{3.21}$$

In equation (3.20) and equation (3.21) the vapour Weber number and the vapour Froude number are as defined by Mori *et al.* (2000) and calculated as follows:

$$We_G = \frac{\dot{m}^2 D_{eq}}{\rho_G \sigma} \tag{3.22}$$

$$Fr_{G,Mori} = \frac{\dot{m}^2}{\rho_G(\rho_L - \rho_G)gD_{eq}} \tag{3.23}$$

The critical heat flux ($q_{crit,C}$) in equation (3.20) and equation (3.21) is calculated with the Kutateladze correlation (Kutateladze, 1948):

$$q_{crit,C} = 0.131\rho_G^{0.5}h_{LG}\big(g\sigma(\rho_L - \rho_G)\big)^{0.25} \tag{3.24}$$

Each of the four local flow boiling heat transfer coefficients for these respective areas will now be discussed with the general equation being:

$$h_C = \frac{\theta_{dry}h_{G,C} + (2\pi - \theta_{dry})h_{L,C}}{2\pi} \tag{3.25}$$

- <u>Intermittent flow</u>

For this flow pattern the dry angle (θ_{dry}) equals zero due to the whole tube perimeter being wet. Therefore the general equation as shown in equation (3.25) reduces to $h_C = h_{L,C}$. Where $h_{L,C}$ is calculated with an asymptotic model which combines the nucleate boiling and

convective boiling heat transfer contributions by the third power, the calculation is as follows:

$$h_{L,C} = \left(\left(S_C h_{nb,C} \right)^3 + h_{cb,C}^3 \right)^{1/3} \tag{3.26}$$

The nucleate boiling transfer coefficient in equation (3.26) is calculated with the Cooper correlation albeit with some modification:

$$h_{nb,C} = 131 p_r^{-0.0063} (-\log_{10} p_r)^{-0.55} M^{-0.5} q^{0.58} \tag{3.27}$$

The nucleate boiling heat transfer suppression factor (S_C) in equation (3.26) equals 1 for this region. The convective boiling heat transfer coefficient ($h_{cb,C}$) in equation (3.26) is calculated as follows:

$$h_{cb,C} = 0.0133 Re_\delta^{0.69} Pr_L^{0.4} \frac{k_L}{\delta} \tag{3.28}$$

The liquid film Reynolds number in equation (3.28) is defined as:

$$Re_\delta = \frac{4\dot{m}(1-x)\delta}{\mu_L(1-\varepsilon)} \tag{3.29}$$

with ε in equation (3.29) being the void fraction which is determined by the Rouhani-Axelsson drift flux model as shown in equation (3.7). The liquid film thickness in equation (3.29) is calculated as follows:

$$\delta = \frac{D_{eq}}{2} - \sqrt{(\frac{D_{eq}}{2})^2 - \frac{2A_L}{2\pi - \theta_{dry}}} \tag{3.30}$$

- Annular flow

For this region the heat transfer coefficient is calculated in a similar way to the one for the intermittent flow region, the only difference being that the value of the suppression factor is no longer equal to 1, it' is calculated as follows:

$$S_C = 1 - 1.14 \left(\frac{D_{eq}}{0.00753} \right)^2 \left(1 - \frac{\delta}{\delta_{IA}} \right)^{2.2} \tag{3.31}$$

with D_{eq} set to 7.53 mm if $D_{eq} > 7.53$, as is the case in this study.

- Dry-out region

The heat transfer coefficient for this region is calculated with linear interpolation as defined by Wojtan *et al.* (2005a):

$$h_{dry,C} = h_C(x_{di}) - \frac{x - x_{di}}{x_{de} - x_{di}}\left(h_C(x_{di}) - h_{M,C}(x_{de})\right) \tag{3.32}$$

where $h_C(x_{di})$ is calculated with equation (3.25) at the dry-out inception quality as defined by equation (3.20). The dry-out region (θ_{dry}) increases from 0 to 2π as the quality increases from x_{di} to x_{de}, which is calculated with the following equation:

$$\begin{aligned}\theta_{dry} = 2\pi - 2\Bigg(&\pi(1-\varepsilon) \\ &+ \left(\left(\frac{3\pi}{2}\right)^{1/3}\left(1 - 2(1-\varepsilon) + (1-\varepsilon)^{1/3} - \varepsilon^{1/3}\right)\right. \\ &\left. - \frac{1}{200}(1-\varepsilon)\varepsilon\left(1 - 2(1-\varepsilon)\right)\left(1 + 4(1-\varepsilon)^2 + \varepsilon^2\right)\right)\Bigg)\end{aligned} \tag{3.33}$$

The vapour phase heat transfer coefficient ($h_{G,C}$) as shown in equation (3.25) is calculated with the Dittus-Boelter correlation:

$$h_{G,C} = 0.023 Re_G^{0.8} Pr_G^{0.4} \frac{k_G}{D_{eq}} \tag{3.34}$$

with the vapour Reynolds number in equation (3.34) defined as:

$$Re_G = \frac{\dot{m} x D_{eq}}{\mu_G \varepsilon} \tag{3.35}$$

The heat transfer coefficient on the wet perimeter is calculated in the same way as for the annular flow with the quality set to x_{di}. Similarly $h_{M,C}(x_{de})$ in equation (3.32) is calculated with the mist flow heat transfer correlation shown below in equation (3.36) at the dry-out completion quality as defined by equation (3.21).

- Mist flow

For the mist flow region the heat transfer coefficient is calculated with the Groeneveld correlation with some modification to improve the accuracy for R-744:

$$h_{M,C} = 2 \times 10^{-8} Re_H^{1.97} Pr_G^{1.06} {Y_C}^{-1.83} \frac{k_G}{D_{eq}} \tag{3.36}$$

where the homogeneous Reynolds number in equation (3.36) is calculated with:

$$Re_H = \frac{\dot{m} D_{eq}}{\mu_G} (x + \frac{\rho_G}{\rho_L}(1 - x)) \tag{3.37}$$

The correction factor (Y_C) in equation (3.36) is defined by:

$$Y_C = 1 - 0.1((\frac{\rho_L}{\rho_G} - 1)(1 - x))^{0.4} \tag{3.38}$$

3.1.4 Pamitran et al. (2011)

Pamitran *et al.* (2011) used the following equation to calculate the two-phase heat transfer coefficients which is a superposition of the nucleate boiling and forced convective evaporation heat transfer coefficients:

$$h_P = F_P h_{L,P} + S_P h_{nb,P} \tag{3.39}$$

Due to the influence of different flow conditions (laminar or turbulent), Zhang *et al.* (2004) proposed a multiplier factor (F_P) which is a function of the Reynolds number and a two-phase frictional multiplier (ϕ_f^2). The general equation for this multiplier is as follows:

$$\phi_f^2 = 1 + \frac{C}{X} + \frac{1}{X^2} \tag{3.40}$$

where C is the Chisholm parameter, the value of which depends on the respective liquid-vapour flow conditions as indicated below:

- Both liquid and vapour are turbulent then $C = 20$.
- Liquid laminar and vapour turbulent then $C = 12$.
- Liquid turbulent and vapour laminar then $C = 10$.
- Both liquid and vapour are laminar then $C = 5$.

The Martinelli parameter (X) in equation (3.40) is calculated with:

$$X = \left(\frac{f_L}{f_G}\right)^{\frac{1}{2}} \left(\frac{1-x}{x}\right) \left(\frac{\rho_G}{\rho_L}\right)^{\frac{1}{2}} \tag{3.41}$$

The value of the two friction factors depends on whether the flow is turbulent or laminar for liquid and vapour respectively. The following equations are used:

$$f = 16Re^{-1} \text{ for } Re < 2300 \text{ (laminar flow)} \tag{3.42}$$

$$f = 0.079Re^{-0.25} \text{ for } Re > 3000 \text{ (turbulent flow)} \tag{3.43}$$

For the liquid friction factor (f_L), the liquid Reynolds number (Re_L) is used and for the vapour friction factor (f_G) the vapour Reynolds number (Re_G) is used. The liquid heat transfer coefficient in equation (3.39) is calculated with the Dittus-Boelter equation as shown below:

$$h_{L,P} = 0.023 \frac{k_L}{d} \left(\frac{\dot{m}(1-x)d}{\mu_L}\right)^{0.8} \left(\frac{c_{pL}\mu_L}{k_L}\right)^{0.4} \tag{3.44}$$

The convective two-phase multiplier (F_P) in equation (3.39) cannot be smaller than 1 and is therefore calculated as follows:

$$F_P = Max\left[\left(0.009(\phi_f^2)^2 + 0.76\right), 1\right] \tag{3.45}$$

The nucleate pool boiling heat transfer coefficient ($h_{nb,P}$) in equation (3.39) is calculated with the Cooper correlation which is given by the following equation, where a surface roughness of 1.0 μm is assumed:

$$h_{nb,P} = 55p_r^{0.12}(-0.4343log_{10}p_r)^{-0.55}M^{-0.5}q^{0.67} \tag{3.46}$$

The same surface roughness is assumed in this study due to similar materials being used. The nucleate pool boiling suppression factor (S_P) in equation (3.39) is calculated by:

$$S_P = C_{ref}(\phi_f^2)^{-0.2093}Bo^{0.7402} \tag{3.47}$$

In the case of R-744 being the working fluid, C_{ref} has a value of 0.25.

3.2 Water correlations

In this section the theory behind the heat transfer correlations for water will be discussed. Both these correlations were used since the Dittus-Boelter is well known and relatively simple to use, whereas Gnielinski is somewhat more complex but has an higher accuracy.

3.2.1 Dittus-Boelter (1930)

The Dittus-Boelter equation (Dittus & Boelter, 1930) in its most well-known form is as follows:

$$Nu_D = 0.023 Re_D^{4/5} Pr^n \tag{3.48}$$

with n given by the following equations:

$$n = 0.4 \text{ if } T_s > T_m \tag{3.49}$$

$$n = 0.3 \text{ if } T_s < T_m \tag{3.50}$$

T_s is referring to the temperature measured at the channel wall; and T_m referring to the temperature of the bulk fluid.

3.2.2 Gnielinski (1975)

The equation for the Nusselt number as proposed by Gnielinski (1975) is given by:

$$Nu_D = \frac{\left(\frac{f}{8}\right)(Re_D - 1000)Pr}{1 + 12.7\left(\frac{f}{8}\right)^{1/2}(Pr^{2/3} - 1)} \tag{3.51}$$

where the friction factor (f) is determined from the Moody diagram.

3.3 Chapter Summary

In Chapter 3 the theory describing each of the correlations chosen from literature was discussed. This includes the four flow boiling heat transfer correlations for R-744 as well as the two Nusselt number correlations for water. These equations will form the basis of the Engineering Equation Solver (EES) software program used to compare the theoretical heat transfer coefficients against the experimental data. The EES program will be discussed in

Chapter 6. In Chapter 4 the experimental setup will be discussed as well as the experimental procedure followed to generate the data for this study.

Chapter 4 – Experimental setup

In this chapter the layout of the existing test bench will be discussed along with the extensive upgrades made to obtain the results required for evaluating the different correlations. The test bench consists of a trans-critical heat pump cycle with two secondary water loops which are used for cooling and heating of the two heat exchangers. In the first part of this chapter the physical layout will be discussed, after which the focus will shift to the data acquisition system, and finally the test procedure will be discussed.

4.1 Test bench physical layout

The test bench can be divided into three independent closed circuit loops, each with its own working fluid as shown in Figure 4.1 with the primary circuit being the R-744 vapour compression cycle, and the two secondary circuits being water cycles. These two secondary cycles have the sole purpose of exchanging heat with the R-744 in the heat exchangers.

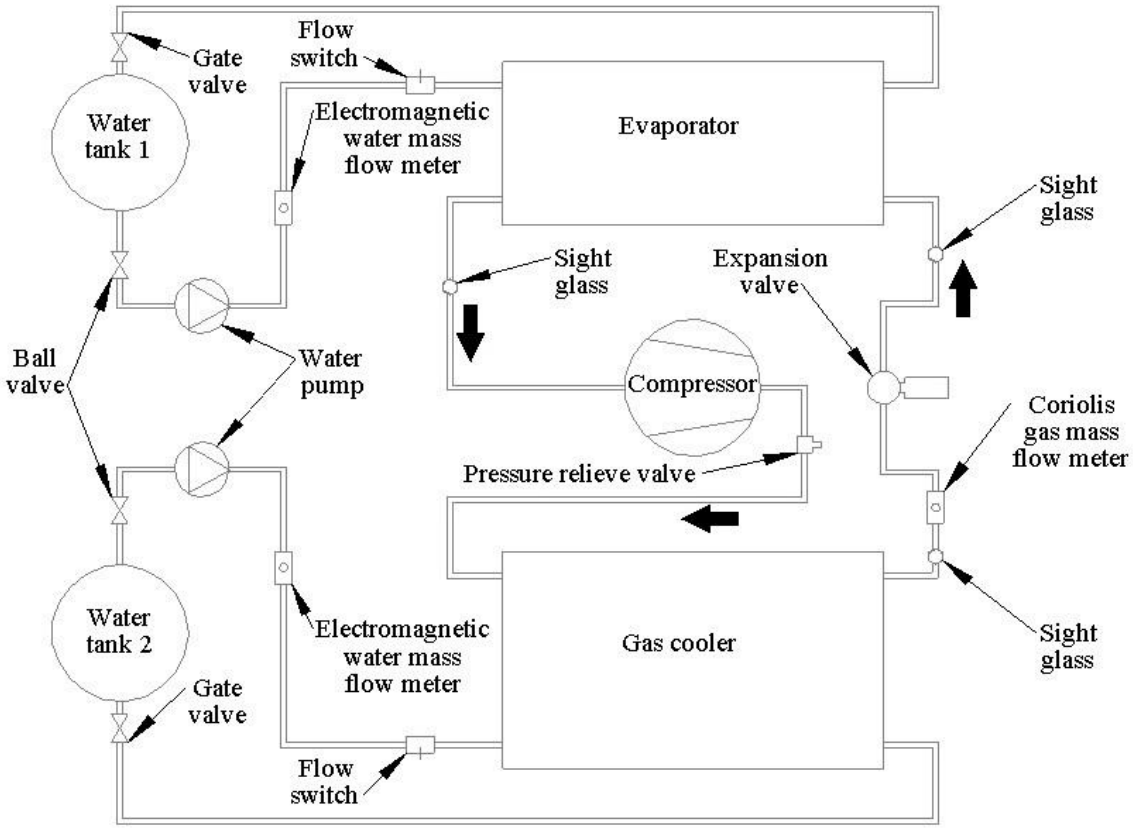

Figure 4.1 – Flow schematic of test bench.

The two water cycles are identical and each consists of a 5000 litre holding tank, a 0.75 kW circulation pump, a flow switch and a manual flow control valve. The flow switch functions as a safety precaution, preventing the compressor from starting unless the water is circulating through the cycle. The size of the holding tanks ensures that tests can be conducted over a long period of time without water temperatures being affected.

The R-744 vapour compression cycle consists of an evaporator, compressor, gas cooler and expansion valve. Each of these components will be briefly discussed with the main focus of this study being the evaporator. In Figure 4.2 the test bench (excluding the water holding tanks) is shown.

Figure 4.2 – Experimental test bench.

4.1.1 Evaporator

The evaporator consists of a tube-in-tube counter flow configuration with R-744 flowing through the inner tube and water through the annulus. The evaporator consists of eight tube-in-tube sections stacked vertically and connected with well insulated independent links where no heat transfer occurs. A schematic diagram of one of these sections is shown in Figure 4.3.

Figure 4.3 – Counter flow diagram of heat exchangers.

The inner channel consists of a schedule 40 stainless steel seamless tube with an inner diameter of 15.7 mm and an outer diameter of 24.2 mm due to the high operating pressures (maximum 120 Bar) it needs to withstand. The outer channel consists of copper pipe with an inner diameter of 26 mm and an outer diameter of 28 mm. Each section is two meters in length with the total length of the evaporator being 16 meters.

Each of the eight sections is well insulated over the outer tube to minimize the effect of heat transfer loss to or gain from the ambient air. The insulation used consists of low density foam with a reflective aluminium tape cladding. The R-744 inlet of the evaporator is connected to the expansion valve via schedule 40 stainless steel piping, and the outlet with the same material to the compressor inlet.

The water inlet is connected via copper tubing to the outlet of the circulation pump which in turn feeds from water tank 1 in Figure 4.1. The inlet to the pump is fitted with a ball valve whereas the water outlet of the evaporator is fitted with a gate valve. This gate valve is used to throttle the pump and allows for manual control of the water flow rate circulation through the evaporator.

4.1.2 Compressor

The compressor used is a Bitzer 4JTC-15K semi-hermetic reciprocating compressor specifically designed to compress R-744. The compressor is capable of delivering a maximum pressure of 130 Bar with a fluid displacement of 9.2 m^3/h. As a safety precaution the R-744 cycle is fitted with a pressure release valve which prevents the system pressure from exceeding 120 Bar.

The compressor rotation speed is controlled with a variable speed drive (VSD) allowing the 3-phase electric motor to operate at different frequencies. The Danfoss VSD used is sized according to the compressor specifications and allows the R-744 mass flow to be varied during testing.

The compressor is only suitable for the compression of super-heated vapour and can be damaged if liquid or a two-phase mixture enters the compression chamber. This is ensured by the design of the evaporator to obtain adequate heat exchange. Additionally a sight glass was fitted on the outlet of the evaporator to visually verify that no liquid enters the compressor.

4.1.3 Gas cooler

The gas cooler configuration is similar to that of the evaporator with the only exemption being that it consists of 12 sections of tube-in-tube heat exchangers instead of eight. The R-744 outlet is connected to the expansion valve inlet and the inlet connected to the compressor outlet. The water cycle is identical to the evaporator water cycle as discussed in section 4.1.1.

4.1.4 Expansion valve

The expansion valve allows the high pressure fluid (R-744) flowing from the gas cooler to expand to a low pressure. The typical pressure drop is from 120 Bar to 30 Bar. During this process the R-744 enthalpy remains constant. An electronic Danfoss valve was installed in conjunction with a controller and pressure sensor by which the valve is automatically controlled to ensure a constant evaporator pressure. During the testing phase of this study the expansion valve was manually operated to ensure the test conditions did not change over time.

4.2 Data acquisition

Along with the test bench as described in the preceding section, instrumentation was installed to complete the experimental setup. The data acquisition system consists of various measuring instruments as well as a data logger with the ability to display in real time. The variables logged include temperatures, pressures, R-744 mass flow rate and water volumetric flow rate.

The data logger digitally captures data from all of the instruments in 5 minute intervals. The positions of the temperature and pressure measurement equipment for the evaporator are shown in Figure 4.4, with the positions of the three flow meters shown in Figure 4.1.

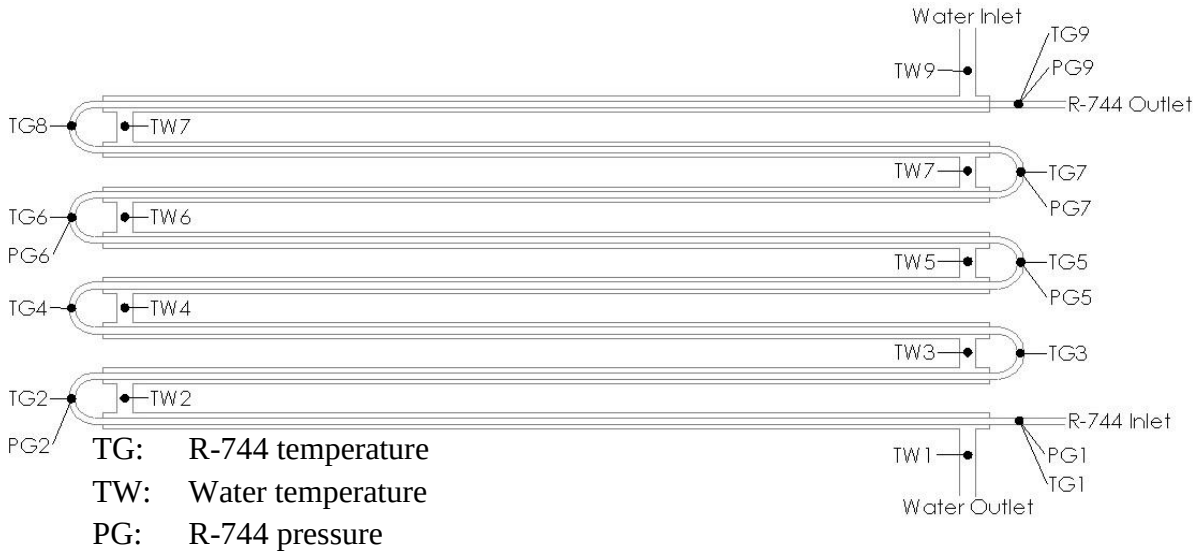

Figure 4.4 – Temperature and pressure measurement points for the evaporator.

The inlet and outlet temperatures for each heat exchanger section are measured in the linkage pipes between sections, for both the R-744 and water cycles. The pressures for the R-744 cycle are also measured at specific links as indicated. The flow rates for each cycle are measured with in-line instruments located on the respective inlet pipes. These instruments will be briefly discussed in the following sections.

4.2.1 Temperature sensors

Temperatures on both the R-744 and water sides are measured with two-wire PT 1000 sensors, although two different models were used. Danfoss AKS 12 sensors were only used on the water side and MBT 3270 sensors were mainly used on the R-744 side and on two instances for the water side. The sensors are inserted into the fluid thus measuring the fluid temperature directly using the prescribed process connection of the supplier to connect these sensors to the heat exchanger. The rated accuracy of both types of sensors is $\pm(0.3 + 0.005T)$ with T being the fluid temperature. This equates to ± 0.425℃ for a fluid at 25℃.

4.2.2 Pressure transmitters

Danfoss AKS 2050 pressure transmitters were used to measure the R-744 pressures. Two different pressure range sensors were used, namely -1 to 159 Bar and -1 to 99 Bar. The lower range type was used for the evaporator cycle.

These sensors are ratiometric pressure transmitters, meaning the output voltage signal is a function of the pressure and the input voltage. These transmitters have a maximum operating temperature of 85°C and were therefore positioned on "pigtails" to protect them against the

effects of high temperatures. The accuracy of these transmitters is ±0.3% x *FS* with *FS* being the full range of each transmitter. This equates to ±0.3 Bar for the low range transmitters and 0.48 Bar for the high range transmitters.

4.2.3 Flow meters

Two types of flow meters were used to measure the mass flow of the water cycles and the R-744 respectively. For the two water cycles Promag electromagnetic flow meters from Endress+Hauser were used. The measuring principle of this instrument is based on a voltage being induced by an electrically conductive fluid flowing through a magnetic field. Hereby the flow velocity is measured and since the fluid is incompressible, the mass flow can be calculated accordingly.

Since R-744 is a compressible fluid, a coriolis mass flow meter was used. The Proline meter from Endress+Hauser makes use of two tubes which oscillate in-phase when there is no flow through them. When a fluid flows through these tubes the oscillation of the tubes at the inlet decelerates and at the outlet accelerates. The phase difference between the inlet and outlet increases as the mass flow increases and electrodynamic sensors are used to measure this change and are then converted to a mass flow reading.

The accuracy of the Promag electromagnetic flow meter is 0.5% ± 1 mm/s of reading. The accuracy of the Proline coriolis flow meter is 0.5% ± ((0.1 ÷ *measured value*) x 100)% which equates to 0.527% with a mass flow of 360 kg/h or 360 ± 1.9 kg/h.

4.2.4 Data logging

The instruments described above combined gives a total of 59 measured data points for the total test bench including the gas cooler. Data was logged in 5-second intervals during tests using a Danfoss AK-CS controller unit. This unit was used in conjunction with AK-CM communication modules and AK2-XM analogue input modules. Data was exported from the controller to Microsoft Excel® for further analysis and storage.

4.3 Experimental tests

4.3.1 Test setup

The aim of the experimental tests was to create a new database with similar ranges to those from which each correlation was developed, as was shown in Table 2.1. The values of these

parameters (mass flux, heat flux and saturation temperature) are directly dependent on the data points measured on the test bench. In order to ensure that the database consists of as a wide a range of data points as possible, no limits were placed on the test ranges, apart from those required by the test bench itself to prevent pressures above 120 Bar and water temperatures below freezing-point. Each data set in the database corresponds to one heat exchanger element as shown in Figure 4.3 and Figure 4.4 with the following measured data points:

- R-744 inlet temperature.
- R-744 inlet pressure.
- R-744 outlet temperature.
- R-744 outlet pressure.
- R-744 mass flow rate.
- Water inlet temperature.
- Water outlet temperature.
- Water mass flow rate.

Due to pressure transmitters not being available on every linkage pipe, an average pressure was calculated at some points between the preceding and the following data point.

Since the test bench itself is an operational closed cycle heat pump it is not possible to control the measured values independently and any intended change to one will affect the others as well. The following can, however, be controlled directly on the test bench:

- Mass flow of the R-744 cycle – by controlling the rotation speed of the compressor with the VSD.
- Mass flow of the two water cycles – by controlling the pump flow with the gate valve on the heat exchanger outlet.
- The evaporator pressure – by changing the degree of opening of the expansion valve or by changing the amount of R-744 in the system.

Preliminary tests were conducted to determine the limits of the test bench based on these controllable values:

- *Compressor speed of rotation:*

As prescribed by the manufacturer the rotational speed of the compressor is limited to a minimum of 30 Hz and a maximum of 60 Hz.

- *Evaporator water mass flow rate:*

  The maximum obtainable water flow rate is 22 l/min due to the specifications of the circulation pump and the high friction factor of the small annulus flow area. The water flow rate requires a minimum of 16 l/min to prevent the water from freezing inside the heat exchanger. This value was determined through empirical testing. The flow rate also needs to be sufficient to ensure the gas is fully superheated on entering the compressor since any liquid can cause damage to the compressor.

- *Gas cooler water mass flow rate:*

  Similarly to the evaporator the maximum water flow rate is based on the specification of the circulation pump which is 16 l/min. Although a similar pump was used as for the evaporator, the flow rate is lower because of the higher friction factor. The friction factor is higher due to the gas cooler being longer than the evaporator. The minimum flow is 8 l/min and was also determined by empirical testing. This is to ensure enough heat is removed from the R-744 to ensure the vapour quality is low after the gas has expanded through the expansion valve. A low quality at the evaporator inlet ensures that a large section of the evaporator area falls within the two-phase region which is the focus of this study.

- *Evaporator pressure:*

  The minimum evaporating pressure was determined empirically to be 25 Bar. A low evaporating pressure corresponds with a low saturation temperature which again can cause the water to freeze in the evaporator. The maximum limit for the evaporator was set at 40 Bar due to safety concerns regarding the corresponding high gas cooler pressure. A gas pressure above 120 Bar will cause the pressure release valve to open and discharge R-744 gas to the atmosphere.

In Table 4.1 below the limits as mentioned above are summarised:

Table 4.1 – Limits of the test bench.

Limit	Maximum	Minimum	Units
Compressor rotation speed	60	30	Hz
Evaporator - water flow rate	22	16	l/min
Gas Cooler - water flow rate	16	8	l/min
Evaporating pressure	40	25	Bar

With these limits in mind tests were conducted over the following intervals.

- Compressor speed: 40; 50; 60 Hz
- Evaporator water flow rate: 16; 19; 22 l/min
- Gas cooler water flow rate: 8; 12; 16 l/min
- Evaporating pressure: 25; 30; 35 Bar

Tests were conducted for all possible combinations of these 12 values which resulted in 81 different tests (3^4). An additional 9 tests were possible with an evaporating pressure of 40 Bar, however at this pressure the test bench is operating close to its maximum pressure, therefore not all combinations were run at 40 Bar evaporation pressure. A further 8 tests were conducted to test the repeatability of the data. In Figure 4.5 below a schematic is shown to indicate the controlled, measured and calculated data points for each test.

During each test the working fluid were super-heated at a different physical point in the heat exchanger. Since this study is only focused on the characteristics of two-phase flow boiling, only the heat exchanger sections (pipe lengths) stream up from the point at which the fluid is superheated are considered for the database. Depending on the controlled parameters for each of the tests, the number of heat exchanger sections differs and for each section one data set consisting of 8 data points forms part of the database.

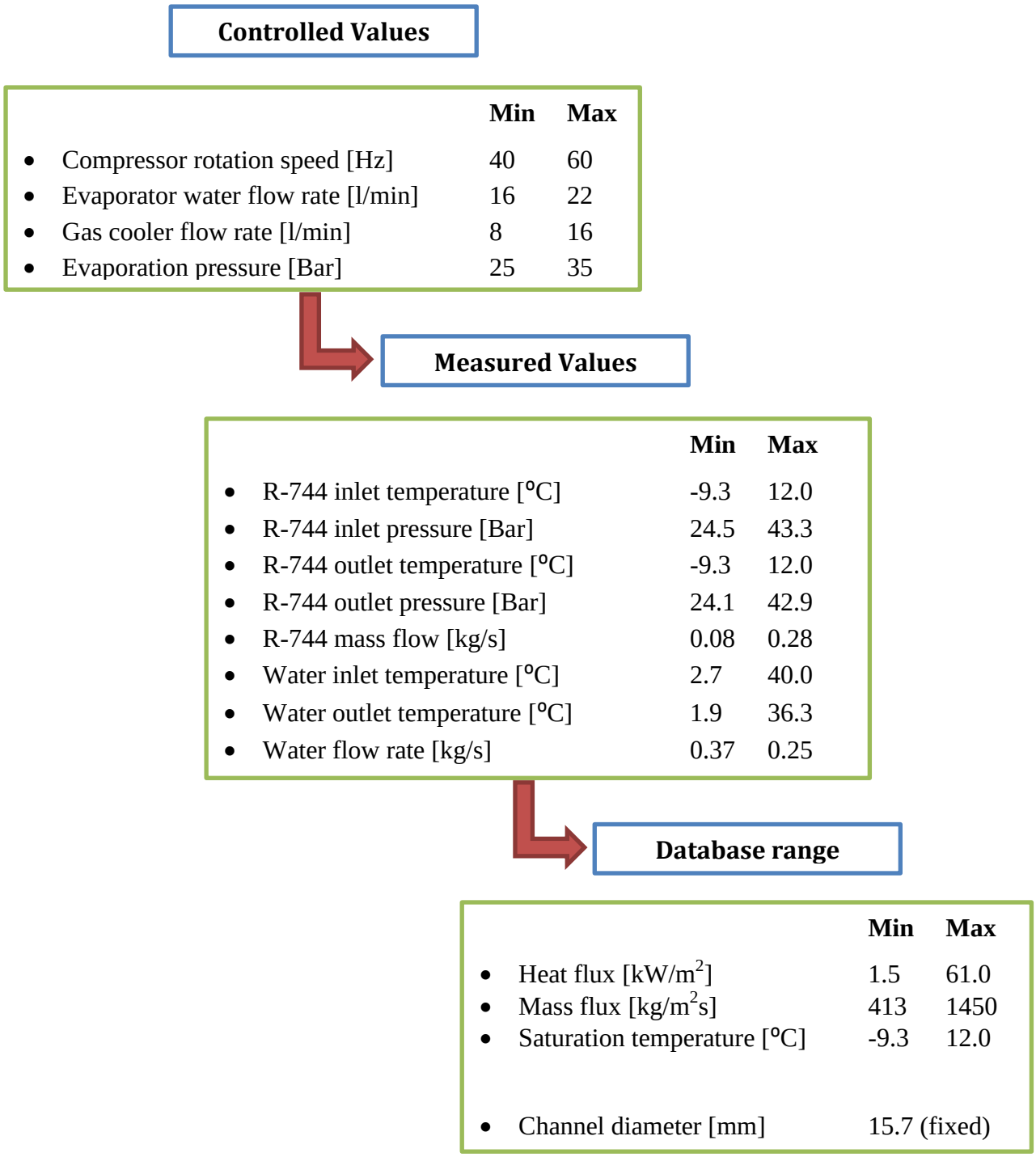

Figure 4.5 – Experimental setup.

4.3.2 Test procedure

Each of the 98 individual tests was conducted according to the following procedure:

- **Step 1**: Test bench is turned on and needs to run for a minimum of 15 minutes. During this period basic diagnostics are carried out. All sensors and transmitters are checked to ensure proper functioning. The data logging system is checked to ensure

all data is logged accurately. During this time the VSD would normally control the compressor on 40 Hz, the water mass flow rates through both cycles are 16 to 20 l/min and the expansion valve is set to an evaporation pressure of 30 Bar.

- **Step 2**: Set the four controllable values according to the requirements for the specific test as discussed in section 4.3.1 by operating the control equipment (gate valves, VSD and expansion valve).

- **Step 3**: The heat pump cycle needs to run for a further 15 minutes with regular checks to ensure the set points stay constant. If needed, adjustments are made to the above-mentioned control equipment.

- **Step 4**: The test phase starts once steady state is reached, with the cycle again running for a minimum of 15 minutes without interruption. During this time no changes are made to the control equipment mentioned in Step 2. This is done to ensure that no external factors affect the test data.

- **Step 5**: Once a specific test has been completed the process is repeated from Step 2 for the next test condition.

- **Step 6**: Once all tests have been completed the test bench needs to run for another 15 minutes with the settings as discussed in Step 1.

- **Step 7**: All data is exported from the controller to a PC and using a standard data template the data is stored for further analysis. Graphs are automatically generated by the template and these are checked for any deviations.

4.4 Chapter summary

In Chapter 4 the test bench layout was discussed with an overview on each of the main components. In the second part the data acquisition system was discussed showing the instruments used as well as the accuracy thereof. The impact of these accuracies will be discussed further in the next two chapters. In the final section the test setup and procedure were discussed showing which values were controlled and the individual ranges of each. Also shown were the ranges of the experimental database which will be used in this study. In Chapter 5 the results of these tests and the final database will be discussed.

Chapter 5 – Experimental results

In Chapter 5 the data generated from the tests as discussed in Chapter 4 will be shown and analysed. The first section will show a typical data report for each of the tests conducted from which the selection of a representative steady state was chosen. The uncertainty of this data will be shown in the second section. In the final section the data acquisition system is analysed with regards to energy balances in the heat exchanger and the repeatability of the data.

5.1 Database

The test procedure described in section 4.3.2 was applied to each of the 98 combinations of input variables as described in section 4.3.1, during which the 59 data points were logged in 5-second intervals. These 59 data points include all the instrumentation installed on the gas cooler which will be mostly excluded from this study. The logged data was exported to a data template from which graphs were automatically generated to determine when steady state was reached. At least 15 minutes of steady state data was logged per test as is indicated in the following four graphs:

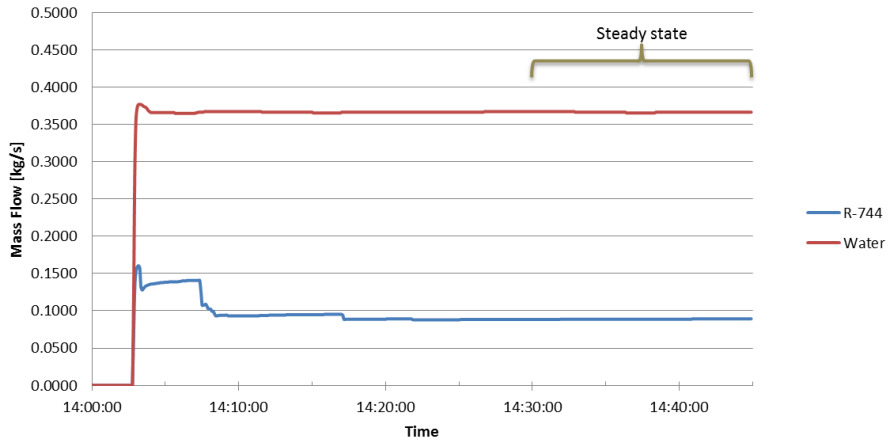

Figure 5.1 – Example of mass flow data as logged for one test.

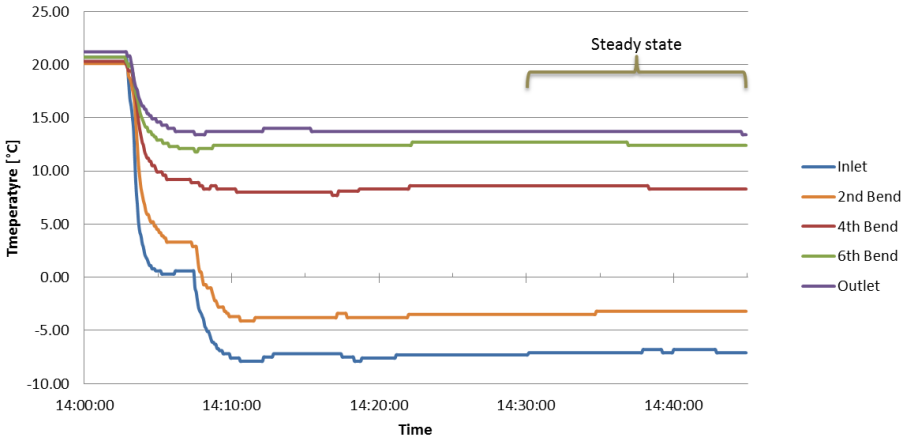

Figure 5.2 – Example of evaporator R-744 temperature as logged for one test.

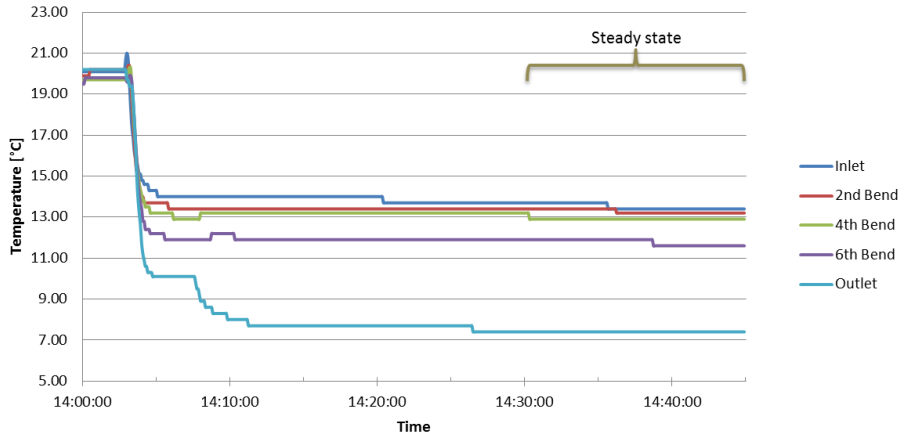

Figure 5.3 – Example of evaporator water temperature data as logged for one test.

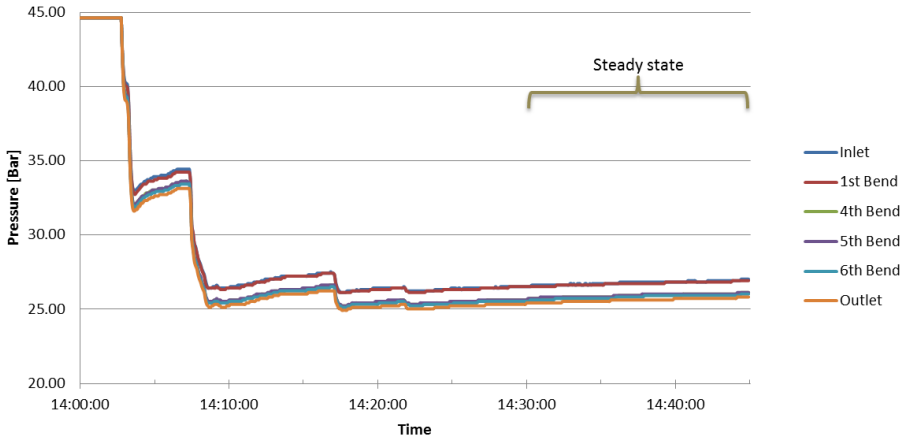

Figure 5.4 – Example of evaporator R-744 pressure data as logged for one test.

For each of the 98 tests conducted a data set was selected from the period during which steady state was obtained. The selection was made by calculating the average of 10 five-

second interval data points. From the database, only the following data points are required for this study:

- 9 x R-744 temperatures.
- 9 x Water temperatures.
- 6 x R-744 pressure.
- Evaporator water mass flow rate.
- Gas mass flow rate.
- Gas cooler outlet pressure and temperature.

Each data set is further divided into eight sections corresponding to the eight pipe sections in the heat exchanger. With the mass flow for water and R-744 being constant throughout the heat exchanger, a total of 784 complete data sets were obtained with each set consisting of the following:

- R-744 inlet temperature.
- R-744 inlet pressure.
- R-744 outlet temperature.
- R-744 outlet pressure.
- Water inlet temperature.
- Water outlet temperature.
- R-744 mass flow rate.
- Water mass flow rate.

From observing the R-744 temperature profile throughout the heat-exchanger it is clear in which pipe section R-744 reach the superheated region. The heat exchanger sections where the gas is in the superheated region falls outside of the scope of this study as stated in Chapter 1 and was therefore excluded from the database. This reduces the number of data sets to a total of 339, which will be used as the experimental database for the remainder of this study.

5.2 Data accuracy

In this section the accuracy of the data logged during each test will be shown. The accuracy of each of the instruments as mentioned in section 4.2 is as follow:

- Coriolis flow meter: $\pm 0.5\% \pm ((0.1 \div \textit{measured value}) \times 100)\%$

- Electromagnetic flow meter: ± 0.5% ± 1
- Temperature sensor: ± (0.3 + 0.05*T*)
- Pressure transmitter: ± 0.3% *Full Span*

The data acquisition system also includes the logging device which is the AK-CS logger that also influences the data accuracy. Both the temperature and pressure transmitters have a pre-set logging interface with the controller. However, for the flow meters three new interfaces needed to be created on the controller.

In Figure 5.5 the accuracy of the coriolis flow meter is shown for the corresponding steady state period shown in Figure 5.1. In this graph the error bars indicate the uncertainty due to the inaccuracy of the flow meter as mentioned above. From this graph it can be seen that the logging device (AK-CS Controller) logs changes in data of ±0.0005 kg/s (blue line) whereas the accuracy of the flow meter in this case is ±0.00047 kg/s (error bars). Therefore the accuracy of the instrument is higher than the accuracy of the logging device.

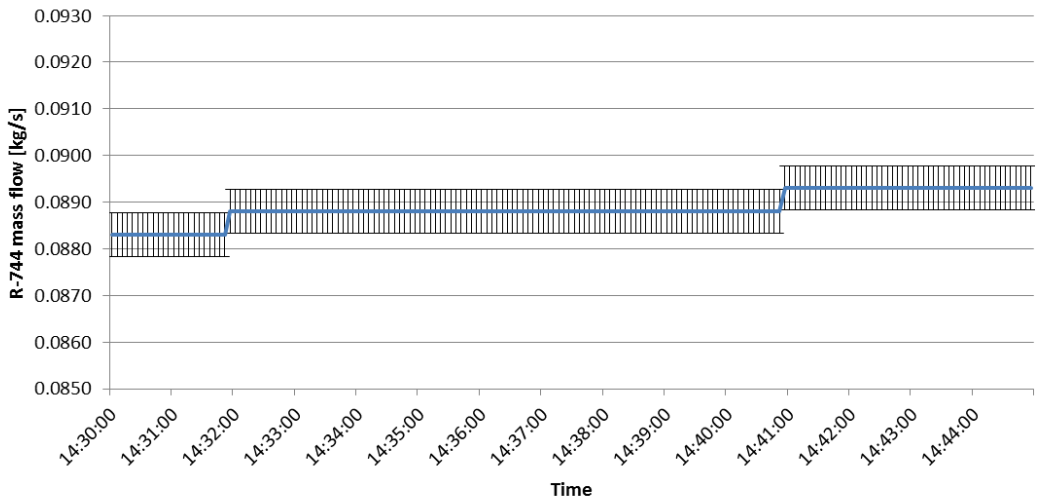

Figure 5.5 – Accuracy of data as logged by the coriolis flow meter.

The accuracy of the logging device will therefore determine the accuracy of the data logged. Similarly the accuracy of the electromagnetic flow meter is shown in Figure 5.6. In this case the flow meter accuracy is approximately ±0.0019 kg/s with the logging device registering changes in increments of ±0.0005 kg/s. Therefore the accuracy of the instrument is lower than the accuracy of the logging device and will hence determine the accuracy of the logged data.

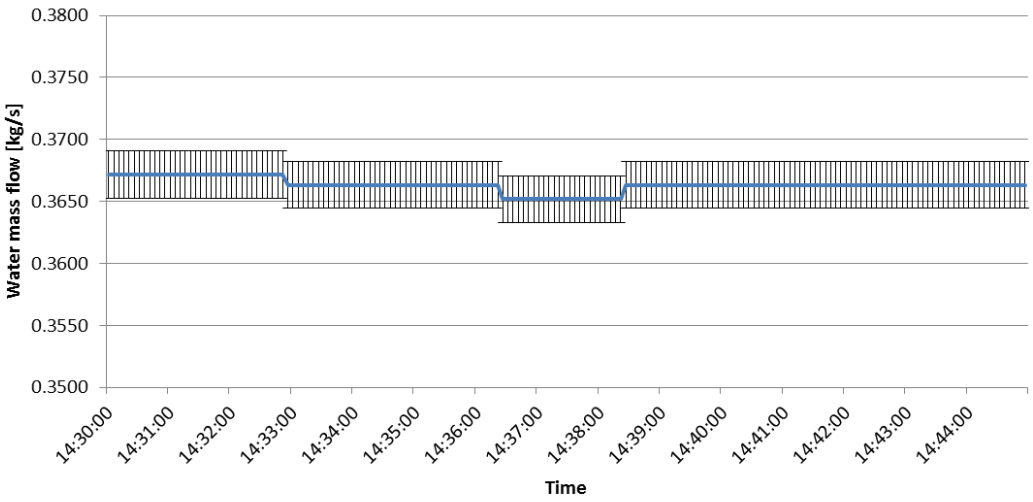

Figure 5.6 – Accuracy of data as logged by the electromagnetic flow meter.

In Figure 5.7 the accuracy of the three temperature sensors are shown indicating the temperature increase of R-744 as it flows through the evaporator (only three shown to simplify graph). This data corresponds to the steady state section shown in Figure 5.1. Due to the pre-set logging interface used for the temperature transmitters, the controller records changes in readings of ±0.3°C. The temperature sensor accuracy in this case is ±0.34°C for the fourth bend reading, however for some data it is below ±0.3°C depending on the specific reading. Therefore the highest possible accuracy obtainable is ±0.3°C due to the equipment being used.

Similarly the pressure transmitters also use a pre-set logging interface with the controller, with data from three instruments shown in Figure 5.8 (only three shown to simplify graph). However the logging device records changes in data of ± 0.1 Bar compared to the transmitter accuracy of ± 0.3 Bar. Therefore unlike the temperature transmitters, the accuracy of the pressure data points is determined by the accuracy of the instrument.

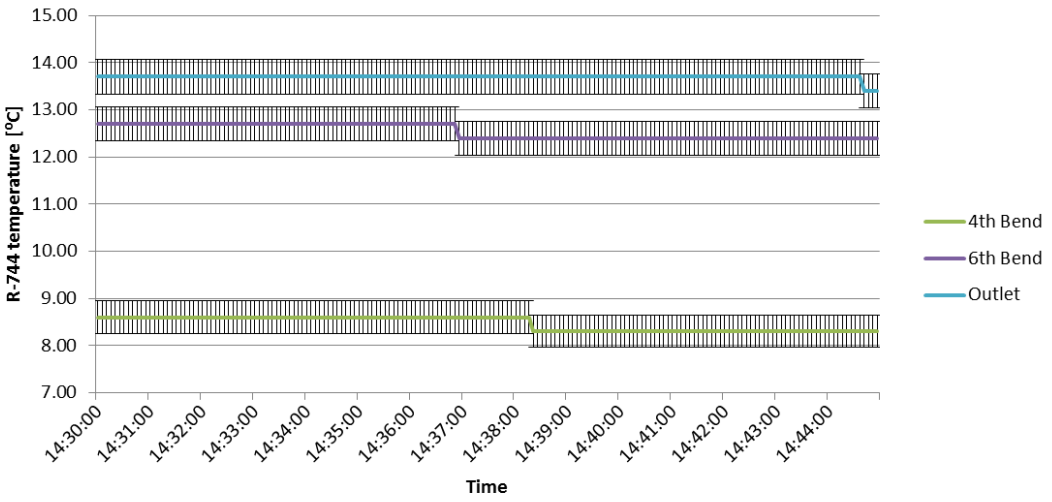

Figure 5.7 – Accuracy of data as logged by the temperature transmitters.

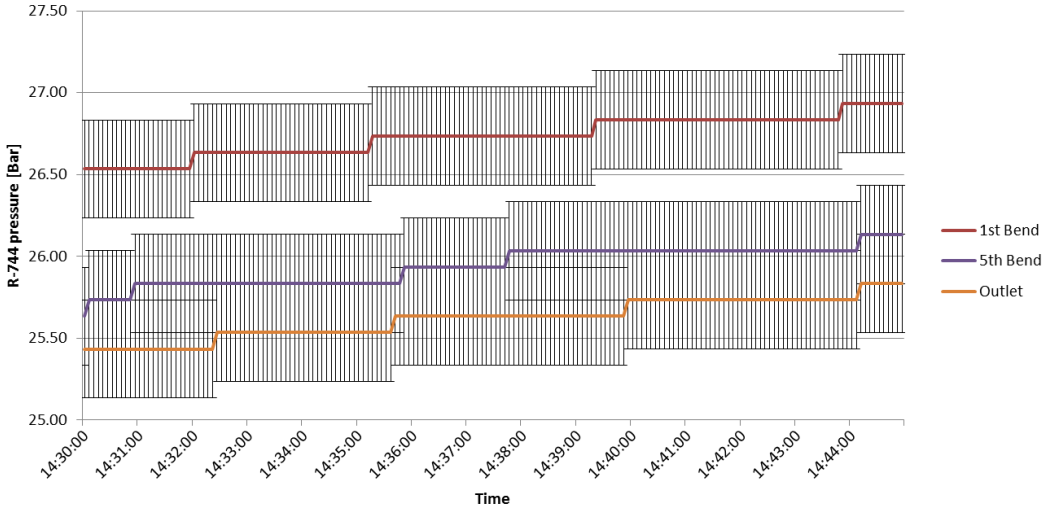

Figure 5.8 – Accuracy of data as logged by the pressure transmitters.

As mentioned in section 4.2.2 each pressure transmitter gives an output voltage as signal to the controller which is a factor of the pressure inside the channel as well as the input voltage to the transmitter. The input voltage needs to be manually selected for the controller and is assumed by the controller to be constant. Through individual testing it was discovered that this was not the case: although the supply voltage was constant for each transmitter during testing, the input voltage differed between transmitters. A correction factor was calculated for each transmitter depending on the specific input voltage of that transmitter whereby the pressure reading was corrected once data was exported to Microsoft Excel®.

From the above-mentioned accuracies and the graphs it can be seen that for both the temperature and the pressure readings the data accuracy is limited due to limitations of the equipment available.

5.3 Data acquisition analysis

In this section the data acquisition system will be analysed and evaluated. In the first section the energy balance between the primary and secondary side in the evaporator will be discussed as well as the uncertainty analysis conducted. In the second section the repeatability of the tests will be discussed.

5.3.1 Energy balance

In order to ensure that the data obtained during testing is accurate, an energy balance check was conducted on the recorded data. Any drastic differences between the measured energy transferred from the water and the measured energy increase of the R-744 would indicate any issue with the data acquisition system. Due to the gas evaporating through the two-phase region where the quality at the relative measuring points is unknown, the energy balance was checked in the pipe sections where R-744 is superheated. In these sections the R-744 condition can be determined from the measured temperature and pressure data. The energy transferred from the water is calculated as follows:

$$Q_{xy} = \dot{m} C_p (T_x - T_y) \tag{5.1}$$

where

$\dot{m}$ is the recorded water flow in kg/s as obtained from the electromagnetic flow meter.

C_p is the theoretical specific heat capacity of water measured in J/kg-K, calculated with EES at the average fluid temperature of each data point.

T_x, T_y is the inlet and outlet temperatures as measured by the respective sensors in ^{0}C.

The energy increase of the R-744 is calculated as follow:

$$Q_{xy} = \dot{m}(\propto_y - \propto_x) \tag{5.2}$$

where:

$\dot{m}$ is the recorded R-744 flow in kg/s as obtained from the coriolis flow meter.

$\propto_x, \propto_y$ is the inlet and outlet enthalpies which are calculated with EES using the temperatures in ^{0}C and the pressures in Bar as recorded by the respective sensors.

For each of the measured input values the measured uncertainty is known as discussed in section 5.2 and therefore a relative uncertainty is applicable to the calculated energy. A demonstrative calculation is shown in Appendix B of the calculations done to determine the uncertainty of the calculated values. This method was applied to the calculation of the uncertainty of the heat transfer correlations as well.

In Figure 5.9 the energy balance for a few test points in the superheat region is shown below with the calculated uncertainty shown by error bars. From this chart it is clear that with the measured uncertainty taken into account the energy gained by the R-744 corresponds to the energy transferred by the water. It is, however, clear that a large uncertainty exists on the water side, which is mainly due to the uncertainty of the temperature measurements. This is reflected by the average uncertainty of the calculated energy reduction on the water side being 21%, while on the R-744 side the average uncertainty of the calculated energy increase is 7%.

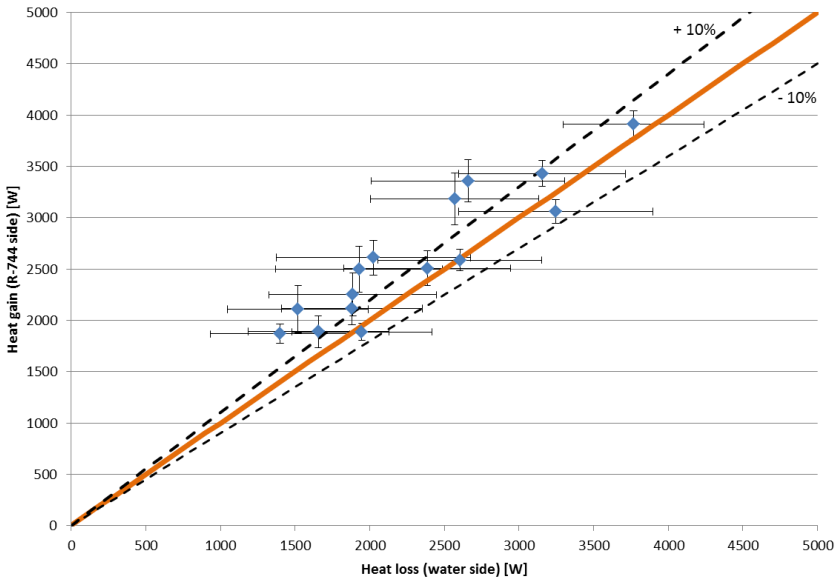

Figure 5.9 – Energy balance in evaporator.

5.3.2 Data repeatability

As discussed in section 4.3.1 a selective eight tests were repeated to determine whether the repeatability of the data can be trusted. Due to the water temperature in the holding tanks not

being controlled and affected by ambient temperature as well as previous tests conducted only a limited number of tests were repeated. For each of these eight tests the heat flux, mass flux and saturation temperatures were calculated as per the diagram in Figure 4.5. The variance for each of the three parameters (mass flux, heat flux, saturation temperature) between the first and second test, for each of the eight repeated tests, was calculated as a percentage and is shown in Table 5.1.

Considering that it is impossible to recreate the conditions of an earlier test exactly due to ambient conditions as well as the uncertainty of the instrumentation, the variance shown in Table 5.1 indicates an acceptable good repeatability of the data.

Table 5.1 – Variance of each of the repeatability tests.

Test Number	Mass Flux	Saturation Temperature	Heat Flux
1	-1.0%	-10.0%	-6.0%
2	2.8%	12.0%	3.2%
3	-0.6%	-3.2%	-8.6%
4	2.1%	-3.3%	-3.1%
5	-1.6%	0.0%	-4.0%
6	-2.3%	12.5%	4.9%
7	-0.6%	-3.3%	-5.3%
8	-0.8%	3.5%	-8.3%

5.4 Chapter summary

In Chapter 5 the data generated from the tests was analysed based on the typical data report generated for each of the tests conducted. The selection of steady state data was discussed in the first section and the uncertainty thereof in the second section. The energy balance in the heat exchanger was shown as well as the repeatability of the data when using the same input values. In Chapter 6 the EES program used to model the correlations will be discussed.

Chapter 6 – Simulation

In Chapter 6 the methodology of the simulation written in Engineering Equation Solver (EES) for this study will be shown and discussed. The EES program is used to simulate the correlations sourced from the literature in Chapter 2 with the theoretical details discussed in Chapter 3. The experimental values contained in the new database, as developed in Chapter 5, were used as input values for the program. The main output from the program is the heat transfer coefficients as predicted by each of the correlations. The EES program can be grouped into two distinct parts namely enthalpy calculation and heat transfer coefficients. Each of these parts will be discussed separately in the following two sections. The complete program code is attached in Appendix B.

6.1 Enthalpy calculation

In order to solve the correlations with EES the inlet and outlet enthalpies of the two-phase R-744 for each of the data sets are required, with each data set corresponding to a physical pipe section in the heat exchanger. For any fluid in the two-phase region two independent properties are needed to calculate the enthalpy (with temperature and pressure not being independent in this region), i.e. temperature or pressure and quality. The quality, however, cannot be measured; therefore the enthalpy cannot be determined by only using the readings on the R-744 side and the readings taken on the water side also needs to be included.

The quality at the inlet to the evaporator can be calculated using the outlet conditions of the gas cooler. The R-744 gas cooler outlet temperature and pressure were also recorded as shown in section 5.1, as part of the experimental database. This is measured prior to the R-744 entering the expansion valve and the fluid is therefore a saturated liquid. In this region temperature and pressure are independent and can be used to calculate enthalpy. Since the enthalpy remains approximately constant for a fluid expanding through an expansion valve, this enthalpy calculated at the gas cooler exit is used as the inlet enthalpy for the evaporator.

With the inlet enthalpy of the heat exchanger known, the inlet and outlet enthalpies for each of the remaining sections are calculated using the energy transferred from the water to the R-744 in that specific section using equation (5.1). Equation (5.2) is then used to calculate the outlet enthalpy for each of the pipe sections. The outlet R-744 enthalpy for each of the pipe sections is also the inlet enthalpy for the following section.

This methodology is used in the EES program to calculate the enthalpy per data set, with the detailed program shown in Appendix D. From this program the inlet and outlet enthalpies are added to the eight existing parameters mentioned in section 5.1 to form a new database containing 339 data sets each with 10 data points.

6.2 Heat transfer coefficients

The updated database was used by the EES program to simulate the R-744 heat transfer correlations. The details of this EES program will be discussed below and can be divided into three sections namely: data and properties, calculated properties and correlation procedures.

6.2.1 Data and properties

In this part of the program the 10 data points for each of the data sets are retrieved from the database and set up in a lookup table. The physical parameters of the test bench required as inputs to the correlations are also defined. These values include the pipe diameters, pipe lengths and basic calculations based on these, including flow area and heat transfer area, as discussed in section 4.1. In this section the gravitational acceleration and the relative roughness of the heat transfer channels are also defined. All values defined in this section are global constants which are applicable for each of the data sets contained in the database.

6.2.2 Calculated properties

This part of the program consists of a duplicate function wherein each calculation is applied to all data sets in the lookup table. The calculations are aimed at determining the additional properties required by the correlations which are specific to each data set and can be divided into the water side and R-744 side.

For the water flowing in the annulus these properties are based on the average water temperature and pressure of a pipe section. Built-in functions of EES are used to calculate the density, specific heat, thermal conductivity, viscosity and the friction factor for which the Moody chart function is used. The Reynolds and Prandtl numbers are required in the water correlations and calculated using equations (6.1) and (6.2) respectively:

$$Re_{water} = \dot{m}_{water}\left(\frac{ID_{water} - OD_{R-744}}{\mu_{water} A_{water}}\right) \tag{6.1}$$

$$Pr_{water} = Cp_{water}\left(\frac{\mu_{water}}{k_{water}}\right) \tag{6.2}$$

For the R-744 flowing inside the inner tube, the built in EES functions were used to calculate the density, specific heat, thermal conductivity, viscosity, surface tension and enthalpy at the evaporation temperature. For each of these both the liquid (quality = 0) and gas properties (quality = 1) were calculated. New functions were defined and used called to calculate average two-phase values for these properties. The liquid and gas Reynolds numbers were calculated with equations (6.3) and (6.4):

$$Re_L = \dot{m}_{R-744}(1 - x_{R-744})\left(\frac{ID_{R-744}}{\mu_{LG}}\right) \tag{6.3}$$

$$Re_G = \dot{m}_{R-744}x_{R-744}\left(\frac{ID_{R-744}}{\mu_{LG}}\right) \tag{6.4}$$

Each of the heat transfer correlations evaluated differ in the calculation of other dimensionless numbers. The remaining dimensionless numbers were therefore calculated in the respective correlation sub-procedures. The equations forming part of each correlation were shown in Chapter 3 and the implementation procedures will be discussed below.

6.2.3 Correlation procedures

In this part of the program six user-defined procedures were written, one for each of the four R-744 heat transfer correlations as well as the two water correlations. For each of the four R-744 procedures the global constants and calculated properties discussed in sections 6.2.1 and 6.2.2 are used as input values. The output value of each procedure is the heat transfer coefficient as predicted by the respective correlations.

In the case of the two water procedures similar input values are used in these procedures. By applying the correlations the heat transfer coefficient for the water side is calculated. With this heat transfer coefficient, the heat loss in the water, as well as the physical properties of the channel known, equation (6.5) is used to calculate the experimental R-744 heat transfer coefficient.

$$\frac{1}{UA} = \frac{1}{\eta_{op}h_{R-744}A_p} + \frac{R_{fp}}{\eta_{op}A_p} + R_w + \frac{1}{\eta_{os}h_{water}A_s} + \frac{R_{fs}}{\eta_{os}A_s} \tag{6.5}$$

This equation is solved twice for h_{water}, firstly with the Dittus-Boelter correlation and secondly with the Gnielinski correlation. This resulted in two different experimental R-744 heat transfer coefficients (h_{R-744}) calculated per pipe section for comparison with the theoretical outputs from the four R-744 procedures.

6.3 Chapter summary

In Chapter 6 the EES program logic was discussed, including how the data contained in the database was used to calculate the heat transfer coefficients. The program uses the database as input and calculates four predicted heat transfer coefficients per data set based on the four R-744 correlations. Similarly two experimental heat transfer correlations were calculated per data set based on the two water heat transfer correlations. The four predicted coefficients will be compared to the two experimental heat transfer coefficients in Chapter 7.

Chapter 7 - Results

In Chapter 7 the predicted heat transfer coefficients, for the different R-744 correlations, will be evaluated against the experimental heat transfer coefficients. The results from each correlation will be evaluated individually in the following sections, firstly based on the ranges of the three parameters as discussed in Chapter 2 and summarised in Table 2.1. Secondly, the correlations will be evaluated using the Reynolds number as reference and finally the results per correlation will be discussed.

- *Results relative to parameter ranges*

The three parameters influencing heat transfer is divided into three ranges as shown in Table 7.1. These ranges are simply based on the limits of the test bench as discussed in section 4.3.1.

Table 7.1 - Ranges to assist in correlation evaluation.

Factor	Low	Medium	High
Mass flux [kg/m^{2}s]	410 – 755	755 – 1100	1100 – 1450
Evaporating temperature [K]	262 – 270	270 – 278	278 – 286
Heat flux [W/m^2]	1500 – 21500	21500 – 41500	41500 – 61500

The data points in the graphs to follow were grouped to indicate whether the points fall within the correlation ranges (blue) as discussed in Chapter 2 and listed in Table 7.2 or not (red).

Table 7.2 – Ranges for each of the four R-744 correlations.

	Channel diameter [mm]	Mass velocities [kg/m^{2}s]	Heat flux [kW/m^2]	Saturation temperatures [^{o}C]
Thome & El Hajal (2004)	0.79 – 10.06	85 – 1440	5 – 36	-25 – 25
Yoon *et al. (2004)*	7.53	200 – 530	12 – 20	-4 – 20
Cheng *et al. (2008b)*	0.6 – 10.0	50 – 1500	1.8 – 46	-28 – 25
Pamitran *et al. (2011)*	3.0 & 1.5	50 – 600	5 – 70	0 – 10

The uncertainty of each data point will be shown in each graph. As discussed in Chapter 5 the uncertainty of the measured values are converted through an uncertainty analysis to the effective uncertainty of the heat transfer coefficients. This was calculated by making use of the built-in uncertainty propagation function of EES. These uncertainties translate to an effective uncertainty of the heat transfer coefficients when calculated with the respective correlations.

Each correlation's uncertainty will therefore differ since the propagation of an uncertainty is dependent on the formulas used in the calculation thereof. The propagation of uncertainty is calculated by EES similarly to the sample calculation done in Appendix B. The uncertainties included in this study are limited to that of the experimental measurements only.

- *Results relative to Reynolds numbers.*

In the second section for each correlation, the results are grouped according to the Reynolds numbers of the R-744 for each data set. The Reynolds number range tested in these experiments are between 29 000 and 130 000. This range is divided as follows for further analysis:

Low Reynolds number:	$29\,000 \leq Re < 62\,000$
Medium Reynolds number:	$62\,000 \leq Re < 95\,000$
High Reynolds number:	$95\,000 \leq Re < 130\,000$

7.1 Thome and El Hajal (2004)

7.1.1 Range comparison

Graphs will be used to compare the predicted versus the experimental heat transfer coefficients of each correlation. For all graphs the experimental heat transfer coefficient will be shown on the x-axis and the predicted heat transfer coefficient from the correlations will be shown on the y-axis. The uncertainty of each reading is indicated in the graphs with the use of "error bars".

Although this comparisons were done using both the Dittus-Boelter and Gnielinski equations on the water side, only the Gnielinski comparisons are shown here. The Gnielinski data consist of wider range since some data which uncertainty is too high (uncertainties exceeding

40% for the experimental coefficients and 20% for the predicted coefficients) have been excluded.

A comparison between the Thome and El Hajal (2004) predicted heat transfer coefficient and the experimental heat transfer coefficient using the Gnielinski equation is shown in Figure 7.1.

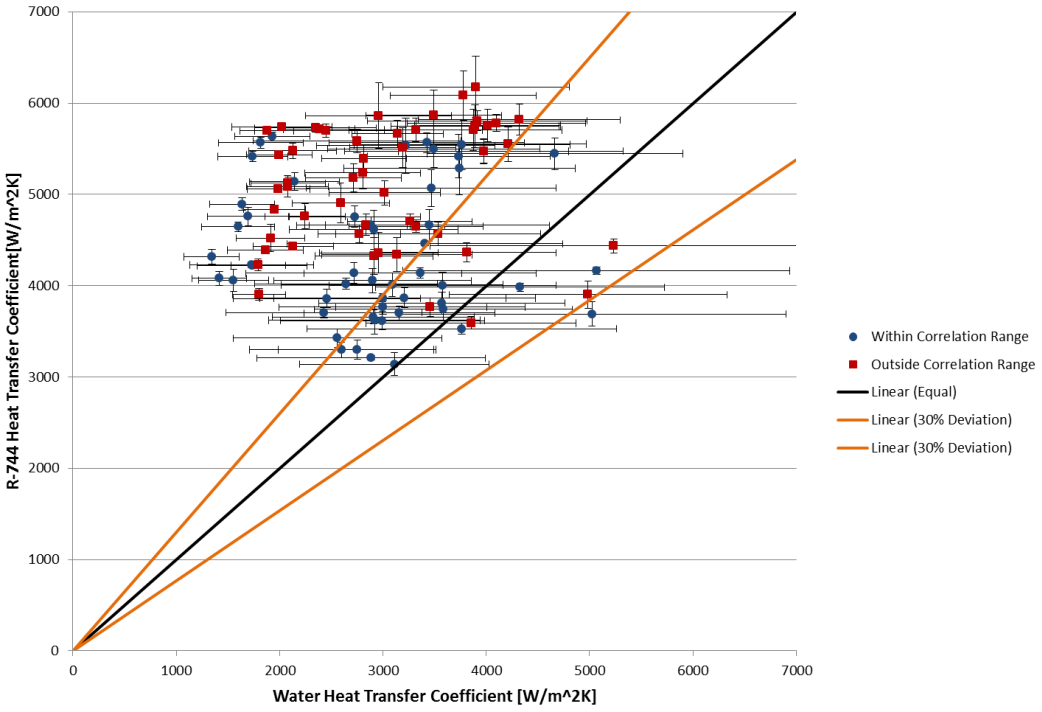

Figure 7.1 - Results of Thome and El Hajal (2004) using Gnielinski on the water side.

The correlation predicted 39% of the data within ±10% and 64% of the data within ±30% of the experimental value. A further breakdown is given in Table 7.3 including the accuracies shown when compared with Dittus-Boelter.

Table 7.3 - Results of Thome and El Hajal (2004) using Gnielinski on the water side.

	Mass Flux				**Evaporation Temperature**				**Mass Flux**			
	Dittus Boelter		Gnielinski		Dittus Boelter		Gnielinski		Dittus Boelter		Gnielinski	
	±10%	±30%	±10%	±30%	±10%	±30%	±10%	±30%	±10%	±30%	±10%	±30%
Low	*74%*	*91%*	*70%*	*87%*	*72%*	*91%*	*71%*	*86%*	-	-	-	-
Medium	*41%*	*59%*	*12%*	*48%*	*63%*	*75%*	*27%*	*82%*	*57%*	*60%*	*46%*	*66%*
High	*33%*	*38%*	*17%*	*42%*	*36%*	*49%*	*14%*	*42%*	*41%*	*81%*	*19%*	*59%*

7.1.2 Reynolds number comparison

Results of Thome and El Hajal (2004) using Gnielinski on the water side to calculate the experimental heat transfer coefficient, with data grouped according to Reynolds numbers, are shown in Figure 7.2.

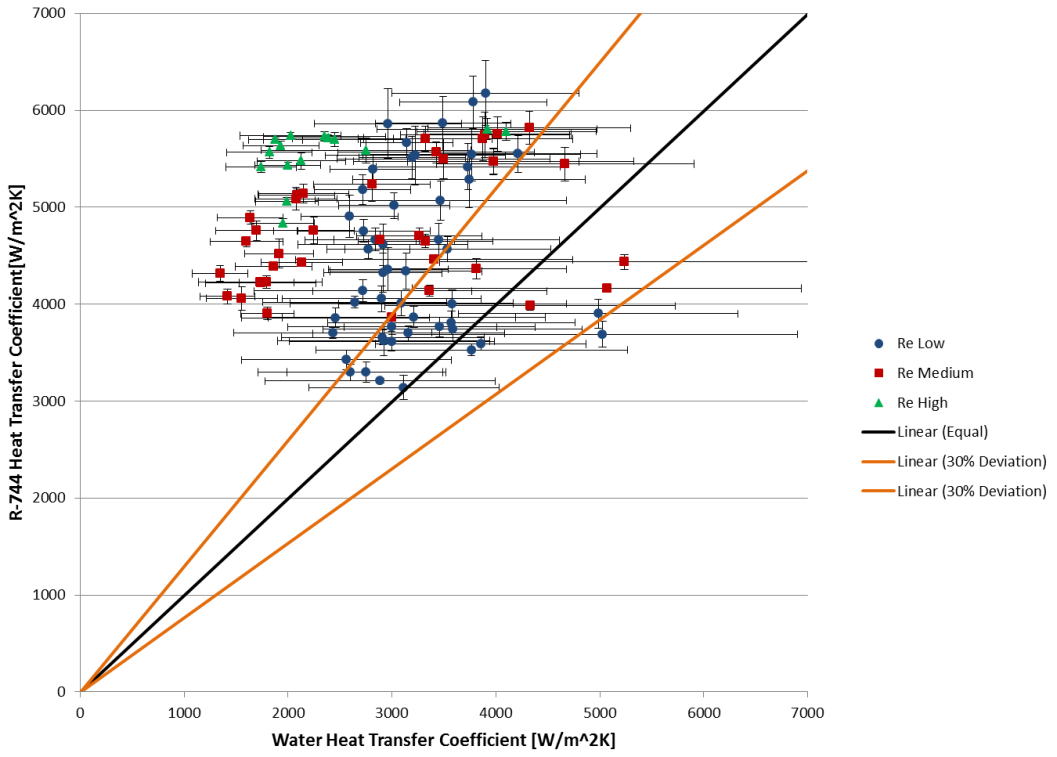

Figure 7.2 - Results of Thome and El Hajal (2004) using Gnielinski on the water side, grouped according to Reynolds numbers.

7.1.3 Result

As mentioned earlier the uncertainty of each heat transfer coefficient is different depending on the specific measurements and calculations. In a few cases these uncertainties exceeded 40% for the experimental coefficients and 20% for the predicted coefficients. Due to this high uncertainty these data points were excluded from the study, and the number of data points per correlation differs.

The uncertainty on the predicted heat transfer coefficients is due to each of the correlations requiring heat flux as an input value. The heat flux is calculated from the measured values on the water side which has an effect on the accuracy of the heat transfer coefficient when calculated with the respective correlations.

With the stated requirements that only those predicted heat transfer coefficients with an uncertainty of 20% or less and experimental coefficients with an uncertainty of 40% or less will be considered, the number of data points were 103 and 87 respectively when compared to Gnielinski and Dittus-Boelter. Of these data points 51% and 44% respectively falls within the factor ranges of the Thome and El Hajal (2004) correlation as shown in Table 2.1.

In the case of using Gnielinski for determining the experimental water convection heat transfer coefficient, this correlation predicts 39% of the values within ±10% and 64% within ±30%. This increases to 60% and 77% when reducing the data points to those falling within the correlation's specific range.

In the case of using Dittus-Boelter this correlation predicts 52% of the values within ±10% and 67% within ±30%. This increases slightly to 66% and 68% when reducing the data points to those falling within the correlation's specific range.

In both cases (Gnielinski and Dittus-Boelter) this correlation shows a reduction in accuracy with an increase in mass flux and evaporation temperature. The data for the low heat flux region was excluded due to the low accuracy and no clear pattern in terms of accuracy emerges for changes in heat flux within the medium and high ranges. When data is grouped according to Reynolds numbers the accuracy decreases with an increase in Reynolds number.

7.2 Yoon *et al.* (2004)

7.2.1 Range comparison

A comparison between the Yoon *et al.* (2004) predicted heat transfer coefficient and the experimental heat transfer coefficient using the Gnielinski equation is shown in Figure 7.3.

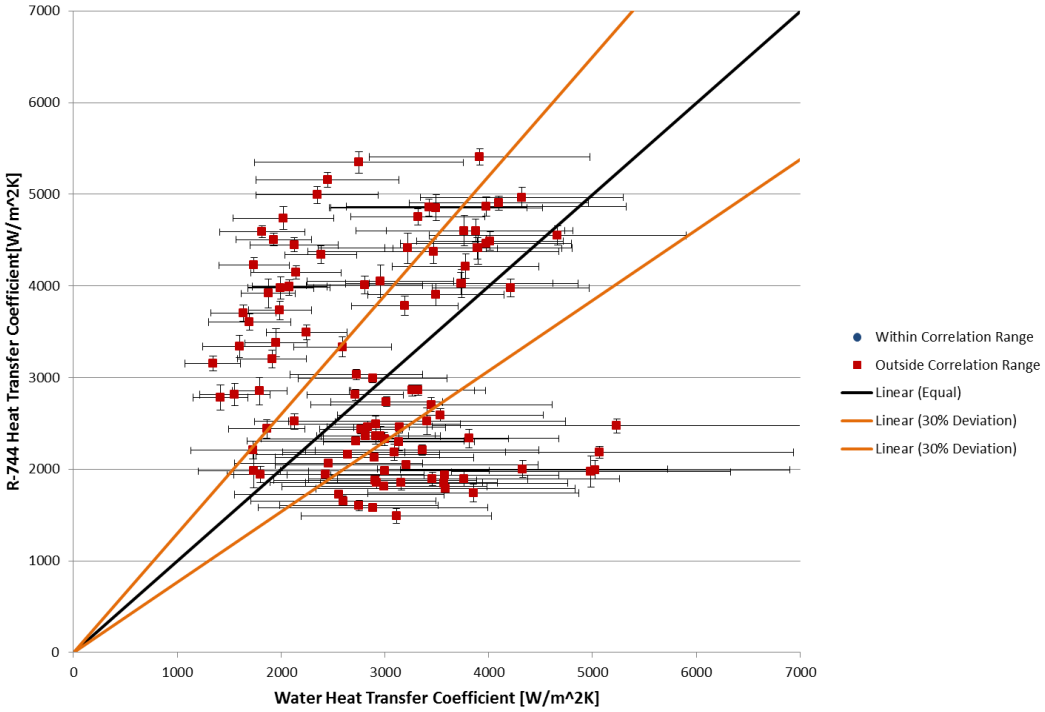

Figure 7.3 - Results of Yoon *et al.* (2004) using Gnielinski on the water side.

The correlation predicted 39% of the data within ±10% and 64% of the data within ±30% of the experimental value. A further breakdown is given in Table 7.4 including the accuracies shown when compared with Dittus-Boelter.

Table 7.4 - Results of Yoon *et al.* (2004) using Gnielinski on the water side.

	Mass Flux				**Evaporation Temperature**				**Mass Flux**			
	Dittus Boelter		Gnielinski		Dittus Boelter		Gnielinski		Dittus Boelter		Gnielinski	
	±10%	±30%	±10%	±30%	±10%	±30%	±10%	±30%	±10%	±30%	±10%	±30%
Low	*74%*	*91%*	*65%*	*76%*	*72%*	*91%*	*63%*	*75%*	-	-	-	-
Medium	*41%*	*59%*	*66%*	*81%*	*63%*	*75%*	*100%*	*100%*	*57%*	*60%*	*52%*	*65%*
High	*33%*	*38%*	*38%*	*48%*	*36%*	*49%*	*49%*	*64%*	*41%*	*81%*	*74%*	*85%*

7.2.2 Reynolds number comparison

Results of Yoon *et al.* (2004) using Gnielinski on the water side to calculate the experimental heat transfer coefficient, with data grouped according to Reynolds numbers, is shown in Figure 7.4.

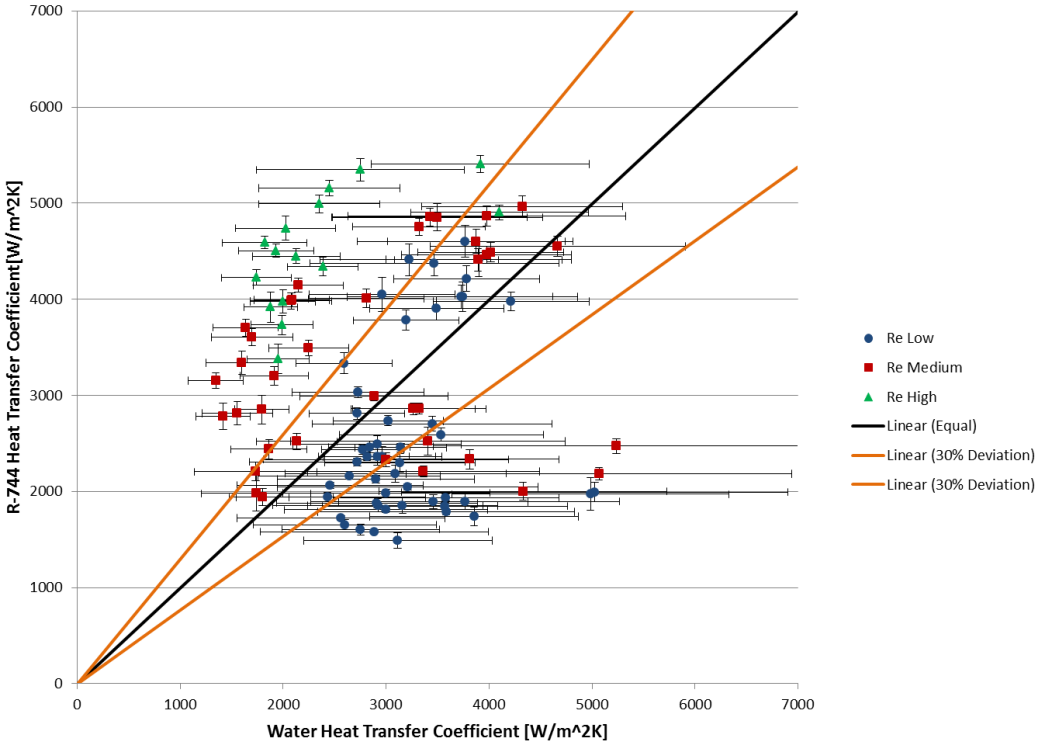

Figure 7.4 - Results of Yoon *et al.* (2004) using Gnielinski on the water side, grouped according to Reynolds numbers.

7.2.3 Result

In the case of Yoon *et al.* (2004) the number of data points is 103 and 87 respectively when using Gnielinski and Dittus-Boelter. None of these data points fall within the factor ranges as shown in Table 2.1. This is mainly due to the low mass flux range for which this correlation has been developed. Most of the data points meeting the uncertainty requirement have a mass flux exceeding the mass flux range from which this correlation was developed as shown in Table 7.2.

In the case of using Gnielinski for the experimental water heat transfer coefficients, this correlation predicts 58% of the values within ±10% and 74% within ±30%, whereas with Dittus-Boelter; the correlation predicts 59% of the values within ±10% and 71% within ±30%.

With Dittus-Boelter this correlation shows a reduction in accuracy with an increase in mass flux and evaporation temperature, however this reduction is less drastic than in the case of the Thome and El Hajal (2004) correlation. Again no data is available for the low heat flux region and no clear pattern in terms of accuracy emerges for changes in heat flux within the medium and high ranges.

With Gnielinski this correlation shows a similar accuracy within the low and medium mass flux and evaporation temperature ranges with a slight decrease in the high range. Again no data is available for the low heat flux region and an increase in accuracy is shown for an increase in heat flux from the medium to the high range. When data is grouped according to Reynolds numbers the accuracy decreases with an increase in Reynolds number.

7.3 Cheng *et al.* (2008b)

7.3.1 Range comparison

A comparison between the Cheng *et al.* (2008b) predicted heat transfer coefficient and the experimental heat transfer coefficient using the Gnielinski equation is shown in Figure 7.5.

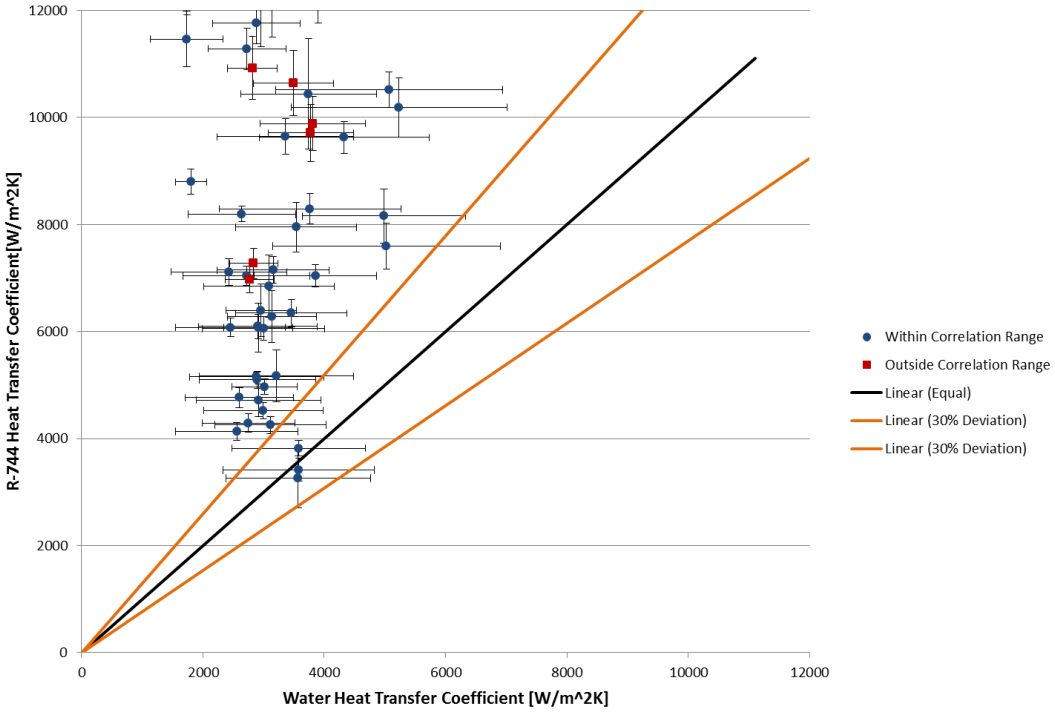

Figure 7.5 - Results of Cheng *et al.* (2008b) using Gnielinski on the water side.

The correlation predicted 8% of the data within ±10% and 19% of the data within ±30% of the experimental value. A further breakdown is given in Table 7.5 including the accuracies shown when compared with Dittus-Boelter.

Table 7.5 - Range accuracy of Cheng *et al.* (2008b) using Gnielinski on the water side.

	Mass Flux				**Evaporation Temperature**				**Mass Flux**			
	Dittus Boelter		Gnielinski		Dittus Boelter		Gnielinski		Dittus Boelter		Gnielinski	
	±10%	±30%	±10%	±30%	±10%	±30%	±10%	±30%	±10%	±30%	±10%	±30%
Low	*0%*	*0%*	*19%*	*42%*	*0%*	*0%*	*21%*	*46%*	*13%*	*29%*	-	-
Medium	*0%*	*0%*	*0%*	*0%*	*0%*	*0%*	*0%*	*0%*	*4%*	*12%*	*11%*	*23%*
High	*0%*	*0%*	*0%*	*0%*	*0%*	*0%*	*0%*	*0%*	*13%*	*29%*	*0%*	*8%*

7.3.2 Reynolds number comparison

The results of Cheng *et al.* (2008b) using Gnielinski on the water side to calculate the experimental heat transfer coefficient, with data grouped according to Reynolds numbers, are shown in Figure 7.6.

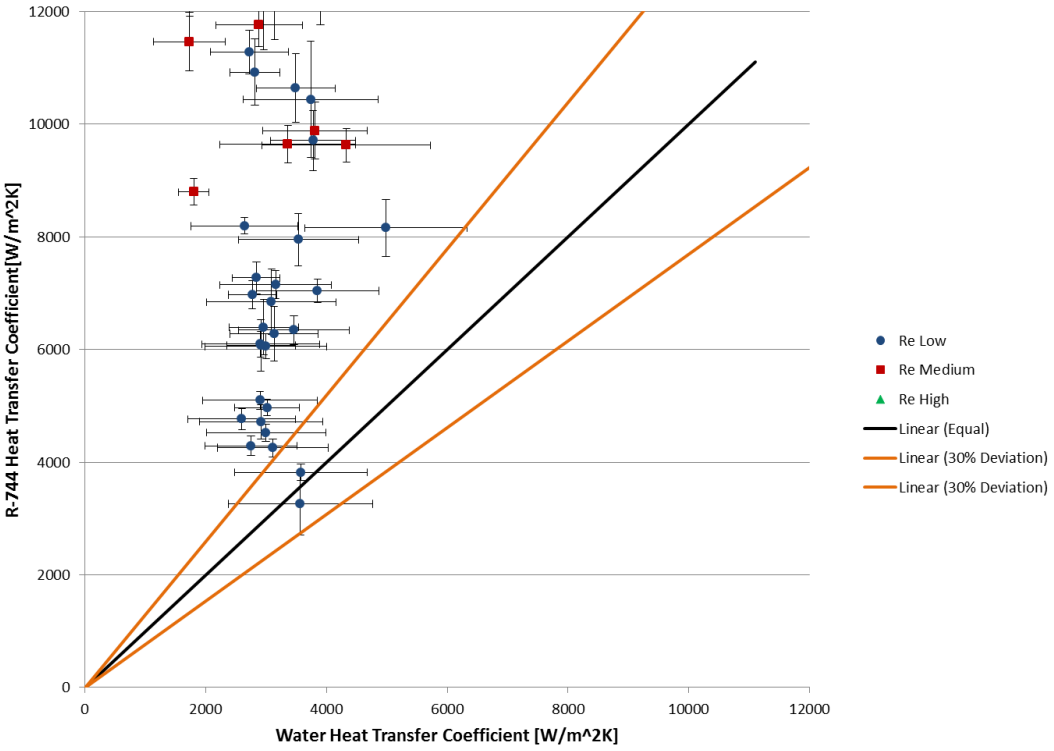

Figure 7.6 - Results of Cheng *et al.* (2008b) using Gnielinski on the water side, grouped according to Reynolds numbers.

7.3.3 Result

With the given accuracy requirements the number of data points is 96 and 81 respectively when using Gnielinski and Dittus-Boelter. For both cases 83% of these data points fall within the factor ranges of the Cheng *et al.* (2008b) correlation as shown in Table 2.1.

With Gnielinski this correlation predicts 8% of the values within ±10% and 19% within ±30%. This increases slightly to 10% and 23% when reducing the data points to those falling within the correlation ranges.

With Dittus-Boelter this correlation predicts 10% of the values within ±10% and 23% within ±30%. This increases slightly to 12% and 28% when reducing the data points to those falling within the correlation ranges.

In both cases (Gnielinski and Dittus-Boelter) this correlation shows a sharp reduction in accuracy with an increase in mass flux and evaporation temperature. No data is available for the low heat flux region and an increase in accuracy is shown for an increase in heat flux. When data is grouped according to Reynolds numbers the accuracy decreases with an increase in Reynolds number.

This correlation is heavily based on flow pattern maps, more so than the correlation by Yoon *et al.* (2004), with each flow region utilising a different correlation. Due to the inaccuracy of the test data the flow pattern of most data points can easily be predicted incorrectly by this correlation. In such a case the correlation applied to calculate the heat transfer coefficient will do so incorrectly although it is applied correctly.

7.4 Pamitran *et al.* (2011)

7.4.1 Range comparison

A comparison between the Pamitran *et al.* (2011) predicted heat transfer coefficient and the experimental heat transfer coefficient using the Gnielinski equation is shown in Figure 7.7.

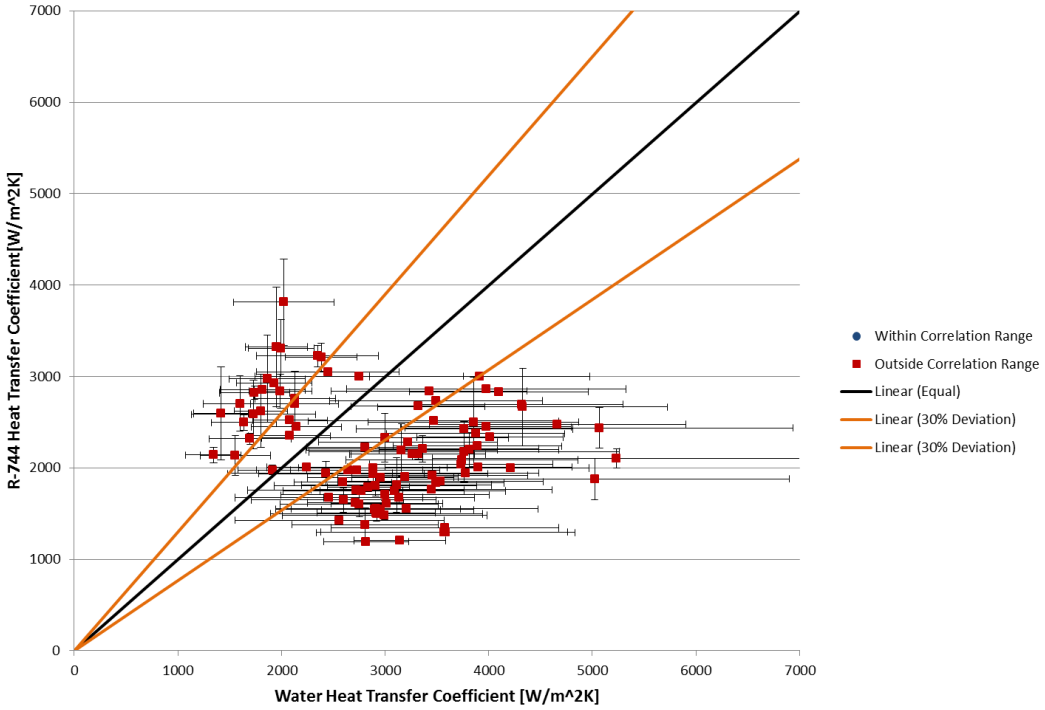

Figure 7.7 - Results of Pamitran *et al.* (2011) using Gnielinski on the water side.

The correlation predicted 40% of the data within ±10% and 73% of the data within ±30% of the experimental value. A further breakdown is given in Table 7.6 including the accuracies shown when compared with Dittus-Boelter.

Table 7.6 - Range accuracy of Pamitran *et al.* (2011) using Gnielinski on the water side.

	Mass Flux				**Evaporation Temperature**				**Mass Flux**			
	Dittus Boelter		Gnielinski		Dittus Boelter		Gnielinski		Dittus Boelter		Gnielinski	
	±10%	±30%	±10%	±30%	±10%	±30%	±10%	±30%	±10%	±30%	±10%	±30%
Low	*27%*	*42%*	*40%*	*60%*	*29%*	*45%*	*39%*	*61%*	-	-	-	-
Medium	*29%*	*61%*	*32%*	*74%*	*25%*	*50%*	*50%*	*80%*	*41%*	*73%*	*50%*	*82%*
High	*50%*	*85%*	*52%*	*96%*	*38%*	*71%*	*40%*	*81%*	*16%*	*28%*	*12%*	*44%*

7.4.2 Reynolds number comparison

Results of Pamitran *et al.* (2011) using Gnielinski on the water side to calculate the experimental heat transfer coefficient, with data grouped according to Reynolds numbers, are shown in Figure 7.8.

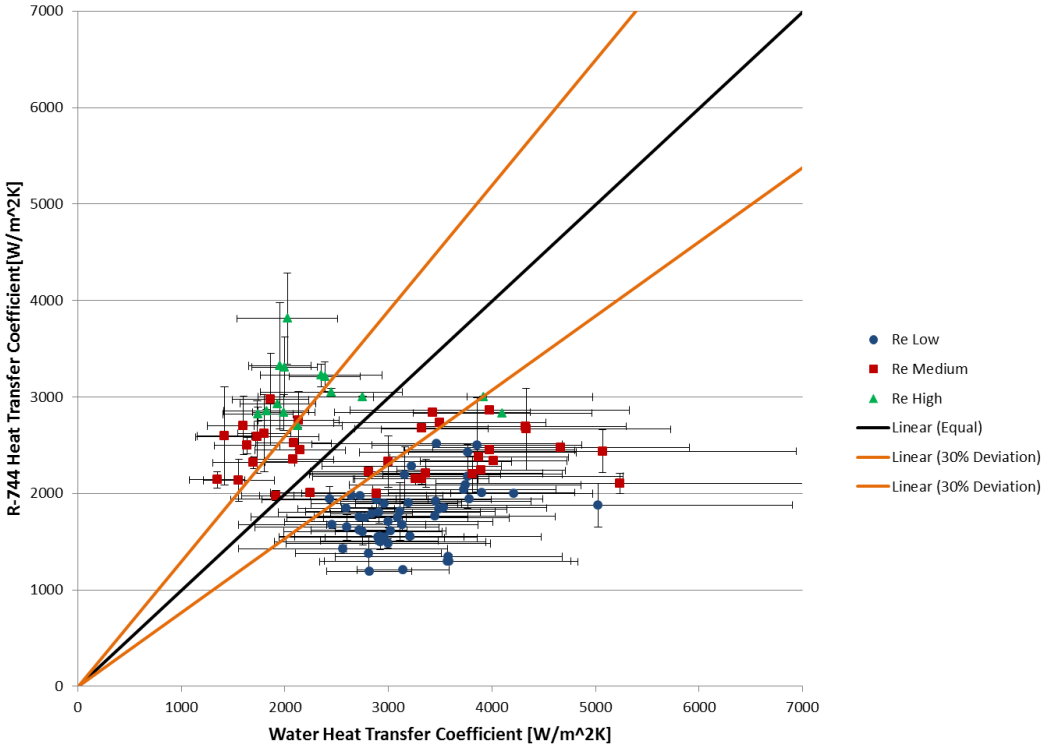

Figure 7.8 - Results of Pamitran *et al.* (2011) using Gnielinski on the water side, grouped according to Reynolds numbers.

7.4.3 Result

In the case of Pamitran *et al.* (2011) the number of data points is 99 and 84 respectively when using Gnielinski and Dittus-Boelter. None of these data points fall within the factor ranges as shown in Table 2.1. This is mainly due to the low mass flux and evaporation temperature ranges for which this correlation has been developed. Most of the data sets for the current study's mass flux exceed this range and no below zero degree evaporation temperature data were used in the development of this correlation.

With Gnielinski this correlation predicts 40% of the values within ±10% and 73% within ±30%. With Dittus-Boelter this correlation predicts 33% of the values within ±10% and 60% within ±30%.

With both Dittus-Boelter and Gnielinski this correlation shows an increase in accuracy with an increase in mass flux and evaporation temperature. Again no data is available for the low heat flux region. A reduction in accuracy is shown with an increase in heat flux from the medium to the high range. When data is grouped according to Reynolds numbers the accuracy increases with an increase in Reynolds number.

7.5 Chapter summary

The results as given in this chapter can be summarised as follows:

7.5.1 Range comparison

From the graphs for the four R-744 correlations, grouped according to the correlation ranges, the following is noted:

- Overall the correlation by Pamitran *et al.* (2011) showed the highest accuracy over the entire range of data. The correlation predicted 40% of the data within ±10% and 73% of the data within ±30% of the experimental value.
- The correlation by Cheng *et al.* (2008b) showed the lowest accuracy with 8% of the data predicted within ±10% and 19% of the data within ±30% of the experimental value. The possible incorrect prediction of the flow pattern per data point is proposed to be the reason for the inaccuracy.
- For Pamitran *et al.* (2011) no data fell within the range of the correlation due to the low mass flux and evaporation temperature for which this correlation was developed.
- Although tests were conducted in the low heat flux range, this data has a high uncertainty factor and were therefore excluded from the results. The effect of the uncertainty of the temperature instruments was higher at lower temperatures when calculating the heat flux.

7.2 *Reynolds number comparison*

In Table 7.7 the results from the Reynolds number comparison are summarised, comparing the percentage accuracy for the different Reynolds number regions.

Table 7.7 - Results of correlations using Gnielinski on the water side, grouped according to Reynolds numbers.

	Reynolds Numbers							
	All		**Low**		**Medium**		**High**	
	±10%	±30%	±10%	±30%	±10%	±30%	±10%	±30%
Thome and El Hajal	*39%*	*64%*	*60%*	*88%*	*26%*	*53%*	*0%*	*13%*
Yoon *et al.*	*58%*	*74%*	*76%*	*92%*	*53%*	*71%*	*13%*	*20%*

	Reynolds Numbers							
	All		**Low**		**Medium**		**High**	
	±10%	±30%	±10%	±30%	±10%	±30%	±10%	±30%
Cheng *et al.*	*8%*	*19%*	*19%*	*40%*	*0%*	*3%*	*0%*	*0%*
Pamitran *et al.*	*40%*	*73%*	*32%*	*54%*	*54%*	*89%*	*36%*	*100%*

From Table 7.7 it can be seen that the results for Cheng *et al.* (2008b) again shows a very low accuracy. For both Thome and El Hajal (2004) and Yoon *et al.* (2004) the correlations showed a decrease in accuracy with an increase in Reynolds number. The opposite was seen for the correlation by Pamitran *et al.* (2011) where data with a high Reynolds number showed the highest accuracy, with only the correlation by Pamitran *et al.* (2011) showing reasonable results here.

Chapter 8 – Conclusion

8.1 Study background

This study was conducted with the focus on adding engineering value to the understanding of heat transfer characteristics of evaporating R-744. Due to the increased need for energy efficient and environmentally friendly technologies in industry, heat pumps are receiving renewed attention in replacing conventional electrical water heaters. Specifically heat pumps which make use of natural refrigerants are being explored, due to the low ODP and GWP value thereof.

Currently the understanding of the heat transfer characteristics of R-744 is still limited due to the lack of heat transfer correlations specifically developed for R-744. Existing heat transfer correlations in literature tends to under-predict the heat transfer coefficient of R-744 and therefore do not deliver accurate results on which heat exchanger designs can be based. Correlations have been developed specifically for R-744, however the accuracy thereof is still relatively unknown.

The purpose of this study was therefore to determine the accuracy of these correlations in predicting the heat transfer coefficients of flow boiling R-744. The study focused on the two-phase area only and is based on a new database created from extensive experimental testing.

The methodology followed is summarised as follow:

- Literature survey – to determine the correlations available in literature and the expected characteristics of evaporating R-744.
- Experimental setup – an existing experimental test facility was upgraded and used to create a database to which these correlations can be compared.
- EES program – these correlations were programmed with EES to calculate the predicted heat transfer coefficients for the experimental test conditions. The EES program was also used to calculate the experimental heat transfer coefficients.
- Comparison – these predicted and experimental coefficients were compared with each other to determine the accuracy of the different correlations.

8.2 Conclusion

From the results presented in Chapter 7 the following conclusions are made:

- Due to the uncertainty of the instrumentation (specifically the temperature and pressure transmitters) a high uncertainty is shown in the recorded readings during testing. This affected the accuracy of the calculated experimental heat transfer coefficients negatively and some data points had to be omitted due to the uncertainty thereof.

- The correlation by Cheng *et al.* (2008b) showed the lowest accuracy (8% within ±10% and 19% within ±30%) in predicting heat transfer coefficients in general as well as in specific ranges.

- Overall the correlation by Pamitran *et al.* (2011) showed the highest accuracy over the entire range of data. The correlation predicted 40% of the data within ±10% and 73% of the data within ±30% of the experimental value. However, some correlations showed higher accuracies in specific regions compared to this correlation.

- Both the correlations by Thome and El Hajal (2004) and Yoon *et al.* (2004) showed a decrease in accuracy for an increase in mass flux and evaporation temperature. In contrast to this, Pamitran *et al.* (2011) showed an increase in accuracy for the same.

- Both the correlations by Thome and El Hajal (2004) and Yoon *et al.* (2004) showed an increase in accuracy for an increase in heat flux, with Pamitran *et al.* (2011) showing a decrease in accuracy for the same.

- Yoon *et al.* (2004) showed the highest accuracy in the low and medium Reynolds number region while in the high Reynolds region Pamitran *et al.* (2011) showed the highest accuracy.

From these observations it is therefore concluded that the correlation by Yoon *et al.* (2004) should be used in the low and medium regions of mass flux and evaporation temperature and that of Pamitran *et al.* (2011) in the high region as defined in Table 7.1. As far as heat flux is concerned, Yoon *et al.* (2004) should deliver the highest accuracy in the high heat flux region and Pamitran *et al.* (2011) in the low and medium region.

8.3 Recommendations

The following recommendations should be considered for future studies on this subject:

- Further experimental testing should be conducted with the installation of higher accuracy instrumentation - specifically the temperature and pressure instrumentation requires a higher accuracy than was the case in this study.
- Further studies should include the use of smaller diameter channels since this is the norm in industry. The channel diameter was pre-determined for this study, however through the literature survey it became clear that most correlations are specifically developed for smaller channels.
- Further studies where the flow pattern of the fluid can be determined without being affected by physical readings independently can lead to a better understanding of the accuracy of the correlation by Cheng *et al.* (2008b).

References

Borgnakke, C. & Sonntag, R.E. 2009. *Fundamentals of thermodynamics.* John Wiley & Sons, Inc.

Calm, J.M. 2008. The next generation of refrigerants: historical review, considerations, and outlook. *International journal of refrigeration*, 31:1123-1133.

Cheng, L., Ribatski, G., Quibén, J.M. & Thome, J.R. 2008a. New prediction methods for CO_2 evaporation inside tubes- part i: a two-phase flow pattern map and a flow pattern based phenomenological model for two-phase flow frictional pressure drops. *International journal of heat and mass transfer*, 51(1-2):111-124.

Cheng, L., Ribatski, G. & Thome, J.R. 2008b. New prediction methods for CO_2 evaporation inside tubes - part ii: an updated general flow boiling heat transfer model based on flow patterns. *International journal of heat and mass transfer*, 51(1-2):125-135.

Cheng, L., Ribatski, G., Wojtan, L. & Thome, J.R. 2006. New flow boiling heat transfer model and flow pattern map for carbon dioxide evaporating inside horizontal tubes. *International journal of heat and mass transfer*, 49(21-22):4082-4094.

Choi, K., Pamitran, A.S. & Oh, J. 2007. Two-phase flow heat transfer of CO_2 vaporization in smooth horizontal minichannels. *International journal of refrigeration*, (30)5:767-777.

Cho, E.S., Yoon, S.H. & Kim, M.S. 2000. A study on the characteristics of evaporative heat transfer for carbon dioxide in a horizontal tube. (*In* KSME Spring Annual Meeting. p. 104-107.)

Cooper, M.G. 1984. Heat flow rates in saturated nucleate pool boiling – a wide-ranging examination using reduced properties. *Advances in heat transfer*, 16:157-239.

Dittus, F.W. & Boelter, L.M.K. 1930. Heat transfer in automobile radiators of the tubular type. *University of California publications of engineering*, 2:443-461.

Gasche, J.L. 2006. Carbon dioxide evaporation in a single microchannel. *Journal of the Brazilian Society of Mechanical Science & Engineering*, 28(1):69-83. January-March.

Gnielinski, V. 1975. New equations for heat and mass transfer in the turbulent flow in pipes and channels. *Forschung im ingenieurwesen*, 41(1):8-16.

Gungor, K.E. & Winterton, R.H.S. 1987. Simplified general correlation for saturated flow boiling and comparisons of correlations with data. *Chemical engineering research and design, 65(2)*:148-156.

Huai, X., Koyama, S., Zhao, T.S., Shinmura, E., Hidehiko, K. & Masaki, M. 2004. An experimental study of flow boiling characteristics of carbon dioxide in multiport mini channels. *Applied thermal engineering*, 24(10):1443-1463.

Jung, D.S., McLinden, M., Radermacher, R. & Didion, D. 1989. A study of flow boiling heat transfer with refrigerant mixtures. *International journal of heat and mass transfer,* 32(9):1751-1764.

Kandlikar, S.G. 1990. A general correlation for saturated two-phase flow boiling horizontal and vertical tubes. *Journal of heat transfer, 112(1):219-228*.

Kandlikar, S.G. 2002. Fundamental issues related to flow boiling in minichannels and microchannels. *Experimental thermal and fluid science, 26(204):*389-407.

Kattan, N., Thome, J.R. & Favrat, D. 1998a. Flow boiling in horizontal tubes: part 1 - development of a diabatic two-phase flow pattern map. *Journal of heat transfer, 120(1):*140-147.

Kattan, N., Thome, J.R. & Favrat, D. 1998b. Flow boiling in horizontal tubes: part 2 - new heat transfer data for five refrigerants. *Journal of heat transfer, 120(1):*148-155.

Kattan, N., Thome, J.R. & Favrat, D. 1998c. Flow boiling in horizontal tubes: part 3 - development of a new heat transfer model based on flow pattern. *Journal of heat transfer, 120(1):*156-165.

Kim, M., Petersen, J. & Bullard, C.W. 2004. Fundamental process and system design issues in CO2 vapour compression systems. *Progress in energy and combustion science, 30(2)*:119-174.

Kutateladze, S.S. 1948. On the transition to film boiling under natural convection. *Kotloturbostroenie*:10-12.

Liu, Z. & Winterton, R.H.S. 1991. A general correlation for saturated and subcooled flow boiling in tubes and annuli, based on a nucleate pool boiling equation. *International journal of heat and mass transfer,* 1(34):2759-2766.

Mori, H., Yoshida, S., Ohishi, K. & Kokimoto, Y. 2000. Dryout quality and post dryout heat transfer coefficient in horizontal evaporator tubes. (*In* 3rd European Thermal Sciences Conference. p. 839-844.)

Neksa, P., Rekstad, H., Zakeri, G.R. & Schiefloe, P.A. 1998. CO_2 heat pump water heater: characteristics, system design and experimental results. *International journal of refrigeration, 21(3)*:172-179.

Oh, H. & Son, C. 2011. Flow boiling heat transfer and pressure drop characteristics of CO_2 in horizontal tube of 4.57-mm inner diameter. *Applied thermal engineering, 31(2-3)*:163-172.

Pamitran, A.S., Choi, K., Oh, J. & Nasruddin. 2011. Evaporation heat transfer coefficient in single circular small tubes for flow natural refrigerants of C_3H_8, NH_3, and CO_2. *International journal of multiphase flow, 37(7):794-801*.

Pearson, A. 2005. Carbon dioxide - new uses for an old refrigerant. *International journal of refrigeration*, 28(8):1140-1148.

Pettersen, J. 2003. Two-phase flow pattern, heat transfer and pressure drop in microchannel vaporization of CO_2. (*In* ASHRAE Transaction (Symposia). p. 523-532.)

Thome, J.R. 2005. Update on advances in flow pattern based two-phase heat transfer models. *Experimental thermal and fluid science, 29(3)*:341-349.

Thome, J.R. & El Hajal, J. 2002. Two-phase flow pattern map for evaporation in horizontal tubes: latest version. (*In* 1st International Conference on Heat Transfer, Fluid Mechanics and Thermodynamics. Kruger Park, South Africa. p. 182-187.)

Thome, J.R. & El Hajal, J. 2004. Flow boiling heat transfer to carbon dioxide: general prediction method. *International journal of refrigeration*, 27(3):297-301.

Wojtan, L., Ursenbacher, T. & Thome, J.R. 2005a. Investigation of flow boiling in horizontal tubes: Part I - A new diabatic two-phase flow pattern map. *International journal of heat and mass transfer*, 48(4):2955-2969.

Wojtan, L., Ursenbacher, T. & Thome, J.R. 2005b. Investigation of flow boiling in horizontal tubes: Part II - Development of a new heat transfer model for stratified-wavy,

dryout and mist flow regimes. *International journal of heat and mass transfer*, 48(4):2970-2985.

Yoon, S.H., Cho, E.S., Hwang, Y.W., Kim, M.S., Min, K. & Kim, Y. 2004. Characteristics of evaporative heat transfer and pressure drop of carbon dioxide and correlation development. *International journal of refrigeration*, 27(2):111-119.

Yun, R., Kim, Y. & Kim, M.S. 2005. Flow boiling heat transfer of carbon dioxide in horizontal mini tubes. *International journal of heat and fluid flow*, 26(5):801-809.

Appendix A – Experimental tests

Tabulated below is the detail of the test bench setup for each of the 98 tests conducted as discussed in section 4.3.1, showing the values of the controllable inputs for each test.

Test #	Gas Cooler Water Mass Flow	Evaporator Gas Pressure	Evaporator Water Mass Flow	VSD (Gas Mass Flow)	Date	Approx. Begin Time	Approx. End Time	Expansion Valve	Notes
	[l/min]	*[Bar]*	*[l/min]*	*[Hz]*	*[ccyy/mm/dd]*	*[hh:mm]*	*[hh:mm]*	*[%]*	
1	8	25	22	40	2011/11/30	14:00	14:30	24	NTR
2	8	25	22	50	2011/11/30	14:30	15:00	25	NTR
3	8	25	22	60	2011/11/30	15:10	15:40	27	NTR
4	8	25	19	40	2011/11/30	15:40	16:10	22	NTR
5	8	25	19	50	2011/11/30	16:10	16:40	24	NTR
6	8	25	19	60	2011/11/30	16:40	17:10	28	NTR
7	8	25	16	40	2011/12/02	09:45	10:15	23	NTR
8	8	25	16	50	2011/12/02	10:15	10:45	26	NTR
9	8	25	16	60	2011/12/02	10:45	11:15		Evap Freeze
10	8	30	22	40	2011/11/14	16:30	17:30	30	NTR
11	8	30	22	50	2011/11/14	17:30	18:30	38	NTR
12	8	30	22	60	2011/11/14	18:30	19:30	41	NTR
13	8	30	19	40	2011/11/15	09:00	10:00	29	NTR
14	8	30	19	50	2011/11/15	10:00	11:00	30	NTR
15	8	30	19	60	2011/11/15	11:00	12:00	36	GC Max Pres
16	8	30	16	40	2011/11/15	13:00	14:00	25	NTR
17	8	30	16	50	2011/11/15	14:00	15:00	30	NTR
18	8	30	16	60	2011/11/15	15:00	16:00	44	Evap

									Freeze
19	8	35	22	40	2011/11/17	13:00	14:00	48	NTR
20	8	35	22	50	2011/11/17	14:00	15:00	52	NTR
21	8	35	22	60	2011/11/17	15:00	15:45	57	NTR
22	8	35	19	40	2011/11/17	16:10	17:00	46	NTR
23	8	35	19	50	2011/11/17	17:00	17:45	56	NTR
24	8	35	19	60	2011/11/17	17:45	18:30	61	NTR
25	8	35	16	40	2011/11/17	18:30	19:15	52	NTR
26	8	35	16	50	2011/11/17	19:15	20:00	60	NTR
27	8	35	16	60	2011/11/17	20:00	20:45	64	NTR
28	12	25	22	40	2011/11/30	08:00	08:30	28	NTR
29	12	25	22	50	2011/11/30	08:30	09:00	33	NTR
30	12	25	22	60	2011/11/30	09:00	09:30	37	NTR
31	12	25	19	40	2011/11/30	09:30	10:00	30	NTR
32	12	25	19	50	2011/11/30	10:00	10:30	35	NTR
33	12	25	19	60	2011/11/30	10:30	11:00	41	Evap Freeze
34	12	25	16	40	2011/12/02	11:15	11:45	27	NTR
35	12	25	16	50	2011/12/02	11:45	12:15	32	NTR
36	12	25	16	60	2011/11/30	12:30	13:00	35	Evap Freeze
37	12	30	22	40	2011/11/18	07:15	08:00	32	NTR
38	12	30	22	50	2011/11/18	08:00	08:45	34	NTR
39	12	30	22	60	2011/11/18	08:45	09:30	36	NTR
40	12	30	19	40	2011/11/18	09:30	10:15	28	NTR
41	12	30	19	50	2011/11/18	10:15	11:00	33	NTR
42	12	30	19	60	2011/11/18	11:00	11:45	38	NTR
43	12	30	16	40	2011/11/18	17:00	17:45	28	NTR
44	12	30	16	50	2011/11/18	17:45	18:30	32	NTR
45	12	30	16	60	2011/11/18	18:30	18:45	35	GC Max Pres
46	12	35	22	40	2011/11/23	07:45	08:30	65	NTR

47	12	35	22	50	2011/11/23	12:40	13:25	68	NTR
48	12	35	22	60	2011/11/23	09:00	09:45	77	NTR
49	12	35	19	40	2011/11/23	09:45	10:30	67	NTR
50	12	35	19	50	2011/11/28	10:30	11:15	76	NTR
51	12	35	19	60	2011/11/23	11:15	12:00	78	NTR
52	12	35	16	40	2011/11/28	08:15	09:00	67	NTR
53	12	35	16	50	2011/11/28	09:00	09:45	74	NTR
54	12	35	16	60	2011/11/28	09:45	10:30	80	NTR
55	16	25	22	40	2011/12/05	14:15	14:45	28	NTR
56	16	25	22	50	2011/12/05	14:45	15:15	31	NTR
57	16	25	22	60	2011/12/05	15:15	15:45	35	NTR
58	16	25	19	40	2011/12/05	15:45	16:15	26	NTR
59	16	25	19	50	2011/12/05	16:15	16:45	32	NTR
60	16	25	19	60	2011/12/05	16:45	17:00	38	Evap Freeze
61	16	25	16	40	2011/12/05	17:00	17:30	28	NTR
62	16	25	16	50	2011/12/05	17:30	18:00	32	Evap Freeze
63	16	25	16	60	2011/12/02	13:00	13:30	38	Evap Freeze
64	16	30	22	40	2011/12/02	13:30	14:00	44	NTR
65	16	30	22	50	2011/12/02	14:00	14:30	54	NTR
66	16	30	22	60	2011/12/02	14:30	15:00	61	NTR
67	16	30	19	40	2011/12/02	15:00	15:30	46	NTR
68	16	30	19	50	2011/12/02	15:30	16:00	56	NTR
69	16	30	19	60	2011/12/02	16:00	16:45	53	NTR
70	16	30	16	40	2011/12/02	16:45	17:15	37	NTR
71	16	30	16	50	2011/12/02	17:15	17:45	46	NTR
72	16	30	16	60	2011/12/02	17:45	18:15	52	NTR
73	16	35	22	40	2011/12/05	08:00	08:30	67	NTR
74	16	35	22	50	2011/12/05	08:30	09:00	73	NTR
75	16	35	22	60	2011/12/05	09:00	09:30	78	NTR

76	16	35	19	40	2011/12/05	09:30	10:00	68	NTR
77	16	35	19	50	2011/12/05	10:00	10:30	74	NTR
78	16	35	19	60	2011/12/05	10:30	11:00	78	NTR
79	16	35	16	40	2011/12/05	11:00	11:30	69	NTR
80	16	35	16	50	2011/12/05	11:30	12:00	74	NTR
81	16	35	16	60	2011/12/05	12:00	12:30	79	NTR
82	8	30	19	40	2011/11/29	10:15	10:45	34	NTR
83	8	30	19	60	2011/11/29	10:45	11:15	42	NTR
84	8	25	19	40	2011/11/29	11:15	11:45	22	NTR
85	8	25	19	60	2011/11/29	11:45	12:15	26	NTR
86	8	30	16	40	2011/11/29	12:15	12:45	34	NTR
87	8	30	16	60	2011/11/29	12:45	13:15	43	NTR
88	8	25	16	40	2011/11/29	13:15	13:45	22	NTR
89	8	25	16	60	2011/11/29	13:45	14:15	26	NTR
90	12	40	16	40	2011/12/06	07:15	08:00	39	NTR
91	12	40	16	50	2011/12/06	08:00	08:30	50	NTR
92	12	40	16	60	2011/02/06	08:30	09:00	60	NTR
93	12	40	19	40	2011/02/06	09:00	09:45	32	NTR
94	12	40	19	50	2011/02/06	09:45	10:15	40	NTR
95	12	40	19	60	2011/02/06	10:15	10:45	48	NTR
96	12	40	22	40	2011/02/07	06:30	07:20	28	NTR
97	12	40	22	50	2011/02/07	07:20	07:40	34	NTR
98	12	40	22	60	2011/02/07	07:40	07:50	38	GC Max Pres
99	12	45	22	60	2011/02/07	07:50	08:20	64	NTR

Appendix B – Uncertainty propagation

In Appendix B the detailed calculation of the uncertainty analysis conducted is shown at the hand of the energy balance calculations discussed in section 5.3.1. This calculation is applied by EES to calculate the uncertainty of each of the heat transfer coefficients. The basic equation used for the uncertainty analysis is as follows:

$$\Delta q = \sqrt{(\frac{\partial q}{\partial x}\Delta x)^2 + \cdots + (\frac{\partial q}{\partial z}\Delta z)^2} \tag{B.1}$$

Where q is the calculated value which is a function of various variables $(x \ldots z)$ which has a known uncertainty $(\Delta x \ldots \Delta z)$. The formula calculates the uncertainty of q due to the uncertainty of the known variables. In section 5.3.1 the following equations are used to calculate the heat transfer for the water and R-744 sides respectively:

$$Q_g = \dot{m}_g(\alpha_{go} - \alpha_{gi}) \tag{B.2}$$

$$Q_w = \dot{m}_w C_p(T_{wi} - T_{wo}) \tag{B.3}$$

The uncertainty in the calculated heat transferred is dependent on the uncertainty in the mass flow, pressure and temperature readings. The application of equation (B.1) will be demonstrated at the hand of an example. Consider the following data set as example:

Table B.1 - Data set used in uncertainty propagation example.

Variable	Value	Unit
R-744 inlet temperature	280.4	K
R-744 outlet temperature	299.1	K
Water inlet temperature	305.0	K
Water outlet temperature	301.5	K
R-744 mass flow	0.1560	kg/s
Water mass flow	0.2668	kg/s
R-744 inlet pressure	3.02×10^6	Pa
R-744 outlet pressure	2.96×10^6	Pa

For each of these data points the uncertainty is determined from the instrument accuracy as discussed in section 5.2 and listed below. When applying these formulas the specific uncertainties for this data set are calculated as shown in Table B.2.

- Coriolis Flow Meter: $\pm 0.5\% \pm ((0.1 \div measured\ value) \times 100)\%$
- Electromagnetic Flow Meter: $\pm 0.5\% \pm 1\ mm\ /\ s$
- Temperature sensor: $\pm(0.3 + 0.005T)$
- Pressure transmitter: $\pm 0.3\%\ Full\ Span$

Table B.2 – Data set specific uncertainty

Variable	Sensor Uncertainty	Logging Uncertainty	Effective Uncertainty
R-744 inlet temperature [K]	± 0.34	± 0.3	280.4 ± 0.34
R-744 outlet temperature [K]	± 0.43	± 0.3	299.1 ± 0.43
Water inlet temperature [K]	± 0.46	± 0.3	305.0 ± 0.46
Water outlet temperature [K]	± 0.44	± 0.3	301.5 ± 0.44
R-744 mass flow [kg/s]	± 0.000780	± 0.0005	0.1560 ± 0.00078
Water mass flow [kg/s]	± 0.0014	± 0.0005	0.2668 ± 0.0014
R-744 inlet pressure [Pa]	± 30000	± 10000	3.02×10^6 ± 30000
R-744 outlet pressure [Pa]	± 30000	± 10000	2.96×10^6 ± 3000

For the uncertainty calculation the larger of the two uncertainties (instrument or logging uncertainty) was chosen as the effective uncertainty of that data point. The value for the heat transferred from the gas side is calculated as follows:

$$Q_g = \dot{m}_g(\alpha_{go} - \alpha_{gi}) = (0.1560)\big(-30715 - (-54846)\big) = 3764.4 \qquad \text{(B.4)}$$

In order to use equation (B.1) to calculate the uncertainty of the value in equation (B.4) the partial derivative of Q_g to each of the independent factors is required:

$$\frac{\partial Q_g}{\partial \dot{m}_g} = \big(\alpha_{go} - \alpha_{gi}\big) = -30715 - (-54846) = 24131 \qquad \text{(B.5)}$$

$$\frac{\partial Q_g}{\partial p_{gi}} = 0.002752 \tag{B.6}$$

$$\frac{\partial Q_g}{\partial p_{go}} = -0.001981 \tag{B.7}$$

$$\frac{\partial Q_g}{\partial T_{gi}} = -209.9 \tag{B.8}$$

$$\frac{\partial Q_g}{\partial T_{go}} = 180.9 \tag{B.9}$$

Thus Equation (B.1) can be rewritten as follow:

$$\Delta Q_g = \sqrt{(\frac{\partial Q_g}{\partial \dot{m}_g}\Delta \dot{m}_g)^2 + (\frac{\partial Q_g}{\partial p_{gi}}\Delta p_{gi})^2 + (\frac{\partial Q_g}{\partial p_{go}}\Delta p_{go})^2 + (\frac{\partial Q_g}{\partial T_{gi}}\Delta T_{gi})^2 + (\frac{\partial Q_g}{\partial T_{go}}\Delta T_{go})^2} \tag{B.10}$$

Substituting equation (B.5) through to equation (B.9) and the respective uncertainties of each of the factors into equation (B.10) results in the following:

$$\Delta Q_g = \sqrt{354.3 + 6816.2 + 3531.9 + 5049.5 + 6060.8} = 147.8 \tag{B.11}$$

Therefore the heat transferred to the gas side is as follow:

$$Q_g = 3764.4 \pm 147.8 \tag{B.12}$$

Similarly for the water side of the heat exchanger the heat loss can be calculated as follow:

$$Q_w = \dot{m}_w C_p (T_{wi} - T_{wo}) = 0.2668 \cdot 4183(305 - 301.5) = 3906 \tag{B.13}$$

Again the partial derivative of Q_w to each of the independent factors is calculated:

$$\frac{\partial Q_w}{\partial \dot{m}_w} = c_p(T_{wi} - T_{wo}) = \ 4183(305 - 301.5) = 14641 \tag{B.14}$$

$$\frac{\partial Q_w}{\partial T_{wi}} = 1116 \tag{B.15}$$

$$\frac{\partial Q_w}{\partial T_{wo}} = -1116 \tag{B.16}$$

Equation (B.1) can be rewritten as follow:

$$\Delta Q_w = \sqrt{(\frac{\partial Q_w}{\partial \dot{m}_w}\Delta \dot{m}_w)^2 + (\frac{\partial Q_w}{\partial T_{wi}}\Delta T_{wi})^2 + (\frac{\partial Q_w}{\partial T_{wo}}\Delta T_{wo})^2} \tag{B.17}$$

Substituting equation (B.14) through to (B.16) and the respective uncertainties of each of the factors into equation (B.17) results in the following:

$$\begin{aligned}\Delta Q_w &= \sqrt{(14641 \cdot 0.0014)^2 + (1116 \cdot 0.46)^2 + (-1116 \cdot 0.44)^2} \\ &= 710.7\end{aligned} \tag{B.18}$$

Therefore heat transferred from the water side is as follows:

$$Q_w = 3906 \pm 710.7 \tag{8.19}$$

From the results obtained in equation (B.12) and equation (8.19) it is clear that the instruments are functioning correctly. Due to the uncertainty on the temperature and pressure instruments the calculated heat transfer does have a large uncertainty; however the measurements on the two sides do correspond well.

Appendix C – Enthalpy calculation

Shown below is the EES model with which the enthalpy for each of the data points was calculated:

```
From = {# of first data set}
To = {# of last data set}

h_i[From] = Enthalpy(R744,T=T_gg[From],P=P_gg[From])
T_gg[From] = Lookup('EnthalpyData.txt',From,8) + 273.15
P_gg[From] = Lookup('EnthalpyData.txt',From,9) * 100000

    T_g[From] = Lookup('EnthalpyData.txt',From,1) + 273.15
    T_wo[From] = Lookup('EnthalpyData.txt',From,2) + 273.15
    T_wi[From] = Lookup('EnthalpyData.txt',From,3) + 273.15
    m_w[From] = Lookup('EnthalpyData.txt',From,7)
    m_g[From] = Lookup('EnthalpyData.txt',From,6)
    p_i[From] = Lookup('EnthalpyData.txt',From,4) * 100000
    p_o[From] = Lookup('EnthalpyData.txt',From,5) * 100000
    T_wavg[From] = Average(T_wo[From],T_wi[From])
    cp[From] = cp(water,T=T_wavg[From],P=85000)
    Q[From] = m_w[From] * cp[From] * (T_wi[From] - T_wo[From])
    h_e[From] = h_i[From] + Q[From] / m_g[From]

Duplicate k = (From+1),To
    h_i[k] = h_e[k-1]
    T_g[k] = Lookup('EnthalpyData.txt',k,1) + 273.15
    T_wo[k] = Lookup('EnthalpyData.txt',k,2) + 273.15
    T_wi[k] = Lookup('EnthalpyData.txt',k,3) + 273.15
    m_w[k] = Lookup('EnthalpyData.txt',k,7)
    m_g[k] = Lookup('EnthalpyData.txt',k,6)
    p_i[k] = Lookup('EnthalpyData.txt',k,4) * 100000
    p_o[k] = Lookup('EnthalpyData.txt',k,5) * 100000
    T_wavg[k] = Average(T_wo[k],T_wi[k])
    cp[k] = cp(water,T=T_wavg[k],P=85000)
    Q[k] = m_w[k] * cp[k] * (T_wi[k] - T_wo[k])
    h_e[k] = h_i[k] + Q[k] / m_g[k]
End
```

Appendix D – EES program

Shown below is the EES program used to calculate the four R-744 heat transfer coefficients as well as the two water coefficients:

```
"-----------------------------------------------------------------------------------------------------------------------"
"Procedure - Yoon et al."

Procedure Yoon (MassFlux, ID, mu_l, HeatFlux, h_fg, g, rho_l, rho_g, sigma, x_g, k_l, cp_l, k_g,
mu_g, cp_g, A_g, Per_g : h_g_tp, x_res)
    If x_g < 1 Then
        Epsilon =  (x_g / rho_g) * ((1 + 0.12 * (1 - x_g)) * ((x_g / rho_g) + ((1 - x_g) / rho_l)) + (1.18 /
MassFlux) * ((g * sigma * (rho_l - rho_g)) / rho_l^2)^(1/4) * (1 - x_g))^(-1)
        Re_lo = MassFlux * ID / mu_l
        Bo = HeatFlux / (MassFlux * h_fg)
        Bd = (g * (rho_l - rho_g) * ID^2) / sigma
        x_crit = 0.0012 * Re_lo^2.79 * (1000 * Bo)^0.06 * Bd^(-4.76)
        Re_l = MassFlux * (1 - x_g) * ID / mu_l
        Pr_l = mu_l * cp_l / k_l
        Re_g = MassFlux * x_g * ID / (mu_g * Epsilon)
        Pr_g = mu_g * cp_g / k_g
        X = ((1 - x_g) / x_g)^0.9 * (rho_g / rho_l)^0.5 * (mu_l / mu_g)^0.1
        x_res = x_crit
        If x_g < x_crit Then
        Else
            E = 1 + 3000 * Bo^0.86 + 1.12 * (x_g / (1 - x_g))^0.75 * (rho_l / rho_g)^0.41
            h_l = k_l * 0.023 * Re_l^0.8 * Pr_l^0.4 / ID
            h_g = k_g * 0.023 * Re_g^0.8 * Pr_g^0.4 / ID
            h_wet = E * h_l
            Theta_dry = 2 * pi * 36.23 * Re_l^3.47 * Bo^4.84 * Bd^(-0.27) * (1 / X)^2.6
            Theta_strat = 2 * pi - 2 * (pi * (1 - Epsilon) + (3 * pi / 2)^(1 / 3) * (1 - 2 * (1 - Epsilon) + (1 -
Epsilon)^(1 / 3) - Epsilon^(1 / 3)) - (1 / 200) * (1 - Epsilon) * Epsilon * (1 - 2 * (1 - Epsilon)) * (1 + 4 * (1
- Epsilon)^2 + Epsilon^2))
            h_g_tp = (Theta_strat * h_g + (2 * pi - Theta_strat) * h_wet) / (2 * pi)
        Endif
    Else
        x_res = 99999
        h_g_tp = 99999
    Endif
End
```

```
"-----------------------------------------------------------------------------------------------------------------------------------"
"Procedure - Pamitran"

Procedure Pamitran (k_l, ID, MassFlux, x_g, mu_l, cp_l, mu_g, rho_g, rho_l, HeatFlux, T_g, h_fg :
h_g_tp)
    If x_g < 1 Then
      Re_l = MassFlux * (1 - x_g) * ID / mu_l
      Re_g = MassFlux * x_g * ID / mu_g
      h_lo = 0.023 * (k_l / ID) * (Re_l)^0.8 * (cp_l * mu_l / k_l)^0.4
       If Re_l < 2300 Then
         If Re_g< 2300 Then
            f_f = 16 / Re_l                          "Liquid Laminar, Vapour Laminar"
            f_g = 16 / Re_g
         Else
            f_f = 16 / Re_l                           "Liquid Laminar, Vapour Turbulent"
            f_g = 0.079 * Re_g^(-0.25)
         EndIf
      Else
         If Re_g< 2300 Then
            f_f = 0.079 * Re_l^(-0.25)               "Liquid Turbulent, Vapour Laminar"
            f_g = 16 / Re_g
         Else
            f_f = 0.079 * Re_l^(-0.25)               "Liquid Turbulent, Vapour Turbulent"
            f_g = 0.079 * Re_g^(-0.25)
        EndIf
      EndIf
      X = (f_f / f_g)^0.5 * ((1 - x_g) / x_g) * (rho_g / rho_l)^0.5
      If Re_l < 2300 Then
         If Re_g< 2300 Then
            PHI = 1 + (5 / X) + (1 / X^2)            "Liquid Laminar, Vapour Laminar"
         Else
            PHI = 1 + (12 / X) + (1 / X^2)           "Liquid Laminar, Vapour Turbulent"
         EndIf
      Else
         If Re_g< 2300 Then
            PHI = 1 + (10 / X) + (1 / X^2)           "Liquid Turbulent, Vapour Laminar"
         Else
            PHI = 1 + (20 / X) + (1 / X^2)           "Liquid Turbulent, Vapour Turbulent"
        EndIf
      EndIf
```

```
        F = max((0.009 * PHI + 0.76),1)
        p_crit = P_crit(R744)
        p_sat = P_sat(R744,T=T_g)
        P_red = p_sat / p_crit
        M = MolarMass(R744)
        h_pb = 55 * P_red^0.12 * (-0.4343 * ln(P_red))^(-0.55) * M^(-0.5) * HeatFlux^0.67
        Bo = HeatFlux / (MassFlux * h_fg)
        S = 0.25 * PHI^(-0.2093) * Bo^0.7402
        h_g_tp = F * h_lo + S * h_pb
    Else h_g_tp = 99999
End

"-----------------------------------------------------------------------------------------------------------------------------------"
"Procedure - Thome & El Hajal"

Procedure Thome (ID, MassFlux, mu_l, x_g, T_g, HeatFlux, cp_l, k_l, rho_g, rho_l, g, sigma : h_g_tp)
    If x_g < 1 Then
        Re_l = MassFlux * ID / mu_l
        S = (1 - x_g)^(1/2) / (0.121 * Re_l^0.225)
        p_crit = P_crit(R744)
        p_sat = P_sat(R744,T=T_g)
        P_red = p_sat / p_crit
        M = MolarMass(R744)
        h_nb = 55 * P_red^0.12 * (-ln(P_red))^(-0.55)*M^(-0.5)*HeatFlux^0.67
        const = 3970
        h_nb_CO2 = 0.71 * h_nb + const
        FilmThick = 0.005
        Epsilon = (x_g / rho_g) * ((1 + 0.12 * (1 - x_g)) * ((x_g / rho_g) + ((1 - x_g) / rho_l)) + (1.18 /
MassFlux) * ((g * sigma * (rho_l - rho_g)) / rho_l^2)^(1/4) * (1 - x_g))^(-1)
        h_cb = 0.0133 * ((4* MassFlux * (1 - x_g) * FilmThick) / ((1 - epsilon) * mu_l))^0.69 * (cp_l *
mu_l / k_l)^0.4 * (k_l / FilmThick)
        h_g_tp = ((S * h_nb_CO2)^3 + h_cb^3)^(1/3)
    Else h_g_tp = 99999
End

"-----------------------------------------------------------------------------------------------------------------------------------"
"Procedure - Cheng et al."

Procedure Cheng (ID, x_g, rho_g, rho_l, mu_g, mu_l, T_g, HeatFlux, k_l, MassFlux, cp_l, g, sigma,
h_fg, cp_g, k_g : h_g_tp, Phase)
```

```
    If x_g < 1 Then
        Epsilon =  (x_g / rho_g) * ((1 + 0.12 * (1 - x_g)) * ((x_g / rho_g) + ((1 - x_g) / rho_l)) + (1.18 /
MassFlux) * ((g * sigma * (rho_l - rho_g)) / rho_l^2)^(1/4) * (1 - x_g))^(-1)
        x_ia = (1.8^(1/0.875) * (rho_g / rho_l)^(-1 / 1.75) * (mu_l / mu_g)^(-1 / 7) + 1)^(-1)
        We_g = MassFlux^2 * ID / (rho_g * sigma)
        Fr_g_Mori = MassFlux^2 / (rho_g * (rho_l - rho_g) * g * ID)
        HeatFlux_crit = 0.131 * rho_g^0.5 * h_fg * (g * sigma * (rho_l - rho_g))^0.25
        const1 = exp(0.52 - 0.236 * We_g^0.17 * Fr_g_Mori^0.17 * (rho_g /rho_l)^0.25 * (HeatFlux /
HeatFlux_crit)^0.27)
        x_di = 0.58 * const1
        const2 = exp(0.57 - 0.502 * We_g^0.16 * Fr_g_Mori^0.15 * (rho_g / rho_l)^(-0.09) * (HeatFlux /
HeatFlux_crit)^0.72)
        x_de = 0.61 * const2
        If x_g < x_ia Then                                  "Intermittent Flow"
            Theta_dry = 0
            FilmThick = 1
            FilmThick_ia = 1
            S = 1
            p_crit = P_crit(R744)
            p_sat = P_sat(R744,T=T_g)
            P_red = p_sat / p_crit
            M = MolarMass(R744)
            h_nb = 131 * P_red^(-0.0063) * (-ln(P_red))^(-0.55)*M^(-0.5)*HeatFlux^0.58
            Pr_l = mu_l * cp_l / k_l
            h_cb = 0.0133 * ((4 * MassFlux * (1 - x_g) * FilmThick) / ((1 - Epsilon) * mu_l))^0.69 * Pr_l^0.4
* (k_l / FilmThick)
            h_g_tp = ((S * h_nb)^3 + h_cb^3)^(1/3)
            Phase = 1
        Else
            If x_g < x_di Then                              "Annular Flow"
                Theta_dry = 0
                D_ref = 7.53 / 1000
                D = 7.53 / 100                              "ID > D_ref therefore set D = 7.53"
                FilmThick = 1
                FilmThick_ia = 1
                S = 1 - 1.14 * (D / D_ref)^2 * (1 - FilmThick/FilmThick_ia)^2.2
                p_crit = P_crit(R744)
                p_sat = P_sat(R744,T=T_g)
                P_red = p_sat / p_crit
                M = MolarMass(R744)
```

```
        h_nb = 131 * P_red^(-0.0063) * (-ln(P_red))^(-0.55)*M^(-0.5)*HeatFlux^0.58
        Pr_l = mu_l * cp_l / k_l
        h_cb = 0.0133 * ((4 * MassFlux * (1 - x_g) * FilmThick) / ((1 - Epsilon) * mu_l))^0.69 *
Pr_l^0.4 * (k_l / FilmThick)
        h_g_tp = ((S * h_nb)^3 + h_cb^3)^(1/3)
        Phase = 2
      Else
        If x_g < x_de Then                              "Dry-out Region"
          Theta_strat = 2 * pi - 2 * (pi * (1 - Epsilon) + (3 * pi / 2)^(1 / 3) * (1 - 2 * (1 - Epsilon) + (1 -
Epsilon)^(1 / 3) - Epsilon^(1 / 3)) - (1 / 200) * (1 - Epsilon) * Epsilon * (1 - 2 * (1 - Epsilon)) * (1 + 4 * (1
- Epsilon)^2 + Epsilon^2))
          Re_g = (MassFlux * x_di * ID) / (mu_g * Epsilon)
          Pr_g = mu_g * cp_g / k_g
          h_v = 0.023 * Re_g^0.8 * Pr_g^0.4 * (k_g / ID)
          D_ref = 7.53 / 1000
          D = 7.53 / 100                                "ID > D_ref therefore set D = 7.53"
          FilmThick = 1
          FilmThick_ia = 1
          FilmThick = 1
          S = 1 - 1.14 * (D / D_ref)^2 * (1 - FilmThick/FilmThick_ia)^2.2
          p_crit = P_crit(R744)
          p_sat = P_sat(R744,T=T_g)
          P_red = p_sat / p_crit
          M = MolarMass(R744)
          h_nb =  131 * P_red^(-0.0063) * (-ln(P_red))^(-0.55)*M^(-0.5)*HeatFlux^0.58
          Pr_l = mu_l * cp_l / k_l
          h_cb = 0.0133 * ((4 * MassFlux * (1 - x_di) * FilmThick) / ((1 - Epsilon) * mu_l))^0.69 *
Pr_l^0.4 * (k_l / FilmThick)
          h_wet =  ((S * h_nb)^3 + h_cb^3)^(1/3)
          h_tp = (Theta_strat * h_v + (2 * pi - Theta_strat) * h_wet) / (2 * pi)
          Re_hom = ((MassFlux * ID) / mu_g) * (x_de + (rho_g / rho_l) * (1 - x_de))
          Pr_g = mu_g * cp_g / k_g
          Y = 1 - 0.1 * (((rho_l / rho_g) - 1) * (1 - x_g))^0.4
          h_m = 2 * 10^(-8) * Re_hom^1.97 * Pr_g^1.06 * Y^(-1.83) * k_g / ID
          h_g_tp =  h_tp - ((x_g - x_di) / (x_de - x_di)) * (h_tp - h_m)
          Phase = 3
        Else                                            "Mist Flow"
          Re_hom = ((MassFlux * ID) / mu_g) * (x_g + (rho_g / rho_l) * (1 - x_g))
          Pr_g = mu_g * cp_g / k_g
          Y = 1 - 0.1 * (((rho_l / rho_g) - 1) * (1 - x_g))^0.4
```

```
                h_g_tp = 2 * 10^(-8) * Re_hom^1.97 * Pr_g^1.06 * Y^(-1.83) * k_g / ID
                Phase = 4
            Endif
        Endif
    Endif
Else h_g_tp = 99999
     Phase = 5
End

"-----------------------------------------------------------------------------------------------------------------------------------"
"Procedure - Dittus-Boelter"

Procedure ActualDB (Q, T_g, T_w, r_o, r_i, l_pipe, A_hx_g, A_hx_w, Re_w, Pr_w, k_w, ID_w, OD_g :
h_actDB)
    DELTAT = T_w - T_g
    UA = Q / (DELTAT)
    AverageT = Average(T_w,T_g)
    k_alu = k_ ('Aluminum', AverageT)
    R = log10(r_o / r_i) / (2 * pi * k_alu * l_pipe)
    If Re_w < 4000 Then
       Nus_w = 3.66
    Else
       Nus_w = 0.023 * Re_w^0.8 * Pr_w^0.3
    Endif
    h_w = Nus_w * k_w / (ID_w - OD_g)
    h_actDB = 1 / (A_hx_g * ((1 / UA) - R - (1 / (h_w * A_hx_w))))
End

"-----------------------------------------------------------------------------------------------------------------------------------"
"Procedure - Gnielinski"

Procedure ActualG (Q, T_g, T_w, r_o, r_i, l_pipe, A_hx_g, A_hx_w, Re_w, Pr_w, k_w, ID_w, OD_g,f :
h_actG)
    DELTAT = T_w - T_g
    UA = Q / (DELTAT)
    AverageT = Average(T_w,T_g)
    k_alu = k_ ('Aluminum', AverageT)
    R = log10(r_o / r_i) / (2 * pi * k_alu * l_pipe)
    Nus_w = ((f / 8) * (Re_w - 1000) * Pr_w) / (1 + 12.7 * (f / 8)^0.5 * (Pr_w^(2 / 3) - 1))
    h_w = Nus_w * k_w / (ID_w - OD_g)
```

```
    h_actG = 1 / (A_hx_g * ((1 / UA) - R - (1 / (h_w * A_hx_w))))
End
"-----------------------------------------------------------------------------------------------------------------------------------------------"
"Function - Density of Two-phase Fluid"

Function TwoPhaseDensity(x_in, x_out, rho_liq, rho_gas, p_avg, T_avg)
    If x_in = 100 Then
        TwoPhaseDensity := Density(R744,T=T_avg,p=p_avg)
    Else
        If x_out = 100 Then
            TwoPhaseDensity := (1 - (x_in + 1) / 2) * rho_liq + (x_in + 1) / 2 * rho_gas
        Else
            TwoPhaseDensity := (1 - (x_in + x_out) / 2) * rho_liq + (x_in + x_out) / 2 * rho_gas
        Endif
    Endif
End
"-----------------------------------------------------------------------------------------------------------------------------------------------"
"Function - Conductivity of Two-phase Fluid"

Function TwoPhaseConductivity(x_in, x_out, k_liq, k_gas, p_avg, T_avg)
    If x_in = 100 Then
        TwoPhaseConductivity := Conductivity(R744,T=T_avg,p=p_avg)
    Else
        If x_out = 100 Then
            TwoPhaseConductivity := (1 - (x_in + 1) / 2) * k_liq + (x_in + 1) / 2 * k_gas
        Else
            TwoPhaseConductivity := (1 - (x_in + x_out) / 2) * k_liq + (x_in + x_out) / 2 * k_gas
        Endif
    Endif
End
"-----------------------------------------------------------------------------------------------------------------------------------------------"
"Function - Viscosity of Two-phase Fluid"

Function TwoPhaseViscosity(x_in, x_out, mu_liq, mu_gas, p_avg, T_avg)
    If x_in = 100 Then
        TwoPhaseViscosity := Viscosity(R744,T=T_avg,p=p_avg)
    Else
        If x_out = 100 Then
            TwoPhaseViscosity := (1 - (x_in + 1) / 2) * mu_liq + (x_in + 1) / 2 * mu_gas
        Else
```

```
            TwoPhaseViscosity := (1 - (x_in + x_out) / 2) * mu_liq + (x_in + x_out) / 2 * mu_gas
        Endif
    Endif
End
```

```
"-----------------------------------------------------------------------------------------------------------------------------------------"
"Function - Average Quality of Increment"

Function AverageQuality(x_in, x_out)
    If x_in = 100 Then
        AverageQuality := 1
    Else
        If x_out = 100 Then
            AverageQuality := Average(x_in,1)
        Else
            AverageQuality := Average(x_in,x_out)
        Endif
    Endif
End
"-----------------------------------------------------------------------------------------------------------------------------------------"
"Enthalpy Calculation"

Procedure EnthalpyCalc(Check, T_g, T_wo, T_wi, m_w, m_g, p_i, p_o, T_gg, P_gg, h_ex : h_i, h_e)
    If Check = 1 Then
        h_i = Enthalpy(R744,T=T_gg,P=P_gg)
        T_wavg = Average(T_wo,T_wi)
        cp = cp(water,T=T_wavg,P=85000)
        Q = m_w * cp * (T_wi - T_wo)
        h_e = h_i + Q / m_g
    Else
        h_i = h_ex
        T_wavg = Average(T_wo,T_wi)
        cp = cp(water,T=T_wavg,P=85000)
        Q = m_w * cp * (T_wi - T_wo)
        h_e = h_i + Q / m_g
    Endif
End
```

```
"-----------------------------------------------------------------------------------------------------------------------------------"
"Lookup Table"

h_go[0] =0

From =1
To = 252

Dup1 = 1
Dup2 = 252

Duplicate k = Dup1,Dup2
    Check[k]= Lookup('DataB.txt',((From - 1) + k),10)
    T_g[k] = Lookup('DataB.txt',((From - 1) + k),1)
    T_wo[k] = Lookup('DataB.txt',((From - 1) + k),2)
    T_wi[k] = Lookup('DataB.txt',((From - 1) + k),3)
    p_gi[k] = Lookup('DataB.txt',((From - 1) + k),4)
    p_go[k] = Lookup('DataB.txt',((From - 1) + k),5)
    m_dot_g[k] = Lookup('DataB.txt',((From - 1) + k),6)
    m_dot_w[k] = Lookup('DataB.txt',((From - 1) + k),7)
    T_ggc[k] = Lookup('DataB.txt',((From - 1) + k),8)
    P_ggc[k] = Lookup('DataB.txt',((From - 1) + k),9)
    Call EnthalpyCalc(Check[k], T_g[k], T_wo[k], T_wi[k], m_dot_w[k], m_dot_g[k], p_gi[k], p_go[k],
T_ggc[k], P_ggc[k], h_go[k-1] : h_gi[k], h_go[k])
End

"-----------------------------------------------------------------------------------------------------------------------------------"
"Physical Properties & Constants"

"R-744"

"Diameter"
ID_g = 0.0158
OD_g = 0.02134
"Radii"
r_i_g = ID_g / 2
r_o_g = OD_g / 2
"Area"
A_g = pi * r_i_g^2
"Perimeter"
```

```
Per_g = 2 * pi * r_i_g

"Water"

"Diameter"
ID_w = 0.03
OD_w = 0.032
"Radii"
r_i_w = ID_w / 2
r_o_w = OD_w / 2
"Area"
A_w = pi * r_i_w^2 - pi * r_o_g^2

"Length"

N_pipes = 8
L_pipe = 2
L_tot = L_pipe * N_pipes

A_hx_g = pi * ID_g * L_pipe
A_hx_w = pi * OD_g * L_pipe

g = 9.81
RR = 0.0025

"-----------------------------------------------------------------------------------------------------------------------------------------"
"Increments"

Duplicate k = Dup1,Dup2
    T_w_avg[k] = Average(T_wo[k],T_wi[k])
    rho_w_avg[k] = Density(Water,T=T_w_avg[k],P=85000)
    cp_w_avg[k] = Cp(Water,T=T_w_avg[k],P=85000)
    Q_w[k] = m_dot_w[k] * cp_w_avg[k] * (T_wi[k] - T_wo[k])
    k_w_avg[k] = Conductivity(Water,T=T_w_avg[k],P=85000)
    m_dot_w[k] = rho_w_avg[k] * V_w_avg[k] * A_w
    HeatFlux[k] = Q_w[k] / A_hx_g
    mu_w_avg[k] = Viscosity(Water,T=T_w_avg[k],P=85000)
    Re_w[k] = m_dot_w[k] * (ID_w - OD_g) / (mu_w_avg[k] * A_w)
    Pr_w[k] = cp_w_avg[k] * mu_w_avg[k] / k_w_avg[k]
    f_w[k] = MoodyChart(Re_w[k], RR)
```

```
x_gi[k] = Quality(R744,T=T_g[k],h=h_gi[k])
x_go[k] = Quality(R744,T=T_g[k],h=h_go[k])
x_g_avg[k] = Average(x_gi[k],x_go[k])

p_g_avg[k] = Average(p_gi[k],p_go[k])
cp_gl_avg[k] = cp(R744, T=T_g[k], x=0)
cp_gg_avg[k] = cp(R744, T=T_g[k], x=1)
rho_gl_avg[k] = Density(R744, T=T_g[k], x=0)
rho_gg_avg[k] = Density(R744, T=T_g[k], x=1)
k_gl_avg[k] = Conductivity(R744, T=T_g[k], x=0)
k_gg_avg[k] = Conductivity(R744, T=T_g[k], x=1)
mu_gl_avg[k] = Viscosity(R744, T=T_g[k], x=0)
mu_gg_avg[k] = Viscosity(R744, T=T_g[k], x=1)
k_g_avg[k] = TwoPhaseConductivity(x_gi[k], x_go[k], k_gl_avg[k], k_gg_avg[k], p_g_avg[k], T_g[k])
mu_g_avg[k] = TwoPhaseViscosity(x_gi[k], x_go[k], mu_gl_avg[k], mu_gg_avg[k], p_g_avg[k], T_g[k])
sigma_g[k] = SurfaceTension(R744,T=T_g[k])
h_g_l[k] = Enthalpy(R744,x=0,T=T_g[k])
h_g_g[k] = Enthalpy(R744,x=1,T=T_g[k])
h_g_fg[k] = h_g_g[k] - h_g_l[k]
MassFlux[k] = m_dot_g[k] / A_g

Re_l_avg[k] = MassFlux[k] * (1 - x_g_avg[k]) * ID_g / mu_gl_avg[k]
Re_g_avg[k] = MassFlux[k] * x_g_avg[k] * ID_g / mu_gg_avg[k]
Re_hom_avg[k] = ((MassFlux[k] * ID_g) / mu_gg_avg[k]) * (x_g_avg[k] + (rho_gg_avg[k] / rho_gl_avg[k]) * (1 - x_g_avg[k]))

Call  Yoon (MassFlux[k], ID_g, mu_gl_avg[k], HeatFlux[k], h_g_fg[k], g, rho_gl_avg[k], rho_gg_avg[k], sigma_g[k], x_g_avg[k], k_gl_avg[k], cp_gl_avg[k],k_gg_avg[k], mu_gg_avg[k], cp_gg_avg[k], A_g, Per_g : h_Yoon[k], x_res[k])
Nus_YoonF[k] = h_Yoon[k] * ID_g / k_g_avg[k]

Call Pamitran (k_gl_avg[k], ID_g, MassFlux[k], x_g_avg[k], mu_gl_avg[k], cp_gl_avg[k], mu_gg_avg[k], rho_gg_avg[k], rho_gl_avg[k], HeatFlux[k], T_g[k], h_g_fg[k] : h_Pamitran[k])
Nus_PamitranB[k] = h_Pamitran[k] * ID_g / k_g_avg[k]

Call Thome (ID_g, MassFlux[k], mu_gl_avg[k], x_g_avg[k], T_g[k], HeatFlux[k], cp_gl_avg[k], k_gl_avg[k], rho_gg_avg[k], rho_gl_avg[k], g, sigma_g[k] : h_Thome[k])
```

```
    Nus_Thome[k] = h_Thome[k] * ID_g / k_g_avg[k]

    Call Cheng (ID_g, x_g_avg[k], rho_gg_avg[k], rho_gl_avg[k], mu_gg_avg[k], mu_gl_avg[k], T_g[k],
HeatFlux[k], k_gl_avg[k], MassFlux[k], cp_gl_avg[k], g, sigma_g[k], h_g_fg[k], cp_gg_avg[k],
k_gg_avg[k] : h_Cheng[k], Phase[k])
    Nus_Cheng[k] = h_Cheng[k] * ID_g / k_g_avg[k]

    Call ActualDB (Q_w[k], T_g[k], T_w_avg[k], r_o_g, r_i_g, L_pipe, A_hx_g, A_hx_w, Re_w[k],
Pr_w[k], k_w_avg[k], ID_w, OD_g : h_ActualDB[k])
    Nus_ActualDB[k] = h_ActualDB[k] * ID_g / k_g_avg[k]

    Call ActualG (Q_w[k], T_g[k], T_w_avg[k], r_o_g, r_i_g, L_pipe, A_hx_g, A_hx_w, Re_w[k],
Pr_w[k], k_w_avg[k], ID_w, OD_g, f_w[k] : h_ActualG[k])
    Nus_ActualG[k] = h_ActualG[k] * ID_g / k_g_avg[k]

End
"----------------------------------------------------------------------------------------------------------------------------"
```